Src homology domain-mediated protein interactions

Lindfors, H.E.

Src homology domain-mediated protein interactions

Proefschrift

ter verkrijging van

de graad van Doctor aan de Universiteit Leiden,

op gezag van Rector Magnificus Prof. Mr. P.F. van der Heijden,

volgens besluit van het College voor Promoties

te verdedigen op donderdag 21 Januari 2010

klokke 13.45

door

Hanna Elisabet Lindfors

Geboren te Säter in 1978

Promotiecommissie

Promotor: Prof. Dr. J.P. Abrahams

Co-promotor: Dr. M. Ubbink

Overige leden: Prof. Dr. J. Brouwer

Dr. M.E. Kuil

Prof. Dr. M. Sattler (Technische Universität München)

Dr. G. Siegal

Prof. Dr. G.W. Vuister (Radboud University Nijmegen)

Printed by Wöhrmann Print Service

This is my story both humble and true,
take it to pieces and mend it with glue

John Lennon, Wonsaponatime

Till min familj

Contents

Abbreviations

SH: Src homology

FAK: Focal adhesion kinase

TOAC: 2,2,6,6-tetramethylpiperidine-1-oxyl-4-amino-4-carboxylic acid

Fmoc: 9H-fluorenylmethyloxycarbonyl

HATU: O-(7-azabenzotriazol-1-yl)-1,1,3,3-tetramethyluronium hexafluorophosphate

NMM: N-methylmorpholine

NMP: N-methyl-2-pyrrolidone

PyBOP: Benzotriazol-1-yl-oxy-tris-pyrrolidino-phosphonium hexafluorophosphate

TFA: Trifluoroacetic acid

RP-HPLC: Reversed phase high performance liquid chromatography

MALDI-TOF: Matrix-assisted laser desorption/ionization time-of-flight

NOESY: Nuclear Overhauser effect spectroscopy

TOCSY: Total correlation spectroscopy

HSQC: Heteronuclear single quantum coherence

DTT: Dithiothreitol

INEPT: Insensitive Nuclei Enhanced by Polarization Transfer

TCEP·HCl: Tris(2-Carboxyethyl)phosphine hydrochloride

RT: Room temperature

FBS: Fetal bovine serum

NBS: Newborn bovine serum

IPTG: Isopropyl β-D-1-thiogalactopyranoside

DOTAP: N-[1-(2,3-Dioleoyloxy)propyl]-N,N,N-trimethylammonium methylsulfate

Dpi: Days post-infection

MOI: Multiplicity of infection

TCEP: Tris(2-carboxyethyl) phosphine

HEPES: 4-(2-hydroxyethyl)-1-piperazineethanesulfonic acid

PVDF: Polyvinylidene fluoride

BSA: Bovine serum albumine

TBS: Tris-buffered saline

ECL: Enhanced chemoluminescence

Chapter 1

General introduction

Signal transduction and protein-protein interactions

Cells in multicellular organisms constantly receive and react to external stimuli. Signals from outside the cell initiate signal transduction cascades within the cell, and in this way diverse external signals are detected, amplified and integrated to generate cellular responses such as changes in enzyme activity, gene expression or ion-channel activity. An appropriate response to external signals is necessary for the proper functioning of individual cells and for multicellular life to be possible. A central feature of signal transduction and many biological processes is the ability of proteins to bind each other in a highly specific manner. Studying protein complex formation in detail and understanding the forces that drive the interaction is therefore of great interest.

Protein complexes vary greatly in their properties, with equilibrium dissociation constants (K_d) spanning many orders of magnitude. Some proteins form stable complexes, interacting for a long time, whereas others interact only briefly. The properties of protein complexes are related to their biological functions. Antibody-antigen complexes or enzyme-inhibitor complexes require tight binding and high specificity, to ensure a proper immune response or strict control of enzyme activity. In contrast, proteins involved in signal transduction cascades or in electron transfer often need to interact with multiple partners and maintain a high turnover. Consequently, these protein complexes tend to be more transient and to display a lower binding affinity.

In our current understanding of protein complex formation at least two steps are involved, with the first step being the formation of an encounter complex. This involves the proteins coming together, mainly with the help of long-range electrostatic forces, to form a loosely-bound intermediate state. From the encounter complex the proteins can either dissociate or proceed to form a final complex involving short-range interactions such as hydrogen bonding, van der Waals forces

and the hydrophobic effect. The role of the encounter complex is to accelerate the rate of specific complex formation, by reducing the dimensionality in the diffusional search process and increasing the lifetime of macromolecular collisions [1].

The equilibrium between the encounter complex and the productive complex varies between protein complexes. Some protein complexes exist mainly as a specific, well-defined complex, whereas in other protein-protein interactions the encounter complex is populated for a significant part of the time. Some electron transfer complexes can even exist purely as an encounter complex, never proceeding to form a specific complex [2].

Phosphotyrosine signalling and modular proteins

In order for multicellular life to be possible cell proliferation, differentiation, adhesion and motility need to be strictly controlled. Many of these processes are regulated by tyrosine phosphorylation, which is believed to have been necessary for the transition from single-cell to multicellular organisms [3-5]. Tyrosine phosphorylation, the covalent addition of a phosphate group to the hydroxide group in the side chain of a tyrosine residue in a protein, is regulated by two groups of enzymes: protein tyrosine kinases and protein tyrosine phosphatases. Protein tyrosine kinases catalyze the transfer of a phosphate group from ATP to a tyrosine residue, and this action is opposed by protein tyrosine phosphatases that catalyze the reaction of phosphate removal. Addition of a phosphate group to a tyrosine residue creates a high-affinity binding site for Src homology 2 (SH2) domains. This leads to the formation of new protein complexes, and thereby, to the transmission of the signal. Tyrosine phosphorylation signalling can therefore be considered to consist of three components: A ‘writer’ (the kinase), a ‘reader’ (the SH2 domain) and an ‘eraser’ (the phosphatase), which can be combined to generate

remarkably diverse signalling responses [6], including hormone-, growth factor-, immune-, and adhesion-based signalling [7-10]. Because of their involvement in so many signalling pathways and regulatory events protein tyrosine kinases are important drug targets. Many human diseases are recognized to be associated with abnormal phosphorylation of cellular proteins resulting from disregulation of kinase activity [11].

Despite its importance, tyrosine phosphorylation is still a relatively rare event in cells compared to the more common serine/threonine phosphorylation, and it was discovered only in 1979 [12]. Like many important scientific discoveries the finding of protein tyrosine phosphorylation was a serendipitous event. In the processes of determining whether a protein was phosphorylated on serine or threonine residues, Tony Hunter used an old buffer in which the pH had changed to a point that allowed phosphotyrosine to be separated from phosphothreonine [13].

The main sites of tyrosine phosphorylation in the cell are focal adhesions, the sites of attachment of the cell to the extracellular matrix (ECM). At focal adhesions integrin receptors link ECM proteins to the actin cytoskeleton involving a multitude of signalling and adaptor proteins (Fig. 1.1). Focal adhesions perform at least two important functions in the cell, they transmit force or tension at adhesion sites in order to maintain strong attachments to the ECM, and they are of central importance in many signalling pathways that regulate cell growth, survival and gene expression [14].

Many eukaryotic signalling proteins are modular proteins, containing several individually folded domains connected by linker regions. These domains can be protein-interaction domains or domains with a catalytic function. Common for these signalling proteins is that their activity is tightly regulated. The activity is normally low under basal conditions, but the proteins can be activated by specific ligands binding to the protein-interaction domains. This way the activity is

intrinsically coupled to protein localization. Recognition of short peptide sequences by modular interaction domains plays a central role in regulating cellular behaviour, since it is via these protein-protein interactions that the assembly of signalling protein complexes and larger protein networks can occur [15;16].

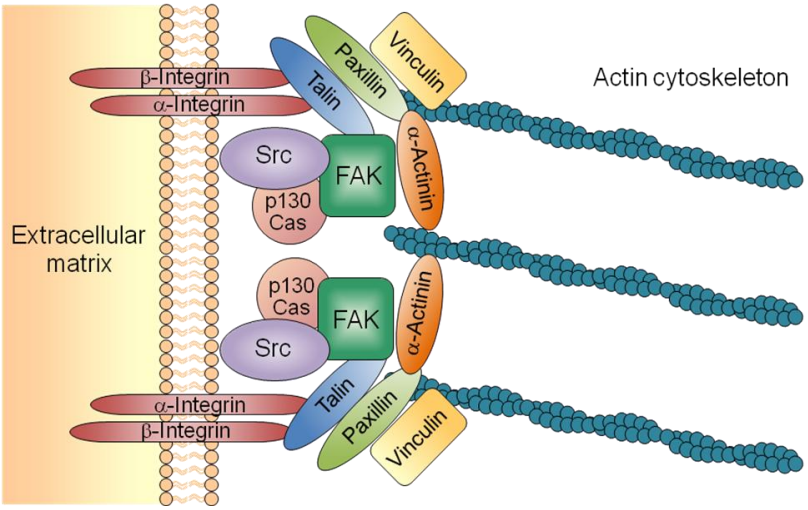

Figure 1.1. Focal adhesions. At focal adhesions integrin receptors bind to extracellular matrix proteins. A number of proteins, including talin, paxillin, vinculin and α-actinin, bind to the cytoplasmic tails of integrins, linking the integrins to the actin cytoskeleton. The large protein complexes also contain signalling proteins such as FAK and Src that promote focal adhesion turnover and cell motility.

Two proteins with a central role at focal adhesions are the non-receptor protein tyrosine kinases focal adhesion kinase (FAK) and Src kinase. FAK and Src are involved in a number of processes such as cell proliferation, survival and migration [17;18]. Increased activity and expression of Src and FAK has been demonstrated in many human cancers and is implicated in increased metastatic potential and invasiveness of tumour cells [19-28].

Proteins

Src

In 1911, Peyton Rous discovered that a cell-free filtrate of a chicken tumour was able to induce the formation of tumours in other chickens. Rous concluded that the tumour was caused by a 'filterable agent', as viruses were known at the time [29]. The idea that the virus, later called Rous sarcoma virus, could cause cancer was at first controversial, but it was later proven that the cancer-causing ability of the virus could be attributed to a viral gene, v-src [30]. A cellular counterpart of v-Src, Src, was subsequently discovered and found to be conserved in the vertebrate genome, indicating that the v-src gene had been incorporated into the viral genome through recombination. V-Src differs from Src in deletions at the C-terminal and in point mutations throughout the gene [31]. Unlike v-Src, Src is not constitutively active and is poorly transforming under normal conditions, but can act as an oncogene when activated [32;33]. This makes Src a proto-oncogene, the first of many to be discovered [34].

Src has a molecular weight of 60 kDa. It is expressed ubiquitously, but with the highest levels in the brain, osteoclasts and platelets [35]. It is a member of the Src family of protein tyrosine kinases that also includes Fyn, Yes, Lck, Hck, Blk, Fgr, Lyn, Yrk, Brk and Srm [36]. The members of the Src family share a conserved domain structure consisting of an N-terminal myristoylated SH4-domain followed by a region unique to each family member, an SH3 domain, an SH2 domain, a kinase domain and a C-terminal regulatory region [37]. The myristoylation facilitates attachment of Src to membranes. The SH3 domain and the SH2 domain are involved in protein-protein recognition, and facilitate the interaction of Src with its substrates.

The Src SH3 domain is about 60 amino acid residues in size. It has a β-barrel structure consisting of five antiparallel β-strands and two loops, known as the RT

and n-Src loops [38] (Fig. 1.2). SH3 domains bind to sequences that can adopt a left-handed helical conformation. These sequences often contain a characteristic proline-rich motif, PxxP. Src SH3 target sequences can be divided into two classes, which bind in opposite orientations to the SH3 domain. The binding orientation is largely determined by the position of an arginine residue close to the proline-rich core motif [39].

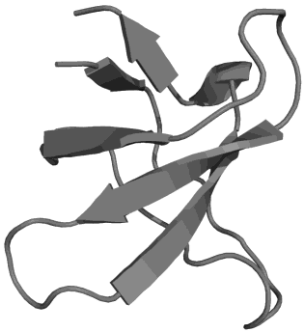

Figure 1.2. Solution structure of the Src SH3 domain (PDB entry 1SRL [40]).

The SH2 domain of Src contains about 100 aminoacids. It recognises and binds to sequences containing a phosphorylated tyrosine residue. The structure consists of a central β-sheet flanked by two α-helices, with connecting loops in-between [41] (Fig. 1.3). The preferred sequence for Src SH2 domain-binding is pYEEI [42], and the binding has been described by the 'two-pronged plug two-holed socket' model, where the phosphotyrosine is inserted into a pocket containing a conserved arginine residue, and the isoleucine at position pY+3 binds to a hydrophobic pocket [43].

The Src kinase domain consists of a small amino-terminal lobe, with a predominantly antiparallel β-sheet structure, and a larger carboxyl-terminal lobe that is mostly α-helical. The catalytic site is situated in a cleft between the two lobes [44].

Figure 1.3. Solution structure of the Src SH2 domain (PDB entry 1HCS [45]).

Activation and regulation of Src

Src is an important component in many signalling pathways, and can be activated in different ways, including activation by receptor tyrosine kinases [46]. Several mechanisms of activation and regulation of Src have been proposed [47].

The C-terminal part of Src contains a regulatory tyrosine residue, Y529 (if not stated otherwise mouse Src numbering is used throughout this work), which can be phosphorylated by the tyrosine kinase c-Src terminal kinase (Csk). When Y529 is phosphorylated the SH2 domain binds to this region, while at the same time the SH3 domain binds to the linker region between the SH2 domain and the kinase domain. Together these intramolecular interactions cause the protein to assume a closed, inactive conformation [48;49]. When the C-terminal phosphate is removed, Src assumes an open, active form (Fig. 1.4). In contrast to Src, v-Src lacks the negative-regulatory element, and is constitutively active. Full activation of Src also requires the phosphorylation of a tyrosine residue in the kinase domain, Y418, through autophosphorylation [50].

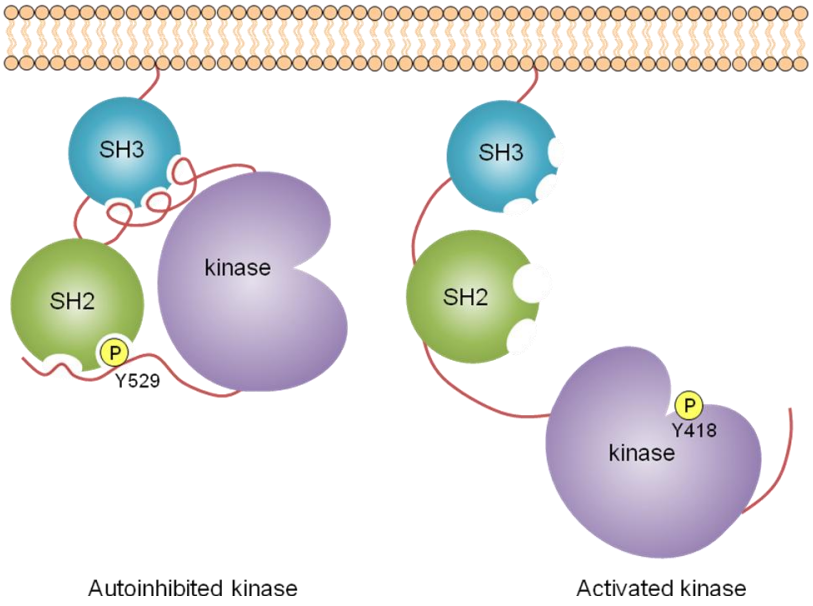

Figure 1.4. Activation of Src. Phosphorylation of Y529 in the C-terminal tail of Src by Csk causes the tail to bind to the SH2 domain. Together with interactions between the SH3 domain and the SH2-kinase linker, this locks the protein into an inactive conformation. Removal of the phosphate group by cellular phosphatases and interactions of the SH3 and SH2 domains with external ligands opens the protein up into an active conformation. Phosphorylation of Y418 in the kinase domain stabilizes the active conformation and is required for full activation of Src. Figure adapted from [51].

A likely mechanism for activation of Src is the removal of the C-terminal phosphate group by protein tyrosine phosphatases. Elevated levels of the protein tyrosine phosphatase PTP1B, which is able to dephosphorylate Src, has been found in breast cancer cell lines [52].

Competition between the low-affinity intramolecular binding sites for the SH2 and SH3 domains and high affinity binding sites in other proteins is another possible mechanism of activation. Upon binding of a ligand by the SH2 or SH3 domain, the closed, inactive conformation of Src would be disrupted and the protein would assume an open, active form instead. The use of domains for autoinhibition enhances the specificity – since the SH2 and SH3 domains already have

intramolecular binding sites, only specific binding sites of higher affinity can bind to the domains and activate the protein [53].

Focal adhesion kinase

FAK, initially identified in 1992 [54;55], is the only member in the FAK family of nonreceptor tyrosine kinases apart from PYK2. FAK can be found in the majority of tissues and cell types, and is evolutionary conserved in mammals and lower eukaryotic organisms [56].

FAK contains a FERM (band 4.1, ezrin, radixin, moesin homology) domain, a tyrosine-kinase domain and a focal adhesion targeting (FAT) domain. The crystal structure of the kinase domain has been determined and displays the typical protein kinase bilobal architecture; with the smaller N-terminal lobe containing a five-stranded antiparallel β-sheet and a single α-helix, and the larger C-terminal lobe being mostly α-helical [57] (Fig. 1.5).

The FAT domain is a four-helix bundle required for localization of FAK to focal adhesions via binding to paxillin [58;59]. The FERM domain is a three-lobed domain thought to mediate protein-protein interactions by binding to cytoplasmic domains of transmembrane receptors, such as the cytoplasmic region of β-integrin subunits [60-62].

The linker region connecting the FERM and the catalytic domain contains a proline-rich site which forms a binding-motif for Src family SH3 domains [63;64]. In the same linker the major autophosphorylation site in FAK, Y397, is situated. When phosphorylated, it forms a high-affinity binding site for the SH2 domains of Src family kinases, the p85 subunit of phosphatidylinositol 3-kinase (PI3K) and growth factor receptor-bound protein 7(Grb7) [65-69].

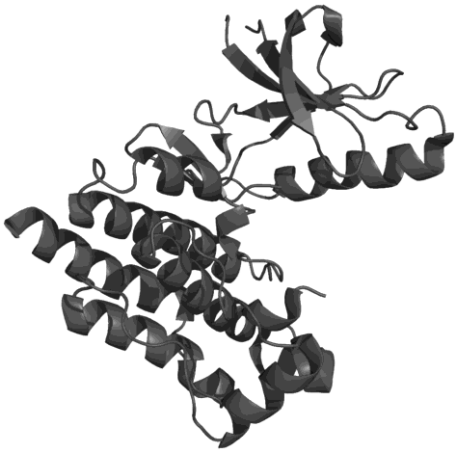

Figure 1.5. Crystal structure of the FAK kinase domain (PDB entry 1MP8 [70]).

Regulation of FAK and interaction with Src

Evidence is mounting that the FERM domain of FAK can interact with the catalytic domain, acting as an autoinhibitor of FAK activity [71-74]. A crystal structure of FAK including the FERM domain, linker region and catalytic domain shows FAK in an autoinhibited state [75]. In this structure the FERM domain binds the kinase domain, blocking access to the active site and to the kinase activation loop, as well as sequestering the Y397 phosphorylation site. This gives rise to a model of FAK activation where the FERM domain is displaced by competitive binding of an activating protein, such as the cytoplasmic regions of β-integrins or growth factor receptors. After FERM domain displacement Y397 is rapidly autophosphorylated and the PxxP sequence in the same linker region is exposed, enabling binding of the SH2 and SH3 domains of Src (Fig. 1.6). The interaction of Src and FAK leads to phosphorylation of other tyrosine residues in FAK and full activation of both proteins. The FAK-Src complex further phosphorylates various adaptor proteins, affecting a number of downstream signalling cascades [76].

Phosphatidylinositol 3-kinase (PI3K)

Phosphatidylinositol 3-kinases, also known as phosphoinositide 3-kinases, are a family of enzymes that phosphorylate inositol lipids at the 3' position of the inositol ring to generate the 3-phosphoinositides PI(3)P, PI(3,4) P2 and PI(3,4,5) P3 [77]. The resulting phosphoinositides act as second messengers in signal transduction cascades controlling cellular activities such as proliferation, differentiation, chemotaxis, survival, trafficking, and glucose homeostasis. PI3Ks therefore play a central role in many processes in the cell, and deregulated PI3K signalling is implicated in diseases such as cancer and diabetes [78].

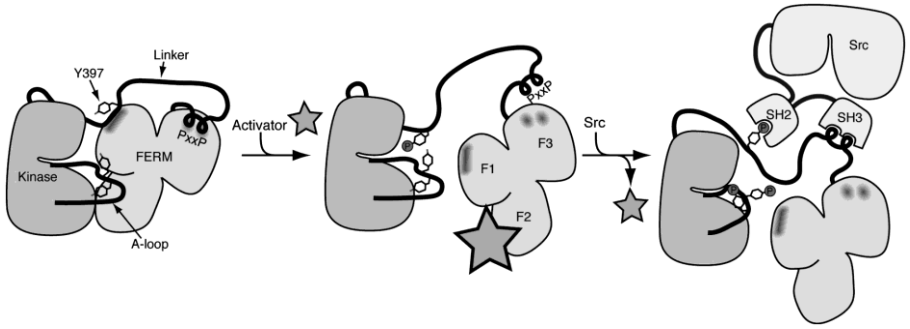

Figure 1.6. Model of activation of FAK and interaction with Src. In the inactive state the FERM domain blocks the access to the kinase domain active site, while sequestering the PxxP and Y397 regions in the FERM-kinase linker. In this model binding of a partner protein to the FERM domain is proposed to be the first step in FAK activation, freeing the kinase domain to autophosphorylate Y397 in cis or in trans. Src recruitment occurs via binding of the SH2 domain to the phosphorylated Y397 and binding of the SH3 domain to the proline-rich region. Phosphorylation of tyrosines Y576 and Y577 in the FAK activation loop by Src leads to full activation of FAK and prevents inhibition by the FERM domain. From Ref. [79] copyright (2007), with permission from Elsevier.

PI3Ks can be divided into different classes depending on their structure and substrate specificity. Class I_A PI3Ks are heterodimers consisting of a catalytic domain with a molecular weight of around 110 kDa (the p110 subunit) and an

adaptor/regulatory subunit known as the p85 subunit, which contains two SH2 domains and one SH3 domain [80]. The SH2 domains bind to phosphotyrosine residues generated by tyrosine kinases, allowing for translocation of PI3K to the membranes where its lipid substrates can be found.

Compared to the SH3 domain of Src, the PI3K p85 subunit SH3 domain contains a 15 aminoacid insertion, and the sequence identity of the two domains is only 21%. Despite these differences, the protein structures are remarkably similar [81;82]. Screening of a combinatorial peptide library for binding to the PI3K p85 SH3 domain lead to the identification of the consensus sequence RXLPPRP [83]. Like the Src SH3 domain the PI3K SH3 domain binds peptides in a left-handed type II polyproline helical conformation [84].

Methods used to study protein complexes

NMR chemical shift perturbation mapping

NMR is a powerful technique for mapping the binding site of a protein upon complex formation with another protein or a ligand [85;86]. In chemical shift perturbation mapping a two-dimensional NMR spectrum such as a [^{15}N,^{1}H]-HSQC spectrum is normally recorded of the free protein, which needs to be ^{15}N-labelled. In the spectrum each peak corresponds to an amide group in the protein, such as the protein backbone amides for all amino acid residues except prolines. N-H groups in sidechains of asparagine, glutamine, histidine and tryptophan residues may also give rise to crosspeaks. After addition of an unlabelled binding partner to the ^{15}N-labelled protein another NMR spectrum is recorded. Nuclei situated at the binding interface may experience a change in their chemical environment upon binding. The chemical shifts in both the nitrogen and proton dimensions are sensitive to this change and the position of the resonance in the spectrum will change. The average

chemical shift perturbation in the nitrogen and proton dimensions can be calculated for each residue using Eq. 1, where $\Delta\delta^{N}{}_{binding}$ and $\Delta\delta^{H}{}_{binding}$ are the chemical shift perturbations of the amide nitrogen and amide proton, respectively.

$$\Delta\delta_{avg} = \sqrt{\frac{(\Delta\delta^{N}_{binding}/5)^2 + (\Delta\delta^{H}_{binding})^2}{2}} \quad (1)$$

By mapping the chemical shift changes onto the protein structure information can be obtained about the binding interface. If the binding induces structural or conformational changes in the protein, chemical shift perturbations can also be seen for residues situated away from the binding site.

In order to determine the binding constant the unlabelled binding partner is titrated into the ^{15}N-labelled protein and a 2D NMR spectrum is recorded at each titration point. The chemical shift perturbations caused by binding can be followed if the chemical exchange rate is large compared to the chemical shift difference between the free and bound forms, measured in radians per second. From the chemical shift perturbations during the titration the binding constant can be determined. The use of deuterated ^{15}N-labelled protein together with TROSY experiments extends the limit of the method to protein complexes of a molecular weight above 100 kDa [87].

Paramagnetic relaxation enhancement NMR

Paramagnetic relaxation enhancement (PRE) NMR is a technique that can be used to determine the structure and dynamics of protein complexes. It is based on the fact that magnetic dipolar interactions between the spins of a nucleus and the unpaired electrons of a paramagnetic centre lead to an increase in the relaxation rate of the nuclear magnetization [88]. The PRE effect is proportional to r^{-6}, where

r is the distance between the unpaired electron and the nucleus. Some metalloproteins contain intrinsic paramagnetic centres, to other proteins a paramagnetic probe can be attached through site-specific labelling. The relaxation rates of the nuclei in the other protein are then measured, and an increase in the relaxation rate indicates that the nucleus has been in the vicinity of the probe. The larger the relaxation effect, the closer that part of the unlabelled protein came to the probe on the other protein. The paramagnetic contribution to the transverse relaxation rate, $R_{2,para}$, can be determined for the amide proton of each aminoacid residue in the protein. This can subsequently be converted into a distance between the paramagnetic centre and the amide proton using Eq. 2:

$$r = \sqrt[6]{\frac{\gamma^2 g^2 \beta^2 \tau_c}{20 R_{2,para}} \left(4 + \frac{3}{1 + \omega_h^2 \tau_c^2} \right)} \qquad (2)$$

where r is the distance between the paramagnetic centre and a given amide proton, τ_c is the correlation time of the dipolar interaction of the electron and the nucleus, ω_h is the proton Larmor frequency, γ is the proton gyromagnetic ratio, g is the electronic g-factor and β is the Bohr magneton. Because of the large magnetic moment of the unpaired electron the PRE effects are large and can provide long-range distance restraints of up to 35 Å [89]. The distance restraints can be used in docking calculations to determine the relative orientation of the macromolecules in the complex. The strong distance-dependence of the PRE enables the detection of protein complex orientations that are populated only a small fraction of the time. This has been exploited to study encounter complexes involved in protein-nucleic acid and protein-protein interactions [90-94].

Isothermal titration calorimetry

Isothermal titration calorimetry (ITC) is a method that is suitable for studying both low-affinity and high-affinity macromolecular interactions. In an ITC experiment a macromolecule is placed in a sample cell, a ligand is injected in a programmed sequence of steps, and the tiny amounts of heat associated with the non-covalent interactions involved in binding are measured. From this, the affinity, the change in enthalpy and the stoichiometry of binding can be estimated and the change in entropy can be calculated, providing a complete thermodynamic characterization of the interaction [95;96].

Scope and outline of thesis

In order to learn more about how protein tyrosine kinases function, it is important not to focus on the kinase domain alone, but also on the interaction with other domains. The main topic of this thesis is the interaction of Src and FAK, mediated via the SH2 and SH3 domains of Src, and the goal is to outline the details of this interaction. To this end, a number of model systems of the FAK-Src interaction are studied, ranging from peptide-protein interaction studies to binding studies involving isolated protein domains. In addition, the interaction of a PI3K SH3 domain with a photocleavable peptide is investigated.

In chapter 2, the interaction of peptides derived from the SH3 domain binding site in FAK with the Src SH3 domain is studied, using paramagnetic relaxation enhancement nuclear magnetic resonance spectroscopy (PRE NMR) together with chemical shift perturbation analysis. In chapter 3, the binding of peptides from the SH2 domain binding site of FAK to the Src SH2 domain are studied using (PRE) NMR and isothermal titration calorimetry (ITC). Chapter 4 contains a study of peptides containing both SH2 domain- and SH3 domain-binding sites interacting

with a Src SH3-SH2 domain fragment, and the effect of decreasing the distance between the binding sites in the peptide is investigated using NMR and ITC. In chapter 5, the expression of the catalytic domain of FAK in insect cells is described, together with the purification and characterization of the protein. In chapter 6, an NMR binding study of the FAK catalytic domain with the Src SH2 domain is presented. In chapter 7, the construction of GFP-labelled SH3 or SH2 domain-containing phosphotyrosine reporter constructs is described, and the behaviour of the constructs in mammalian cells is characterized. In chapter 8, the interaction of the SH3 domain of the p85 subunit of PI3K with a photocleavable peptide is studied, investigating what effect modifying the peptide has on the interaction. Finally, chapter 9 contains a general discussion of the results presented in the previous chapters.

Chapter 2

Mobility of TOAC spin-labelled peptides binding to the Src SH3 domain studied by paramagnetic NMR

Abstract

Paramagnetic relaxation enhancement provides a tool for studying the dynamics as well as the structure of macromolecular complexes. The application of side-chain coupled spin-labels is limited by the mobility of the free radical. The cyclic, rigid amino acid spin-label TOAC (2,2,6,6-Tetramethylpiperidine-1-oxyl-4-amino-4-carboxylic acid), which can be incorporated straightforwardly by peptide synthesis, provides an attractive alternative. In this study, TOAC was incorporated into a peptide derived from focal adhesion kinase (FAK), and the interaction of the peptide with the Src homology 3 (SH3) domain of Src kinase was studied, using paramagnetic NMR. Placing TOAC within the binding motif of the peptide has a considerable effect on the peptide-protein binding, lowering the affinity substantially. When the TOAC is positioned just outside the binding motif the binding constant remains nearly unaffected. Although the SH3 domain binds weakly and transiently to proline-rich peptides from FAK, the interaction is not very dynamic and the relative position of the spin-label to the protein is well-defined. It is concluded that TOAC can be used to generate reliable paramagnetic NMR restraints.

This chapter is based on:

Lindfors, H.E., de Koning, P.E., Drijfhout, J.W., Venezia, B. and Ubbink, M. (2008). Mobility of TOAC spin-labelled peptides binding to the Src SH3 domain studied by paramagnetic NMR. *J. Biomol. NMR* **41**, 157-167.

Introduction

In recent years, paramagnetic relaxation enhancement (PRE) NMR spectroscopy has become a useful tool for studying the structure and dynamics of macromolecular complexes [97-110]. PREs are caused by the magnetic dipolar interaction of a nucleus with the unpaired electron in a paramagnetic centre, leading to an increased relaxation of the nuclear magnetization and a decreased intensity of the corresponding NMR peak. The magnitude of the PRE depends on the distance between the observed nucleus and the paramagnetic centre. Thus, PREs can provide information about the distance between the amino acid residues in one protein and a paramagnetic group in another protein, which can be used to determine the structure of the complex. The non-linear distance dependence of the PREs also makes it possible to detect the presence of alternative protein conformations, even if the proteins only spend a small fraction of the time in the minor state [90;100;111].

A common approach in paramagnetic NMR is to use site-directed spin labelling, in which a spin label is attached to a cysteine residue engineered onto the protein surface. Commonly used spin labels include nitroxide spin labels [100;112-116] or metal-chelating spin labels [117;118]. A disadvantage of these spin labels is their high mobility due to the conformational freedom of the cysteine side chain and the linker of the spin label. This causes the position of the spin label to be ill-defined and leads to averaging of paramagnetic effects. The mobility of the spin-label can be limited by attaching it to the protein via two arms, making it possible to model the position of the paramagnetic centre relative to the protein within a few Å [119;120].

For the study of peptide-protein interactions, labelling with 2,2,6,6-tetramethylpiperidine-1-oxyl-4-amino-4-carboxylic acid (TOAC, Fig. 2.1) provides an alternative. TOAC is an amino acid with a stable nitroxide radical and a reduced

mobility, due to its rigid structure. It can be incorporated directly into peptides via solid-phase synthesis [121-123] and recent advances in chemical protein synthesis [124] may also enable the incorporation of TOAC into proteins for paramagnetic NMR protein interaction studies. TOAC-containing peptides have been used extensively for EPR studies [125-138]. Despite the wide-spread use of TOAC for EPR, to our knowledge it has not been employed for structural studies using paramagnetic NMR. Here, we use PRE NMR spectroscopy to study the structure and dynamics of TOAC-labelled peptides binding to the Src homology 3 (SH3) domain of Src kinase. SH3 domains are ubiquitous interaction domains involved in a vast number of signal transduction pathways. These modular domains generally recognize and bind to proline-rich regions that can form polyproline type II helices, with a core motif of the form PxxP [15]. The Src SH3 domain has been shown to bind to peptides derived from a region in focal adhesion kinase (FAK) with a sequence RALPSIPKL [139]. Using TOAC-labelled peptides derived from this region of FAK, we find that although the peptide-protein interaction is of a weak and transient kind, the peptides bind in a well-defined position relative to the protein.

Experimental Procedures

Cloning and protein expression

A DNA fragment coding for the mouse Src SH3 domain, residues 85-142, was amplified by PCR from the full-length Src plasmid pUSE Src wt (kindly provided by Prof. B. van de Water), and ligated into pET28a, using the NcoI and XhoI restriction sites. The resulting construct was verified by DNA sequencing. The ^{15}N-labelled, His-tagged SH3 domain was produced in *Escherichia coli* BL21 incubated in M9 minimal medium with $^{15}NH_4Cl$ as the sole nitrogen source. A freshly transformed *E.coli* BL21 colony was used to inoculate 10 ml

LB/kanamycin (50 g/L) and incubated overnight at 37 °C and 250 rpm. The preculture was diluted 1:100 into the ^{15}N-minimal medium and incubated to an OD_{600} of 0.6, at which point gene expression was induced by the addition of 0.5 mM isopropyl β-D-1-thiogalactopyranoside. After 4 h the cells were harvested by centrifugation.

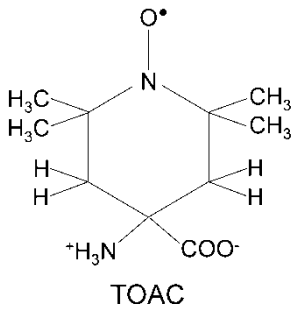

Figure 2.1. Structure of the nitroxide radical-containing amino acid 2,2,6,6-Tetramethylpiperidine-1-oxyl-4-amino-4-carboxylic acid (TOAC).

Protein purification and NMR sample preparation

The cell pellet was resuspended in lysis buffer (20 mM Tris-HCl, pH 8, 0.5 M NaCl, 10 mM imidazole and 1 mM phenylmethanesulfonyl fluoride) and cells were lysed by two passages through a French pressure cell. The cell lysate was centrifuged at 40000 rpm for 30 minutes, the supernatant was loaded onto an affinity column (HisTrap HP, GE Healthcare) and protein was eluted with a gradient of 10-300 mM imidazole. Pure fractions, as judged by SDS-PAGE, were pooled, concentrated and exchanged into NMR buffer (20 mM KPi, pH 6.5, 100 mM NaCl). All NMR experiments were performed in this buffer. The purity of the protein was estimated to be above 95 %. The protein concentration was determined using a theoretical extinction coefficient at 280 nm of 16960 $M^{-1}cm^{-1}$ [140].

Peptide synthesis and preparation

Synthetic peptides were prepared by normal Fmoc-chemistry using preloaded Tentagel resins, PyBop/NMM for in situ activation and 20% piperidine in NMP for Fmoc removal [141]. Couplings were performed for 75 min. The amino acid N-terminally of TOAC was coupled overnight at 37°C using HATU/NMM activation. After final Fmoc removal peptides were cleaved with TFA/H_2O 19/1 containing additional scavengers when a cysteine or a tryptophan was present in the peptide sequence and isolated by ether/pentane precipitation. The peptides were treated 3 h with 10% ammonia, lyophilized and stored at −20°C until use. Peptides were checked on purity using rpHPLC and on integrity using MALDI-TOF mass spectrometry. Fmoc-TOAC-OH was prepared as has been described before [121]. Peptides were kindly provided by Dr. Jan Wouter Drijfhout.

Before the NMR titrations peptides were dissolved in NMR buffer and the pH was adjusted to 6.5 with small aliquots of 0.1-0.5 M solutions of NaOH or HCl. The fraction of paramagnetic peptide was checked by EPR and found to be 53% for peptide P3Tm and 30% for peptide P3Te. Francesco Scarpelli is gratefully acknowledged for help with EPR measurements.

NMR experiments

All NMR experiments were recorded at 303 K on a Bruker DMX600 spectrometer equipped with a TCI-Z-GRAD cryoprobe (Bruker, Karlsruhe, Germany). The data were processed with Azara (ftp://www.bio.cam.ac.uk/pub/azara/) and analyzed using Ansig For Windows [142;143]. For amide backbone resonance assignments 3D NOESY-HSQC and 3D TOCSY-HSQC spectra were recorded on a 1 mM ^{15}N SH3 sample containing 6% D_2O. The protein was assigned with the help of assignments for chicken Src SH3-SH2 domains [144].

Titrations were performed by adding microliter aliquots of concentrated peptide stock solution to 500 µl of ^{15}N SH3 with an initial concentration of 0.2 mM. Two-dimensional ^{15}N-^{1}H HSQC spectra were recorded before addition of peptide and at each titration point. The chemical shift perturbations for the amide ^{15}N nuclei were plotted against the molar ratio of peptide to protein. The data were analysed using a non-linear least squares fit to a one-site binding model (Equation 1) [145] with the programme Origin (OriginLab corporation, Northampton, MA).

$$\Delta\delta_{binding} = \frac{1}{2}\Delta\delta_{\infty}(A - \sqrt{A^2 - 4R/C}) \quad (1)$$

$$A = 1 + R/C + \frac{LR/C + U}{LUK_a}$$

In Eq.1, R is the molar ratio of peptide to protein, $\Delta\delta_{binding}$ is the chemical shift perturbation at a given ratio of peptide to protein, $\Delta\delta_{\infty}$ is the chemical shift perturbation at 100% bound protein, L is the initial concentration of ^{15}N-labelled protein, U is the concentration of the peptide stock solution, K_a is the association constant of the complex and C is a parameter introduced to correct for any error in R, e.g. caused by the use of a theoretical extinction coefficient for the protein. R and $\Delta\delta_{binding}$ are the independent and dependent variables, respectively, and $\Delta\delta_{\infty}$, C and K_a are the fitted parameters.

The averaged amide chemical shift perturbations were calculated according to Eq.2:

$$\Delta\delta_{avg} = \sqrt{\frac{(\Delta\delta^{N}_{binding}/5)^2 + (\Delta\delta^{H}_{binding})^2}{2}} \quad (2)$$

where $\Delta\delta^{N}_{binding}$ and $\Delta\delta^{H}_{binding}$ are the chemical shift perturbations of the amide nitrogen and amide proton, respectively.

Distance restraints

After activation of the nitroxide spin label, peptides were titrated into ^{15}N-labelled Src SH3 domain, and HSQC spectra were recorded with peptide P3 as a diamagnetic control to obtain experimental distance restraints for subsequent docking calculations [114]. To correct for any differences in concentration between the paramagnetic and control samples, the peak intensities of all residues were normalized internally against a residue unaffected by peptide binding. For all residues, the ratio between paramagnetic peak intensity (I_{para}) and diamagnetic peak intensity (I_{dia}), measured by the peak heights, was calculated. The residues were divided into three classes: residues that disappeared in the paramagnetic spectrum, visible residues with an intensity ratio of less than 0.85 and residues with an intensity ratio above 0.90. $R_{2,dia}$, the transverse relaxation rate of a resonance in the diamagnetic sample, was determined from the peaks after processing with a 2 Hz line-broadening exponential window function. The linewidth at half maximum, $\Delta\upsilon_{1/2}$, was extracted from a Lorentzian peak fit using the software MestRe-C [146]. After correction for the artificial line-broadening the $R_{2,dia}$ was obtained according to Eq. 3:

$$R_{2,dia} = \pi\Delta\nu_{1/2} \tag{3}$$

The paramagnetic contribution to the transverse relaxation rate, $R_{2,para}$, was calculated from Eq. 4 [114], where I_{para} and I_{dia} is the peak intensity in the paramagnetic and diamagnetic experiment, respectively, and t is the total INEPT evolution time of the HSQC.

$$\frac{I_{para}}{I_{dia}} = \frac{R_{2,dia}\exp(-tR_{2,para})}{R_{2,dia} + R_{2,para}} \tag{4}$$

The $R_{2,para}$ values were converted into distances between the amide and the spin label, using Eq. 5:

$$r = \sqrt[6]{\frac{\gamma^2 g^2 \beta^2 f_p f_b}{20 R_{2,para}} \left(4\tau_c + \frac{3\tau_c}{1+\omega_h^2 \tau_c^2} \right)} \quad (5)$$

where r is the distance between the unpaired electron of TOAC and a given amide proton of SH3, τ_c is the correlation time of the dipolar interaction of the electron and the nucleus, ω_h is the proton Larmor frequency, γ is the proton gyromagnetic ratio, g is the electronic g-factor and β is the Bohr magneton, f_p is the fraction of peptide that was paramagnetic and f_b is the fraction of protein that was bound to peptide in the experiment. The fraction of protein bound was determined using the titration data, for P3Te it was estimated to 80% and for P3Tm to 44% at the concentrations used. Assuming no internal mobility of the spin label, the correlation time τ_c is defined as $(\tau_r^{-1} + \tau_s^{-1})^{-1}$, where τ_r is the rotational correlation time of the protein-peptide complex and τ_s is the effective electron relaxation time. In the case of organic nitroxide radicals the electronic relaxation times are long and the correlation time is therefore dominated by the rotational correlation. The rotational correlation time of the protein-peptide complex was estimated to 5 ns, using the software hydroNMR [147] and a structure of chicken Src SH3 bound to a similar peptide, PDB Entry 1RLQ [39].

For residues broadened beyond detection in the paramagnetic spectrum the maximum intensity ratio was estimated from the noise level and converted into an upper distance restraint (class 1). Residues with an intensity ratio between 0 and 0.85 were given both upper and lower distance restraints (class 2). For residues with an intensity ratio above 0.9, a common lower distance restraint was estimated, using a $R_{2,dia}$ value representative of the spectrum and an intensity ratio set to 0.90 (class 3). The calculated distances using this $R_{2,dia}$ will differ slightly from the distance calculated using an individual $R_{2,dia}$ value for each residue, but the differences are within the margins used in the docking calculations and it is

therefore not necessary to use a separate $R_{2,dia}$ for each residue in this class. Intensity ratios between 0.85 and 0.90 were not used to generate restraints.

Docking calculations

The PDB file 1RLQ [39], containing a structure of chicken Src SH3 bound to a proline-rich peptide, was modified by mutating residue T125 (chicken Src numbering, corresponding to residue 127 in mouse Src) to S *in silico*, in accordance with the mouse Src SH3 sequence. Random starting positions were generated for the TOAC oxygen atom, and rigid-body docking calculations were performed in Xplor-NIH [148]. Only one energy term, corresponding to the distance restraints, was used. Restraint files can be found in Appendix A.

For the solutions obtained in the docking calculations, Q-factors [97;149] were calculated according to:

$$Q = \sqrt{\frac{\sum_i (r_{calculated,i} - r_{observed,i})^2}{\sum_i r_{observed,i}^2}} \qquad (6)$$

where $r_{observed,i}$ is the distance from the TOAC oxygen atom to the amide proton of residue i derived from the PRE NMR data, and $r_{calculated,i}$ is the spin-label to amide distance for residue i in the docked structure.

All molecular graphics in this work were rendered with PyMol [150].

Results and discussion

To study the interaction of the Src SH3 domain with FAK peptides, three peptides were synthesized: one unlabelled control peptide, P3, with the sequence RALPSIPKL, and two peptides containing a TOAC residue either at one end of the sequence or within the binding motif. The peptide with TOAC within the core binding motif has the sequence RALP-TOAC-IPKL and is referred to as P3Tm, the peptide with TOAC at the end is referred to as P3Te, with the sequence TOAC-RALPSIPKL. All peptides contained acetylated and amidated N- and C-termini, respectively.

Titrations with non-paramagnetic peptides

Upon titration of peptide P3 into ^{15}N-labelled Src SH3 domain, chemical shift perturbations were observed for some backbone amides. Broadening of NMR peaks for residues with large shift changes indicated that the resonances of free and bound SH3 were in intermediate to fast exchange on the NMR timescale. From the binding curves (Fig. 2.2) a K_d of 56 ± 11 μM was determined.

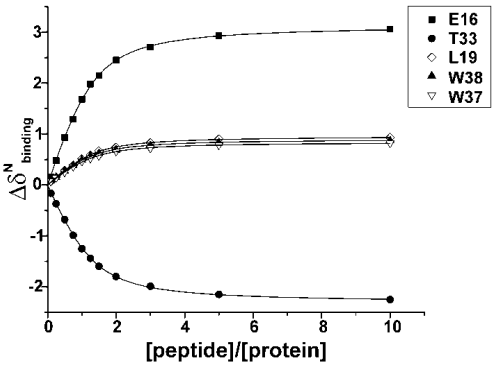

Figure 2.2. ^{15}N Chemical shift perturbations of SH3 resonances upon titration with peptide P3. The curves represent the best global fit to a 1:1 binding model with a K_d of 56 ± 11 μM.

Titration of non-activated peptide P3Te produced very similar chemical shift perturbations (Fig. 2.3) and a K_d of 95 ± 15 μM. This indicates that placing TOAC at the end of the peptide influences the binding of the peptide to the SH3 domain to some extent, although the effect is limited. For peptide P3Tm, which contains a TOAC residue within the binding motif, the observed chemical shift changes are much smaller than for peptides P3 and P3Te at the same ratio of peptide to protein (Fig. 2.3). Fitting of the data to a 1:1 binding model yields a dissociation constant of 0.9 ± 0.1 mM, a 16-fold weaker binding.

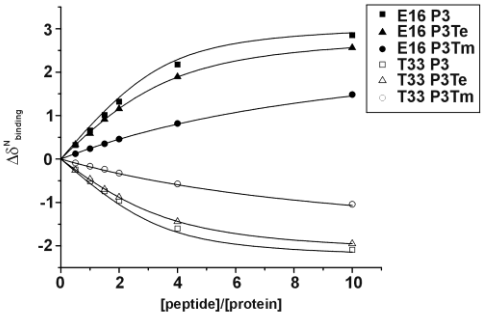

Figure 2.3. Comparison of ^{15}N chemical shift perturbations of two SH3 resonances upon peptide titration. Filled symbols: Residue E16. Open symbols: Residue T33. Squares: Peptide P3, Triangles: Peptide P3Te, Circles: Peptide P3Tm.

The TOAC in P3Tm is within the binding motif, but in a position where it is expected to point outward and not directly make contact with the protein. Pairs of TOAC residues have been shown to promote helical content in short peptides [151], however, no direct spectroscopic evidence exists that a single TOAC residue causes any changes in secondary structure of peptides [134]. For comparison, the average chemical shift perturbations were calculated and extrapolated to 100% bound protein for all three peptides (Fig. 2.4). The binding maps show very similar patterns (Fig. 2.5), indicating that the peptides bind in a similar conformation.

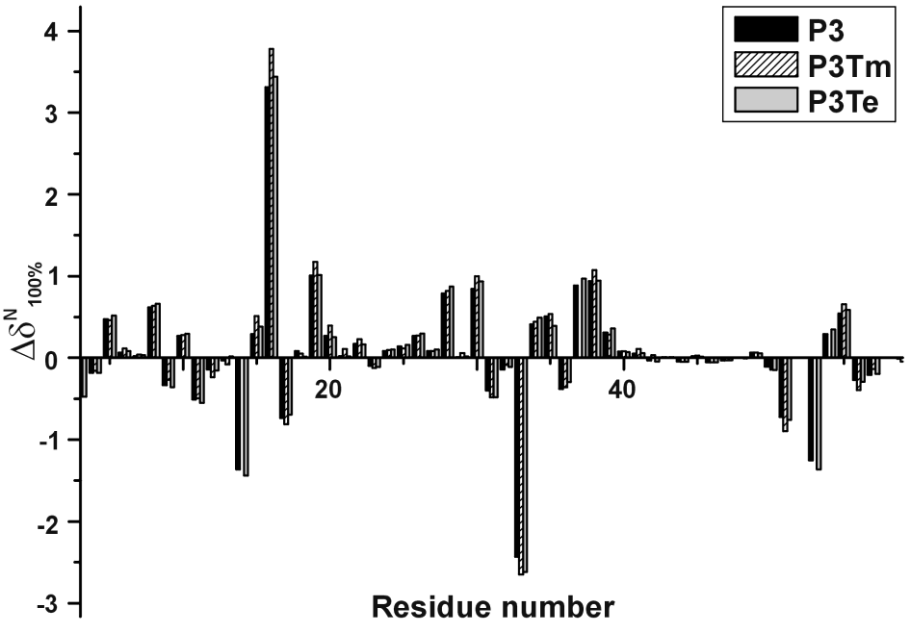

Figure 2.4. Extrapolation of ^{15}N Chemical shift perturbations to infinite peptide:protein ratio for SH3 resonances in the complex of SH3 with peptides P3, P3Te and P3Tm, respectively. Missing resonances in SH3-P3Tm were exchange-broadened beyond detection at the point of extrapolation.

Paramagnetic peptide experiments and docking calculations

After deprotonation of the TOAC nitroxide, peptides were added to ^{15}N-labelled Src SH3 domain, causing a decrease in intensity for some residues (Fig. 2.6).

Distance restraints were calculated from the NMR data and used in docking calculations. For peptide P3Tm multiple rigid-body docking runs with random starting positions for the TOAC nitroxide oxygen atom consistently produced a single low-energy solution (Fig. 2.7A). Analysis of the solution shows that virtually all restraints are satisfied and that the position of the spin-label is well-defined (Fig. 2.7B). Any violations observed can be explained by small movements of residues situated in more flexible regions of the protein. To measure the

agreement between the observed and calculated distances a Q-factor was calculated for the double-bounded restraints (see Experimental Procedures). For peptide P3Tm the Q-factor was 0.08 with a correlation coefficient of 0.96 (Fig. 2.7C). The calculated position of the spin-label is reasonable as judged from comparison with a structure of chicken Src SH3 domain in complex with a similar peptide (Fig. 2.7D). It should be noted that the introduction of the TOAC can have distorted the peptide, given the large reduction in the affinity.

Although the error margins used for the distance restraints are very narrow (Fig 2.7B), almost all restraints are satisfied. To investigate what effect random error in the observed intensity ratios has on the calculations, the observed ratios for P3Tm were randomly varied between −20% and +20% for all residues with both upper and lower distance restraints (class 2). In this way 30 datasets were generated. For two residues the intensity ratios sometimes exceeded 0.9, in those cases the ratio was set to 0.9. New $R_{2,para}$ values were calculated for the 30 data sets, generating new distance restraints. Docking calculations were performed for each set of randomized distance restraints, yielding a cluster of solutions (Fig. 2.8A). Analysis of the solutions shows that the variation in target distance and calculated position due to variation in intensity ratios is small (Fig. 2.8B). An average root mean square deviation (RMSD) from the mean position of 0.7 Å was calculated, with a standard deviation of 0.3 Å, suggesting that any error contributions caused by uncertainty in the determined intensity ratios are likely to be small. Other contributions to the error come from the use of an overall correlation time for all residues, as well as any errors in the estimated fraction bound protein and fraction of peptides containing a radical.

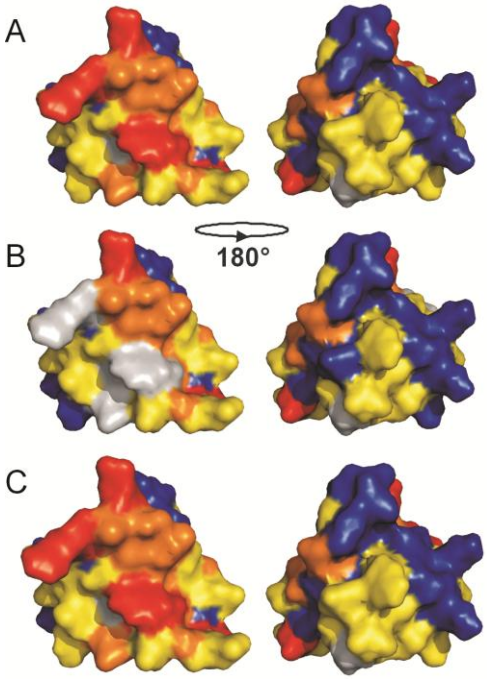

Figure 2.5. Chemical shift perturbations upon titration with peptides P3 **(A)**, P3Tm **(B)** and P3Te **(C)**, mapped onto the surface of Src SH3 domain (PDB entry 1RLQ [39]). Shift changes were extrapolated to 100% bound protein and SH3 residues were coloured according to the size of the average chemical shift perturbation, $\Delta\delta_{avg}$. Red: $\Delta\delta_{avg} \geq 0.3$ ppm; orange: $0.3 > \Delta\delta_{avg} \geq 0.1$ ppm; yellow: $0.1 > \Delta\delta_{avg} \geq 0.04$ ppm; blue: $\Delta\delta_{avg} < 0.04$ ppm. Shown in grey are residues that could not be assigned (proline residues or residues that were exchange-broadened beyond detection at the point of extrapolation).

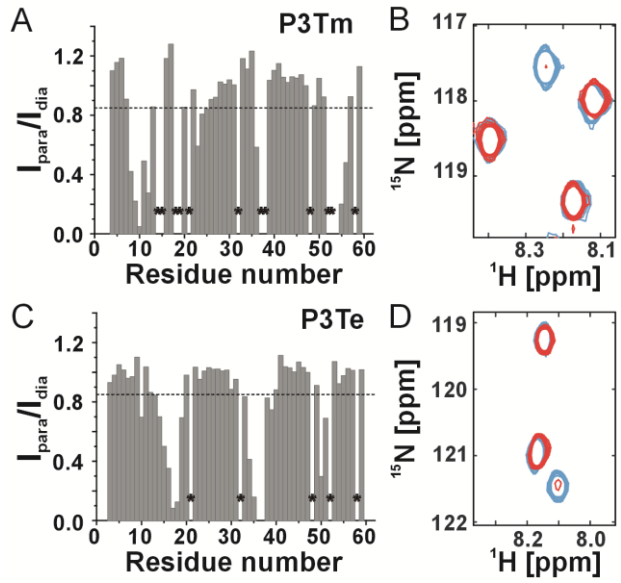

Figure 2.6. A) and **C)**: Intensity ratios of backbone amide SH3 resonances in complex with paramagnetic peptide P3Tm (A) / P3Te (C) and control peptide P3. The dashed horizontal line represents an intensity ratio of 0.85, residues with intensity ratios below this are considered to be affected by TOAC. The asterisks indicate residues for which no intensity ratio data were available. **B)** and **D)**: Detail from the spectrum of SH3 in complex with peptide P3Tm (B) / P3Te (D) in red, overlaid with the spectrum of SH3 with P3 in blue.

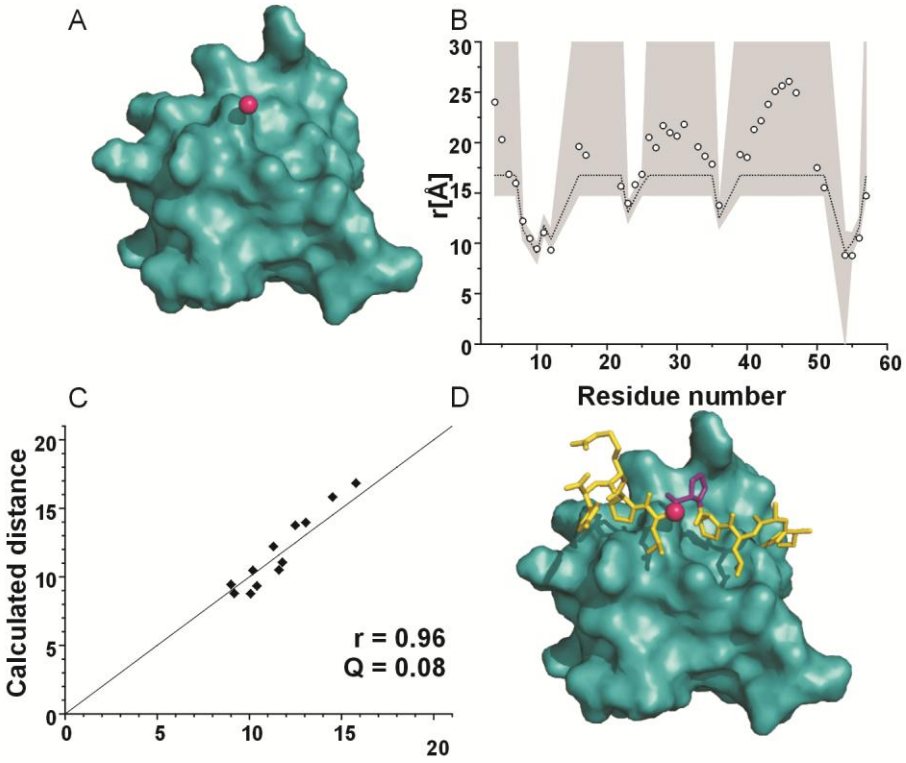

Figure 2.7. A) Calculated position of TOAC oxygen atom, shown as pink sphere, in complex between peptide P3Tm and SH3 (shown in green). **B)** Violations analysis of calculated position of TOAC in P3Tm in complex with SH3. Dotted line: PRE-derived distance; white circles: distance in calculated structure; shaded area: error margins used in calculations. For class 1 residues (upper bound only) the error margin was +2Å, for class 3 residues (lower bound only) a −2Å error margin was used, and for class 2 residues (both upper and lower distance restraints) the error margins were ±1 Å. **C)** Distance from TOAC oxygen atom to backbone amide proton for class 2 residues: distance obtained in rigid-body docking calculations versus PRE-derived distance. **D)** Same as a), overlaid with structure of SH3 in complex with peptide RALPPLPRY, shown in yellow (PDB entry 1RLQ [39]). In purple is shown the residue in peptide RALPPLPRY that corresponds most closely to the position of TOAC in peptide P3Tm.

A consideration for single time-point measurements is that the magnetization recovery levels will differ between the paramagnetic samples and the diamagnetic control, owing to the PRE on the longitudinal relaxation rate [152]. The higher

recovery levels for the paramagnetic sample can lead to a systematic underestimation of the PRE effects, resulting in overestimated distances from the spin-label to the protein. This effect does not seem to be very pronounced in our system, given that the calculated position for the TOAC nitroxide is already close to the protein surface.

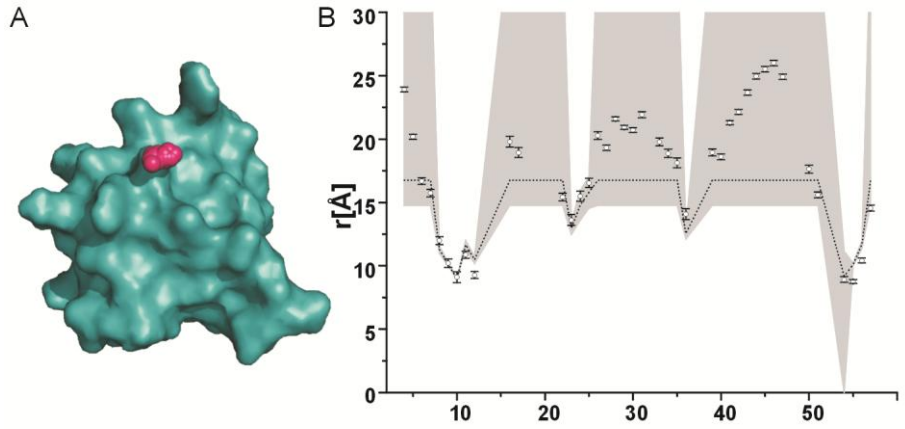

Figure 2.8. A) Influence of variation in intensity ratio on calculated spin-label position. Shown as pink spheres are the resulting TOAC oxygen atom positions for 30 data sets, for which I_{para}/I_{dia} for the class 2 residues has been randomly varied by ±20%. The calculated TOAC positions have an average RMSD from the mean of 0.7 Å, with a standard deviation of 0.3 Å. **B)** combined violation analysis of the 30 "randomized" datasets. Dotted line: mean of the PRE derived distance for the 30 data sets. White circles: Mean of calculated distance from TOAC oxygen atom to backbone amide proton for the 30 data sets, error bars: ± one standard deviation. Shaded area: For class 1 and class 3 residues: error margins used in the calculations, +2Å and −2Å, respectively. For class 2 residues: ± one standard deviation from the PRE derived distance.

Rigid-body docking calculations for the position of TOAC in the complex of SH3 and peptide P3Te also yields a single, reproducible solution (Fig. 2.9A). Analysis of the solution, however, shows violations for several residues (Fig. 2.9B). A Q-factor of 0.17 was calculated together with a correlation coefficient of merely 0.62 (Fig. 2.9C). Closer inspection of the data shows that the poor fit is largely due to one residue, D10 (corresponding to residue D93 in full-length mouse Src). This

residue has an intensity ratio of 0.70, but is located far from the rest of the residues that exhibit an effect from the spin-label, and pulls the calculated final position of the spin-label away from the other residues. Excluding this outlier from the docking calculations changes the final position of the TOAC oxygen atom, the TOAC is now positioned further away from the centre of the peptide in a more realistic position (Fig. 2.10A). This improves the fit, with a new Q-factor of 0.13 and a correlation coefficient of 0.81 (Fig. 2.10B, C). There are still regions where the observed PRE effect is slightly larger than expected from the calculated structure. This is typically seen in systems where dynamics is present [100] and can be accounted for by small movements of the spin-label placed at one end of the peptide, where the flexibility is higher. The effect felt by residue D10 cannot be explained by small peptide movements around the binding site. It is, however, possible to account for this effect by a small percentage of peptide binding in an alternative orientation.

Conclusions

By using TOAC it was demonstrated that the interaction between the Src SH3 domain and a proline-rich peptide derived from FAK is not very dynamic, and the position of the peptide relative to the protein is remarkably well-defined, despite the weak and transient binding. For studies of peptide-protein interactions, paramagnetic NMR with TOAC spin-labelled peptides provides a way to gain information about

the dynamics as well as the structure of the complex. The rigid structure of TOAC makes it an attractive alternative to spin-labelling via cysteine residues, although the introduction of a TOAC residue in a peptide may have a large influence on the binding affinity when introduced in the core of the recognition motif. With the advancements in chemical synthesis of partial or even entire proteins, the

application of TOAC in studies of interactions of proteins with small molecules, nucleic acids or other proteins will be feasible.

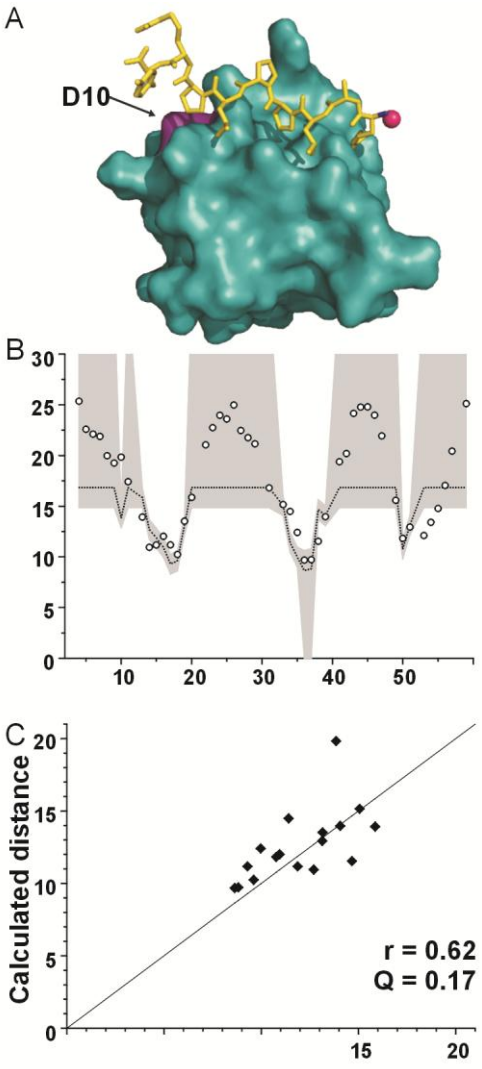

Figure 2.9. A) Calculated position of TOAC oxygen atom, shown as pink sphere, in complex between peptide P3Te and SH3 (in green, residue D10 is shown in purple). Overlaid with structure of SH3 in complex with peptide RALPPLPRY, shown in yellow. (PDB entry 1RLQ [39]). The N-terminus of the peptide, coloured blue, corresponds to the place of attachment of the TOAC amino acid in peptide P3Te. **B)** Violations analysis of calculated position of TOAC in P3Te in complex with SH3. Dotted line: PRE-derived distance; white circles: distance in calculated structure; shaded area: error margins used in calculations. For class 1 residues (upper bound only) the error margin was +2Å, for class 3 residues (lower bound only) a −2Å error margin was used, and for class 2 residues (both upper and lower distance restraints) the error margins were ±1 Å. **C)** Distance from TOAC oxygen atom to backbone amide proton for residues with both upper and lower distance restraints (class 2): distance obtained in rigid-body docking calculations versus PRE-derived distance.

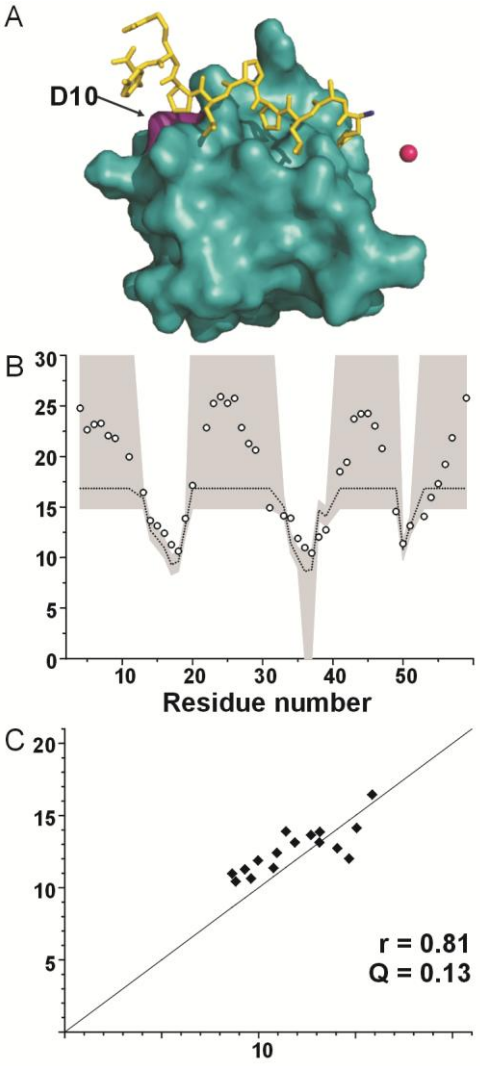

Figure 2.10. A) Calculated position of TOAC oxygen atom, shown as pink sphere, in complex between peptide P3Te and SH3 (in green, residue D10 is shown in purple), after excluding residue D10 from the calculations. Overlaid with structure of SH3 in complex with peptide RALPPLPRY, shown in yellow (PDB entry 1RLQ [39]). The N-terminus of the peptide, coloured blue, corresponds to the place of attachment of the TOAC amino acid in peptide P3Te. **B)** Violations analysis of calculated position of TOAC in P3Te in complex with SH3, after excluding residue D10 from the calculations. Dotted line: PRE-derived distance; white circles: distance in calculated structure; shaded area: error margins used in calculations. For class 1 residues (upper bound only) the error margin was +2Å, for class 3 residues (lower bound only) a −2Å error margin was used, and for class 2 residues (both upper and lower distance restraints) the error margins were ±1 Å. **C)** Distance from TOAC oxygen atom to backbone amide proton for residues with both upper and lower distance restraints (class 2), after exclusion of residue D10 from calculations: distance obtained in rigid-body docking calculations versus PRE-derived distance.

Chapter 3

Dynamics in a high-affinity peptide-SH2 domain complex

Abstract

The interaction between the tyrosine kinases Src and focal adhesion kinase (FAK) is a key step in signalling processes from focal adhesions. The phosphorylated tyrosine residue 397 in FAK is able to bind the Src SH2 domain. To establish the extent of the FAK binding motif, the binding affinity of the SH2 domain for phosphorylated and unphosphorylated FAK-derived peptides of increasing length was determined and compared with that of the internal Src SH2 binding site. It is shown that the FAK peptides have higher affinity than the internal binding site, and that seven negative residues adjacent to the core SH2 binding motif increase the binding constant 30-fold. A rigid spin-label incorporated in the FAK peptides was used to establish on the basis of paramagnetic relaxation enhancement whether the peptide-protein complex is well-defined. The peptide-protein complex exhibits dynamics, despite the high affinity of the peptide. These findings are interpreted in the context of the two step model for complex formation, involving the encounter state as an intermediate in which the proteins form a loose, dynamic complex. The strong electrostatic interaction between the positive side of the SH2 domain and the negative peptide results in a high affinity but may also favour the dynamic encounter state explaining the spread of the paramagnetic effects over the SH2 domain.

This chapter will be published as:

Lindfors, H.E., Drijfhout, J.W., Arendsen, Y. and Ubbink, M (2010). Dynamics in a high-affinity peptide-SH2 domain complex. *Submitted.*

Introduction

Focal adhesion kinase (FAK) and Src kinase are non-receptor protein tyrosine kinases involved in processes such as cell proliferation, cell survival and cell motility. Like many signal transduction proteins FAK and Src are examples of modular proteins, consisting of individually folded protein interaction or catalytic domains separated by linker regions. FAK contains a FERM (erythrocyte band 4.1 ezrin, radixin, moesin homology) domain, a tyrosine kinase domain and a focal adhesion targeting (FAT) domain [153]. whereas Src contains an N-terminal myristoylated membrane targeting region followed by a unique domain, a Src homology 3 (SH3) domain, a Src homology 2 (SH2) domain, a tyrosine kinase domain and a C-terminal regulatory region [154].

SH2 domains, found in many proteins involved in tyrosine kinase signalling, are ~100-amino-acid protein modules that recognize and bind to phosphorylated tyrosine sequences in specific target proteins [155]. Phosphopeptide library studies have shown that the specificity of SH2 domain interactions mainly depends on the three to five residues following the phosphorylated tyrosine [156]. For Src family kinases the SH2 domain consensus sequence is pYEEI [157], of which the phosphotyrosine and the isoleucine are inserted into two binding pockets in the SH2 domain [158]. The Src SH2 domain plays an important role in the regulation of Src activity by binding to a phosphorylated tyrosine, Y527, in the C-terminal tail of Src. Together with interactions between the SH3 domain and the linker connecting the SH2 domain to the kinase domain, this locks the protein into a closed, inactive form [159]. Upon recruitment of FAK by integrins, Y397 in the linker connecting the FERM domain to the kinase domain becomes phosphorylated [160]. The amino acid sequence of this site, YAEI, is close to the Src family SH2 consensus binding motif, and phosphorylation of the tyrosine creates a high-affinity binding site for the Src SH2 domain [139;161-163].

Macromolecular complexes differ not only in binding affinity but also in dynamics, here defined as the motion of one binding partner relative to the other in the complex [100;164-167]. In the two-step model of macromolecular complex formation macromolecules first associate to form a loosely-bound intermediate state known as the encounter state [168] before proceeding to the formation of a well-defined complex. In this model, long-range electrostatic forces serve to bring two randomly diffusing proteins together and help orient them relative to each other [169;170]. This promotes complex formation by a reduced-dimensionality search, where the macromolecules first bind non-specifically and then diffuse along each other [171]. The equilibrium between the encounter state and the well-defined state differs between complexes, some non-physiological electron transfer protein complexes have even been shown to exist mainly as an encounter complex [172]. Dynamics in macromolecular complexes can be studied using paramagnetic relaxation enhancement (PRE) NMR, which has become increasingly popular in recent years [97;100;173]. The strong and highly localized nature of PRE makes it possible to detect lowly populated states in which nuclei in one of the molecules approach the spin-label attached to the other molecule. The spin-labelled amino acid TOAC (2,2,6,6-tetramethylpiperidine-1-oxyl-4-amino-4-carboxylic acid) can be incorporated into peptides via solid-phase synthesis [121;122]. Averaging of the paramagnetic effects caused by motion of the spin-label relative to the peptide can be avoided with TOAC because of its rigid structure. This makes TOAC a useful tool for studying peptide-protein interactions with PRE NMR. Recent PRE NMR studies of the complex of the Src SH3 domain with a TOAC-labelled peptide derived from FAK showed that although the peptide-protein complex is weak, the position of the spin-label relative to the SH3 domain is remarkably well-defined (chapter 2). This indicates that the peptide binds the SH3 domain in a specific manner, rather than the displaying the dynamics that might be expected based on the low-affinity character of the complex. This poses the question whether it is

possible to relate the degree of dynamics in a peptide-protein complex to the binding affinity of the complex.

Here, we have studied the interaction of the Src SH2 domain with phosphorylated and unphosphorylated peptides derived from the C-terminal tail of Src and the Y397 SH2 binding site in FAK, using chemical shift perturbation analysis NMR, PRE NMR and microcalorimetry. First, we established that charged residues outside the SH2 core binding motif have a large influence on the binding affinity. Subsequently, we introduced TOAC in these extended, high affinity peptides and observed that the interaction with the SH2 domain is surprisingly dynamic. These results are discussed in the context of the two-step model for protein complex formation.

Experimental procedures

Peptide synthesis

Peptides were synthesized using the method described in chapter 2 and were kindly provided by Dr. Jan Wouter Drijfhout.

Cloning and protein expression

A DNA fragment encoding the mouse Src SH2 domain, residues 147-250, was generated by PCR and restricted with NcoI and XhoI for insertion into the expression vector pET28a. For protein production *Escherichia coli* BL21 cells were transformed with SH2-pET28 and incubated overnight in LB medium supplemented with 50 mg/L kanamycin at 37°C while shaking at 250 rpm. The preculture was diluted 1:100 into fresh medium, using LB medium with 50 mg/L kanamycin for production of unlabelled protein, and M9 minimal medium with 50

mg/L kanamycin using $^{15}NH_4Cl$ as the sole nitrogen source for ^{15}N-labelled protein. Cultures were incubated at 37°C and 250 rpm until an OD_{600} of 0.6, protein production was induced with 0.5 mM isopropyl β-D-1-thiogalactopyranoside and cells were harvested via centrifugation 3-5 h later.

Protein purification

Cells were resuspended in lysis buffer (20 mM Tris-HCl pH 8, 0.5 M NaCl, 10 mM imidazole, 1 mM phenylmethanesulfonyl fluoride and 50 µg/mL DNAse) and lysed by two passages through a French pressure cell. The lysate was cleared by centrifugation at 40,000 rpm for 30 minutes and the supernatant containing the His-tagged SH2 domain was loaded onto an affinity column (HisTrap HP, GE Healthcare). After washing with 20 mM Tris-HCl pH 8, 0.5 M NaCl and 60 mM imidazole the protein was eluted with the same buffer containg 300 mM imidazole. The eluted protein was diluted 10-fold with 20 mM HEPES pH 6.8, loaded onto an ion-exchange column (HiTrap SP, GE Healthcare) and eluted with a 50-500 mM NaCl gradient. Fractions were checked by SDS-PAGE and the purity of the protein was estimated to be above 95%. The protein concentration was determined using a theoretical extinction coefficient at 280 nm of 14440 M^{-1} cm^{-1} [140].

NMR spectroscopy

NMR experiments were recorded at 303 K on a Bruker DMX600 spectrometer equipped either with a TXI-Z-GRAD probe or a TCI-Z-GRAD cryoprobe (Bruker, Karlsruhe, Germany). The data were processed with Azara (http://www.bio.cam.ac.uk/azara/) and analyzed using Ansig For Windows [142].

For amide backbone resonance assignments 3D [^{15}N, ^{1}H] NOESY-HSQC and 3D [^{15}N, ^{1}H] TOCSY-HSQC spectra were recorded on a 4 mM ^{15}N-SH2 sample in 20 mM KPi pH 6.5, containing 6% D_2O for lock. The resonances were assigned with the help of assignments for the human SH2 domain [174].

For peptide titrations, stock solutions of 4-20 mM peptide were prepared by dissolving peptides in 20 mM KPi, pH 6.5, 0.1 M NaCl and adjusting the pH to 6.5 with small aliquots of 0.1–0.5 M solutions of NaOH or HCl. Titrations with unlabelled peptides were performed by the addition of microliter aliquots of peptide to samples containing 0.20-0.26 mM ^{15}N SH2 in 20 mM KPi pH 6.5, 0.1 M NaCl, 1 mM DTT. [^{15}N, ^{1}H] HSQC spectra were recorded at the start of the titration and after each addition of peptide. Spin-labelled peptides were added to similar samples without DTT. Diamagnetic control experiments were carried out after reduction of the paramagnetic peptides by ascorbate.

Chemical shift perturbation analysis

For titrations with unlabelled peptides the chemical shift perturbations for the amide ^{15}N nuclei were plotted against the molar ratio of peptide to protein. The data were analysed using a non-linear least squares fit to a one-site binding model [145] (Eq. 1) with the programme Origin (OriginLab corporation, Northampton, MA).

$$\Delta\delta_{binding} = \frac{1}{2}\Delta\delta_{\infty}(A - \sqrt{A^2 - 4R/C}) \qquad (1)$$

$$A = 1 + R/C + \frac{LR + U}{LUK_a}$$

In Eq.1, R is the molar ratio of peptide to protein, $\Delta\delta_{binding}$ is the chemical shift perturbation at a given ratio of peptide to protein, $\Delta\delta_{\infty}$ is the chemical shift perturbation at 100% bound protein, L is the initial concentration of ^{15}N-labelled protein, U is the concentration of the peptide stock solution, K_a is the association constant of the complex and C is a parameter introduced to correct for any error in peptide concentration, e.g. caused by the hygroscopicity of the peptides or the uncertainty in connection to the weighing out of milligram amounts of peptide. A

value of C greater than one means that the actual peptide concentration was lower than expected. R and $\Delta\delta_{binding}$ are the independent and dependent variables, respectively, and $\Delta\delta_{\infty}$, C and K_a are the fitted parameters.

The averaged amide chemical shift perturbations were calculated according to Eq. 2:

$$\Delta\delta_{avg} = \sqrt{\frac{(\Delta\delta^{N}_{binding}/5)^2 + (\Delta\delta^{H}_{binding})^2}{2}} \quad (2)$$

where $\Delta\delta^{N}_{binding}$ and $\Delta\delta^{H}_{binding}$ are the chemical shift perturbations of the amide nitrogen and amide proton, respectively, extrapolated to 100% bound protein.

Distance restraints and docking calculations

To correct for any differences in concentration between the paramagnetic and diamagnetic samples, the peak intensities of all residues were normalized internally against a residue unaffected by the peptide binding. The ratio between the paramagnetic and the diamagnetic peak intensities (measured by the peak heights) was calculated for all residues. The residues were subsequently divided into three classes: residues that disappeared in the paramagnetic spectrum (class 1), residues with an intensity ratio equal to or greater than 0.90 (class 2) and visible residues with an intensity ratio of less than 0.85 (class 3). Intensity ratios between 0.85 and 0.90 were not used for generating restraints. The average intensity ratio for class 2 residues was calculated (0.97 for peptide ETDDpYAEIIDEED and 1.11 for peptide ETDDYAEIIDEED) and in order to adjust the average to exactly 1 all intensity ratios in the experiment were divided by this factor and the classes were adjusted according to the scaled intensity ratios.

The paramagnetic contribution to the transverse relaxation rate, $R_{2,para}$, was determined as described in chapter 2 and converted into distances between the amide and the spin label, using Eq. (3):

$$r = \sqrt[6]{\frac{\gamma^2 g^2 \beta^2 f_p f_b}{20 R_{2,para}} \left(4\tau_c + \frac{3\tau_c}{1+\omega_h^2 \tau_c^2} \right)} \qquad (3)$$

where r is the distance between the unpaired electron of TOAC and a given amide proton of SH2, τ_c is the correlation time of the dipolar interaction of the electron and the nucleus, ω_h is the proton Larmor frequency, γ is the proton gyromagnetic ratio, g is the electronic g-factor, β is the Bohr magneton, f_p is the fraction of peptide that was paramagnetic and f_b is the fraction of protein that was bound to peptide in the experiment. The fraction of bound protein, f_b, was estimated from NMR titration data (74% for ETDDpYAEI-Toac-DEED and 31% for ETDDYAEI-Toac-DEED), and the fraction of paramagnetic peptide, f_p, was determined using EPR (59% for peptide ETDDpYAEI-Toac-DEED and 49% for peptide ETDDYAEI-Toac-DEED). The total correlation time of the protein-peptide complex was estimated to 8 ns, using the software hydroNMR [147] and a structure of human Src SH2 bound to a phosphorylated peptide, PDB Entry 1HCS [175]. Francesco Scarpelli is gratefully acknowledged for help with EPR measurements.

For class 2 residues, with an intensity ratio equal to or above 0.9, a common lower distance restraint was estimated using a $R_{2,dia}$ value representative of the spectrum and an intensity ratio set to 0.90. The calculated distances using this $R_{2,dia}$ will differ slightly from the distance calculated using an individual $R_{2,dia}$ value for each residue, but the differences are within the margins used for this class in the docking calculations. Class 3 residues, with an intensity ratio between 0 and 0.85, were given both upper and lower distance restraints. Individual error margins were calculated for class 3 residues by determining the standard deviation of the noise in

the spectra and calculating a maximum and a minimum intensity ratio for each residue according to:

$$I_{ratio}^{\max} = \frac{I_{para} + SD_{para}}{I_{dia} - SD_{dia}} \quad , \; I_{ratio}^{\min} = \frac{I_{para} - SD_{para}}{I_{dia} + SD_{dia}} \tag{4a, b}$$

where SD_{para} and SD_{dia} are the standard deviations of the noise in the paramagnetic and diamagnetic spectra. The maximum and minimum intensity ratios were subsequently used to calculate minimum and maximum $R_{2,para}$ values and converted into upper and lower distance restraints according to Eq. (3) (for $R_{2,para}$ values see Appendix B). For class 1 residues, broadened beyond detection in the paramagnetic spectrum, the maximum intensity ratio was estimated from the noise level and converted into an individual upper distance restraint for each residue. In the docking procedure the SH2 domain was kept fixed and only the TOAC oxygen atom, taken to represent the paramagnetic centre, was free to move. Rigid-body docking calculations were performed in Xplor-NIH [148]. Ten runs were carried out in which random starting positions were generated for the TOAC oxygen atom, and energy minimization was performed until convergence was reached with a maximum of 100 steps. Only one energy term, corresponding to the distance restraints, was used, with the energy term being zero if the calculated distance between the amide proton and the TOAC oxygen atom matches the target distance within the restraint boundaries calculated above. For distances outside the allowed margins a square well energy function was used.

Due to uncertainties in determining the fraction of bound protein and the fraction of paramagnetic peptide, the f_p and f_b values were varied and additional calculations performed. The effect on the calculated TOAC position was marginal and the conclusion that a single position for the spin-label relative to the protein cannot account for the observed PREs remains the same.

Isothermal titration calorimetry

Isothermal titration calorimetry (ITC) experiments were carried out at 303 K on a Microcal (Northampton, MA) VP-ITC microcalorimeter. Unlabelled protein and peptide solutions were dialyzed exhaustively against the same buffer (50 mM HEPES pH 6.8, 0.1 M NaCl, 1 mM TCEP), centrifuged and degassed before experiments. A 25 μM SH2 solution was placed in a sample cell with a volume of 1.4 mL and binding isotherms were recorded following the injection of peptide (stock concentration 250 μM), while continuously stirring at 307 rpm. An initial 4 μL-injection was followed by 27 injections of 10 μL each, with 4-minute intervals between injections. Experiments were performed in triplicate and the standard deviations of the measured values are reported as the error margin. The error in TΔS was calculated using standard error propagation. Dilution heats were determined by titration of peptide into buffer and subtracted from the peptide into protein titration data. Using the Origin software supplied by Microcal, data were analyzed with a non-linear least squares fit to a one site binding model after deletion of the first titration point. In the fits, uncertainty in the peptide stock solution concentration caused the stoichiometry parameter, n, to differ from 1, with an average value of N=1.58 for the three measurements. The original peptide concentration 250 μM was therefore divided by this value (new concentration 158 μM), and the fits were repeated. The reported parameters are the result of these fits.

Molecular graphics were generated using PyMol [150].

Results

Peptide titrations

The peptide-binding face of the Src SH2 domain is predominantly positively charged. Inspection of the sequence surrounding the Y397 SH2 domain binding

site in FAK reveals that the flanking residues are mostly negatively charged. To investigate the influence of the surrounding residues on the interaction with the SH2 domain peptides derived from the FAK Y397 site were synthesized in phosphorylated and unphosphorylated forms, either comprising only the SH2 core binding motif or including the surrounding residues as well. Phosphorylated and unphosphorylated peptides from the C-terminal autoinhibitory region of Src were synthesized in addition (Table 1).

Titration with the unphosphorylated Src C-terminal peptide YQPG did not produce any significant chemical shift perturbations of backbone amide resonances of the SH2 domain, indicating no detectable binding of the SH2 domain to this peptide. The phosphorylated version of the same peptide, pYQPG, caused large chemical shift perturbations for some backbone amides. From the binding curves (Fig. 3.1A) an equilibrium dissociation constant K_d of 63 ± 20 μM was determined. Peptide YAEI, representing the core binding site on FAK, bound extremely weakly to the SH2 domain, with a K_d of at least 10 mM (Fig. 3.1B). For the phosphorylated version of the same peptide, pYAEI, a K_d of 3 ± 2 μM was found (Fig. 3.1C). The unphosphorylated peptide also containing the residues surrounding the core SH2 binding motif, ETDDYAEIIDEED, demonstrated a much higher binding affinity for the SH2 domain compared to the shorter unphosphorylated peptide, yielding a K_d of 0.34 ± 0.16 mM (Fig. 3.1D).

Titration with the long, phosphorylated peptide ETDDpYAEIIDEED also gave rise to large chemical shift perturbations of some amide resonances, but the binding of this peptide to the SH2 domain proved to be too tight to obtain a value of the equilibrium dissociation constant using NMR spectroscopy. In the titrations the resonances of free and bound SH2 domain range from being in fast exchange on the NMR time-scale for peptides YAEI and ETDDYAEIIDEED, via fast-to-

intermediate exchange for peptide pYQPG and intermediate-to-slow exchange for peptide pYAEI, to slow exchange for peptide ETDDpYAEIIDEED (Fig. 3.2).

Table 1. SH2-peptide binding assays. pY=phosphotyrosine. All peptides were acetylated and amidated on the N-, and C-termini, respectively. C is a parameter introduced to correct for any error in peptide concentration (see experimental procedures).

Peptide sequence	**Derived from**	**K_d**	**C**	**Method**
YQPG	Src C-terminal region	No binding detected	-	NMR
pYQPG	Src C-terminal region	63 ± 20 μM	1.56	NMR
YAEI	FAK Y397	≥10 mM	1	NMR
pYAEI	FAK Y397	3 ± 2 μM	1.28	NMR
ETDDYAEIIDEED	FAK Y397	0.34 ± 0.16 mM	0.67	NMR
ETDDpYAEIIDEED	FAK Y397	73 ± 12 nM	1.58	ITC
ETDDYAEI-Toac-DEED	FAK Y397	0.75 ± 0.40 mM	1.89	NMR
ETDDpYAEI-Toac-DEED	FAK Y397	≤ 1 μM	1	NMR

Using ITC, a K_d of 73 ± 12 nM was determined for the interaction of peptide ETDDpYAEIIDEED with the SH2 domain. The binding is driven by an enthalpic change (ΔH) of -10.6±0.1 kcal/mol, with the entropic term (TΔS) being -0.7±0.2 kcal/mol (Fig. 3.3 and Table 2). A comparison of enthalpy and entropy changes of binding of peptides ETDDpYAEIIDEED and PQpYAEIPI [176] under similar conditions with the Src SH2 domain shows a somewhat larger favourable enthalpic

contribution for the former (Table 2). The shorter peptide exhibits a favourable entropic contribution, whereas peptide ETDDpYAEIIDEED displays an unfavourable entropy term.

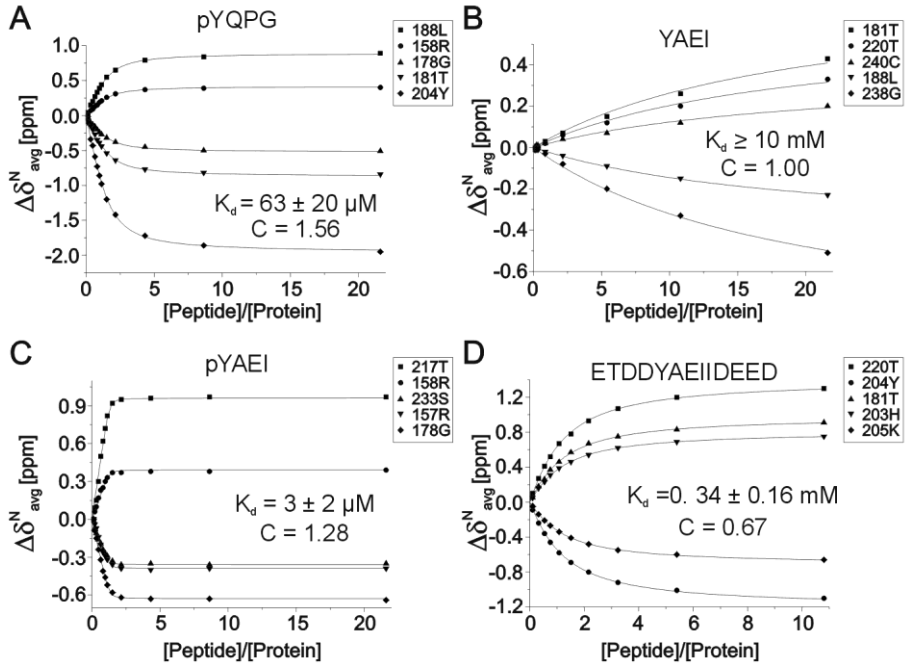

Figure 3.1. ^{15}N chemical shift perturbations of SH2 resonances upon titration with peptides. The curves represent the best global fit to a 1:1 binding model (Eq. 1). **A)** peptide pYQPG **B)** peptide YAEI **C)** peptide pYAEI **D)** peptide ETDDYAEIIDEED.

To compare the effect the different peptides have on the SH2 domain average chemical shift perturbations were extrapolated to 100% bound protein for all assigned residues in the SH2 domain (Fig. 3.4). Peptide pYQPG affects a rather limited set of residues in the SH2 domain, mainly around the phosphotyrosine binding pocket (Fig. 3.4B), whereas peptides derived from FAK affect a larger number of residues, especially the longer peptides (Fig. 3.4C-F). The

unphosphorylated and phosphorylated peptides cause quite similar chemical shift perturbations in the SH2 domain, indicating that they bind in similar ways (Fig. 3.4C and D, E and F).

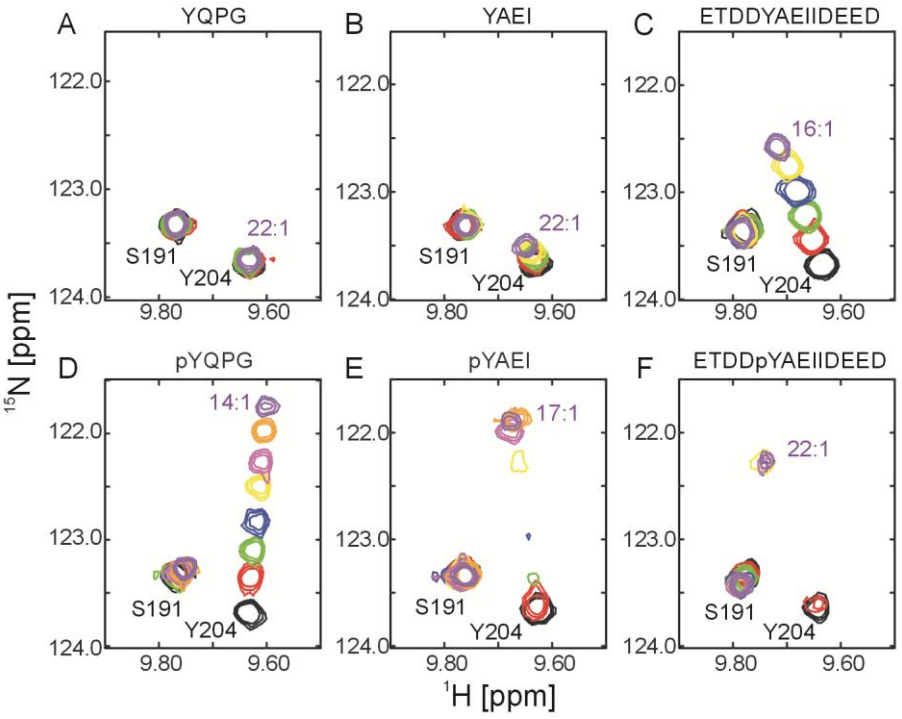

Figure 3.2. Detail from HSQC spectra of SH2 domain in titrations with peptides YQPG **(A)**, YAEI **(B)**, ETDDYAEIIDEED **(C)**, pYQPG **(D)**, pYAEI **(E)** and ETDDpYAEIIDEED **(F)**. Spectra from a few titration points are shown overlaid, with starting points (free protein) in black and titration end points shown in purple. The peptide to protein ratio at the titration end point is noted in the spectra.

Table 2. Thermodynamic parameters for binding of phosphopeptides to Src SH2 obtained by ITC.

Peptide	***K_a (M^{-1})***	***ΔG (kcal/mol)***	***ΔH (kcal/mol)***	***TΔS (kcal/mol)***
ETDDpYAEIIDEED[a]	1.4 (±0.2) x 10^7	-9.9 ± 0.1	-10.6 ± 0.1	-0.7 ± 0.2
PQpYAEIPI[b]	2.9 (±0.4) x 10^6	-8.7 ± 0.1	-7.7 ± 0.2	1.0 ± 0.2

[a] Binding isotherms recorded in 50 mM HEPES, pH 6.8, 1mM TCEP and 100 mM NaClat 303 K.

[b] Values taken from [177], (20 mM HEPES, pH 7.5, and 100 mM NaCl at 298 K).

Dynamics of peptide binding

In order to investigate the dynamics of the interaction between the SH2 domain and the longer peptides derived from FAK, peptides containing the spin-labelled amino acid TOAC were synthesized (Table 1). The paramagnetic TOAC was introduced to determine whether the bound peptide assumes a single, well-defined orientation or samples several orientations. The strong distance dependence of the PRE and the rigidity of the spin-label relative to the peptide should result in highly localized PREs if the peptide orientation is well-defined. To assess the influence of TOAC on the peptide-protein interaction first, NMR titrations were performed with TOAC-labelled peptides in the reduced, non-paramagnetic form. For both the unphosphorylated peptide ETDDYAEI-Toac- DEED and the phosphorylated peptide ETDDpYAEI-Toac-DEED the binding affinity was somewhat reduced compared to the unlabelled peptides, with a K_d of 0.75 ± 0.40 mM for the unphosphorylated TOAC peptide. The exchange between free and peptide-bound

SH2 forms is faster for ETDDpYAEI-Toac-DEED compared to ETDDpYAEIIDEED, suggesting somewhat lower affinity for the former. The binding is, however, still too tight to be determined by NMR.

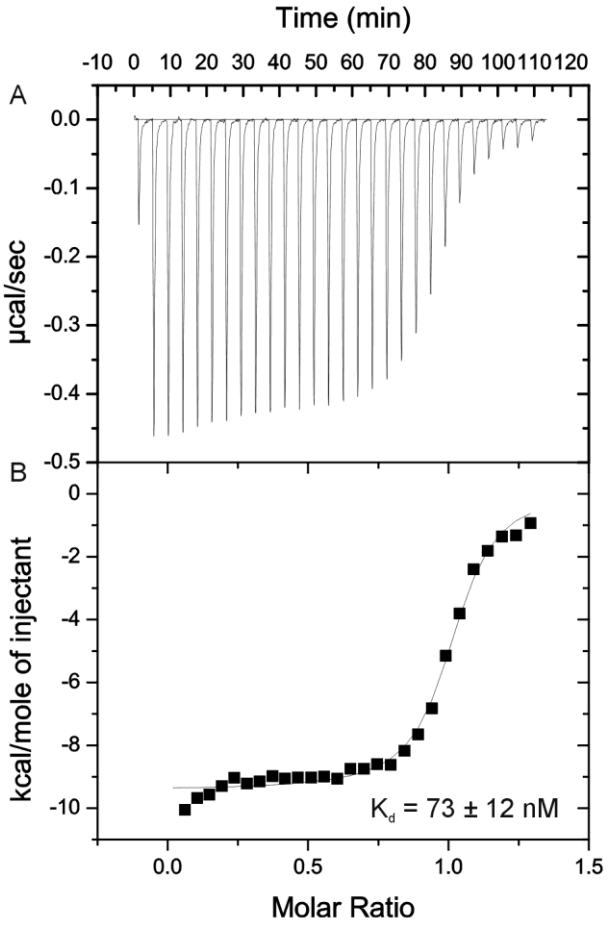

Figure 3.3. Representative isothermal titration calorimetry curves for the binding of Src SH2 to peptide ETDDpYAEIIDEED. **A)** raw data after baseline correction, **B)** integrated data corrected for the heat of dilution of the peptide. The solid line in B) represents the best fit to a 1:1 binding model.

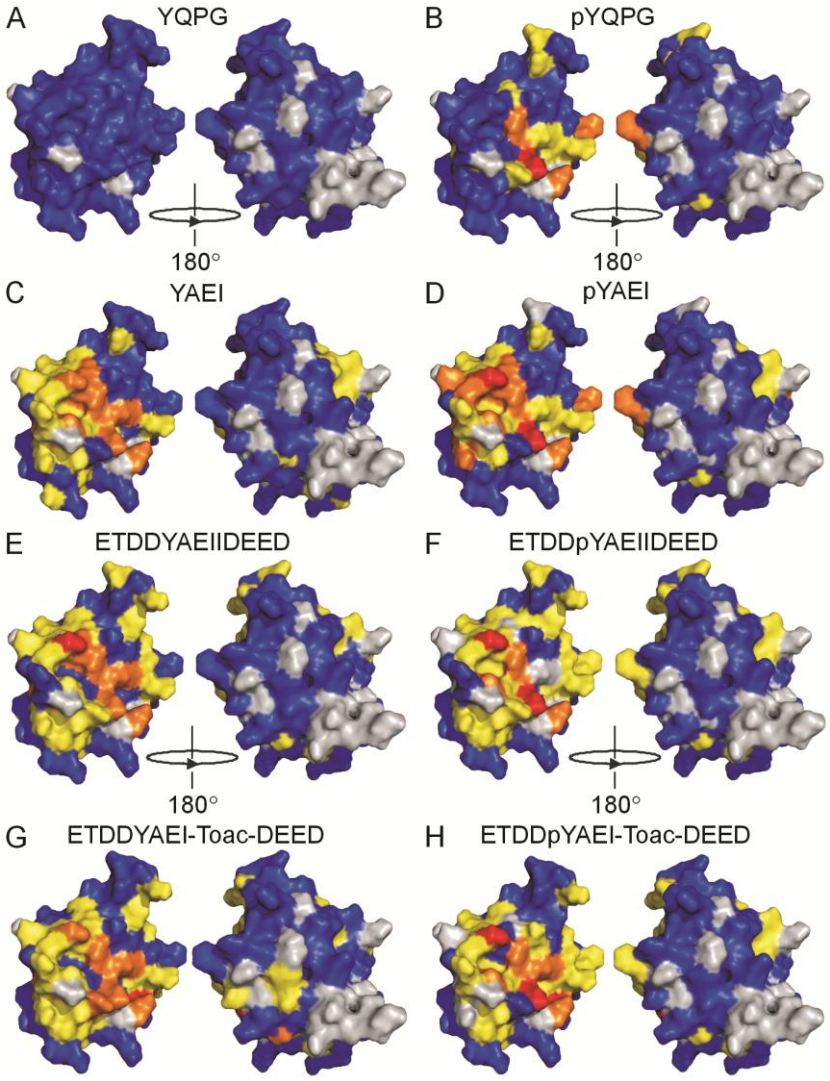

Figure 3.4. Chemical shift perturbations upon titration with peptides **A)** YQPG, **B)** pYQPG, **C)** YAEI, **D)** pYAEI, **E)** ETDDYAEIIDEED, **F)** ETDDpYAEIIDEED, G**)** ETDDYAEI-Toac-DEED (reduced state) **H)** and ETDDpYAEI-Toac-DEED (reduced state) mapped onto the surface of the SH2 domain. Shift changes were extrapolated to SH2 fully bound to peptide and residues were coloured according to the size of the average chemical shift perturbation, $\Delta\delta_{avg}$. Red: $\Delta\delta_{avg} \geq 0.3$ ppm; orange: $0.3 > \Delta\delta_{avg} \geq 0.1$ ppm; yellow: $0.1 > \Delta\delta_{avg} \geq 0.04$ ppm; blue: $\Delta\delta_{avg} < 0.04$ ppm. Non-assigned residues are shown in grey.

From the titration it can only be estimated that the phosphorylated TOAC-peptide binds with a K_d of less than a 1 µM. Due to the limited amount of material no ITC experiments could be carried out to precisely determine the binding constant. Extrapolation of the average chemical shift perturbations to 100% bound protein shows that despite the small changes in affinity, the unphosphorylated peptides ETDDYAEIIDEED and ETDDYAEI-Toac-DEED bind in a similar way (Fig 3.4E and F), as do the phosphorylated peptides ETDDpYAEIIDEED and ETDDpYAEI-Toac-DEED (Fig 3.4G and H).

For PRE NMR studies $^{1}H,^{15}N$-HSQC spectra of the SH2 domain complexed to the paramagnetic TOAC-peptides were recorded, and from a comparison of the peak intensities in the paramagnetic and diamagnetic control samples the PRE ($R_{2,para}$) was derived (see Experimental Procedures), at peptide-to-protein ratios of 2:1 and 2.6:1 for the phosphorylated and unphosphorylated peptide, respectively. Mapping of the experimentally determined $R_{2,para}$-values onto the SH2 domain shows that the observed effects are spread over a large part of the protein for both peptides (Fig 3.5A, B) contrary to the expectation for a well-defined orientation.

To establish whether the PREs agree with a single position of the spin label relative to the protein, distance restraints were derived from the $R_{2,para}$-values and the position of a pseudoatom representing the spin-label was obtained by energy minimization using the restraints as the sole energy term. The calculations converged to a single position for the TOAC nitroxide. However, it differs by approximately 9.5 Å from a prediction based on comparison with the structure of Src SH2 in complex with another phosphopeptide [178] (Fig. 3.6). Furthermore, analysis of the restraint violations shows that many of the amide-spin label distances in the calculated structure fall outside the range set by the paramagnetic effects (Figs. 3.7 and 3.8). This demonstrates that the single calculated position of the spin-label is not sufficient to explain all paramagnetic effects observed. Violations plots based on the $R_{2,para}$-values instead of the distances are shown in

Figs. 3.9 and 3.10. These results provide a clear indication that the TOAC-based spin-label samples a significant part of the SH2 surface.

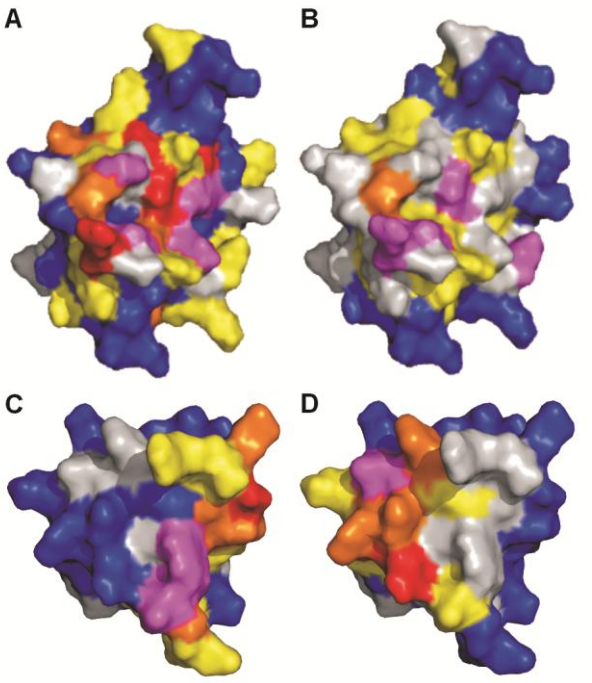

Figure 3.5. $R_{2,para}$ values derived from NMR data of SH2 domain in complex with ETDDYAEI-Toac-DEED **(A)** and ETDDpYAEI-Toac-DEED **(B)** mapped onto the SH2 domain surface. For comparison $R_{2,para}$ values from NMR data of Src SH3 in complex with the spin-labelled peptides Toac-RALPSIPKL **(C)** and RALP-Toac-IPKL **(D)** (chapter 2) are shown. The fraction of paramagnetically labelled peptide (f_p) and the fraction of protein bound to peptide (f_b) are not identical for all four experiments, R_{2para} values have been normalized against the lowest f_p*f_b value. For A) f_p*f_b=0.15, B) 0.44, C) 0.24 and D) 0.23, meaning that R_{2para} values for the phosphorylated peptide (B) have all been divided by 2.9 (=0.44/0.15), and similarly for SH3 R_{2para} values. Purple: residues broadened beyond detection, red: $R_{2para} \geq 50\ s^{-1}$, orange: $50\ s^{-1} > R_{2para} \geq 24\ s^{-1}$, yellow: $24\ s^{-1} > R_{2para} \geq 3.12\ s^{-1}$, blue: $R_{2para} < 3.12\ s^{-1}$. In grey are shown residues not included in docking calculations (non-assigned residues or residues with an intensity ratio greater or equal to 0.85 and less than 0.9).

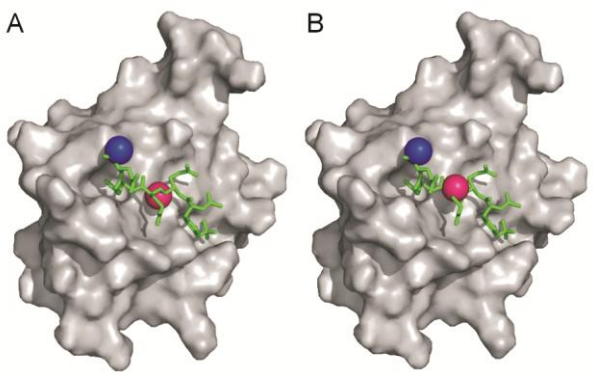

Figure 3.6. Calculated position of TOAC oxygen atom on the basis of PRE data (pink sphere) in complex between peptide ETDDYAEI-Toac-DEED **(A)** or ETDDpYAEI-Toac-DEED **(B)** and the Src SH2 domain, overlaid with a structure of SH2 in complex with peptide pYEEIE, shown in green (PDB entry 1HCS [179]). In blue is shown the expected position of TOAC based on the corresponding residue in peptide pYEEIE.

Discussion

The NMR titrations show that the FAK residues flanking the core binding motif have a large impact on the interaction with the SH2 domain. Including these surrounding residues increases the binding affinity by around 30 fold for both the phosphorylated and unphosphorylated peptides, demonstrating that residues outside the consensus Src family SH2 binding motif can contribute to SH2-mediated protein interactions. Introducing TOAC in the peptides just outside the core SH2 binding motif somewhat reduced the binding affinity for the SH2 domain. It has been shown that introduction of TOAC in a peptide sequence can lower peptide-protein binding affinity if TOAC is placed within the binding motif, but not if placed outside the immediate protein recognition site (chapter 2). Here, we find a small decrease in the affinity when TOAC is placed at the Y+4 position. Based on a published structure of the SH2 domain in complex with a phosphopeptide of the sequence pYEEIE [180] the TOAC is expected to be pointing away from the

protein surface, and therefore interfere minimally with the binding. It is possible though that the rigid structure of the spin-label to some extent restrains the peptide flexibility. However, the similarity of the chemical shift perturbations caused by spin-labelled and unlabelled peptides (Fig. 3.4) suggests that in spite of the effect on the binding affinity the modes of binding are similar.

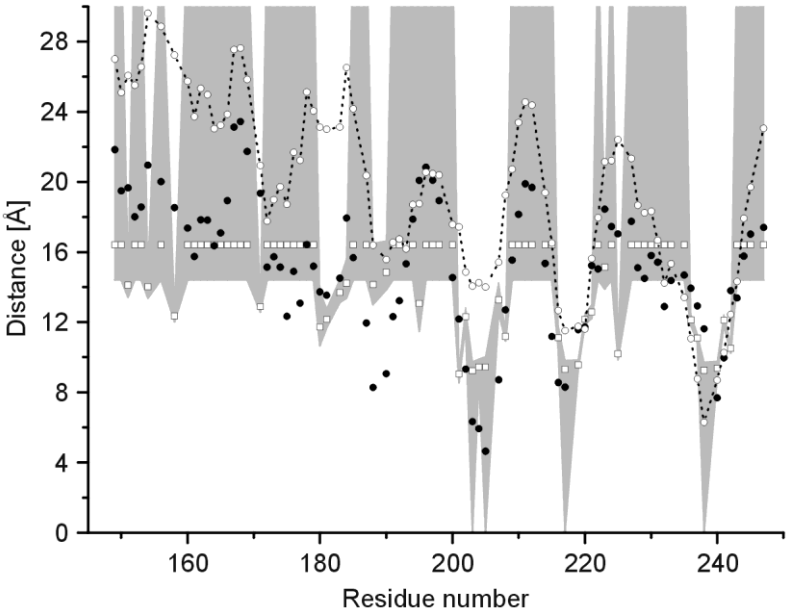

Figure 3.7. Violations analysis of calculated position of TOAC nitroxide in the complex of peptide ETDDYAEI-Toac-DEED with Src SH2. Spin-label to amide distances derived from the NMR data are shown as white squares, with the allowed distance range (error margins used in calculations) shown as a shaded area. Distances in the converged structure are shown as black circles, black circles outside the shaded area signify violations of the distance restraints. For comparison predicted amide-spin label distances based on a structure of peptide pYEEIE in complex with the SH2 domain (PDB entry 1HCS, from [181]) are shown as white circles connected by a dotted line. Predicted distances were obtained by placing the TOAC in the Y+4 position in this peptide, which corresponds to the position of TOAC in ETDDYAEI-Toac-DEED.

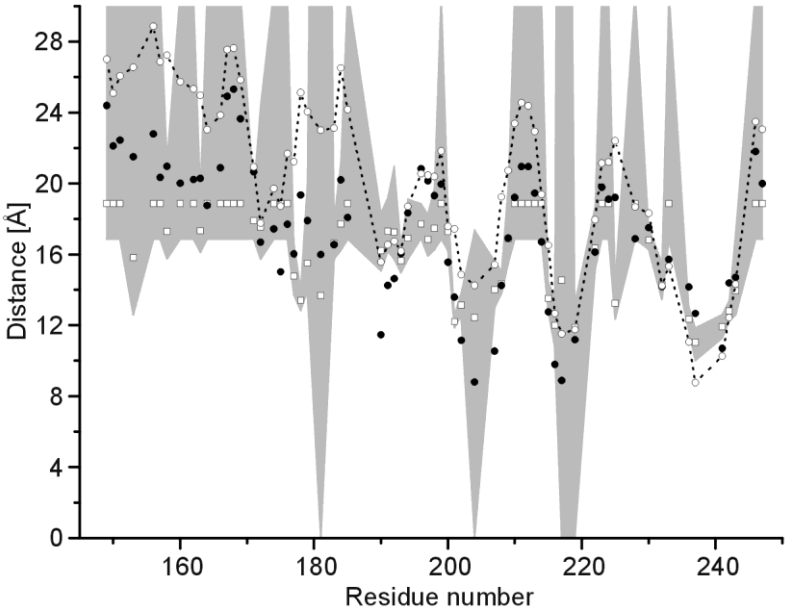

Figure 3.8. Violations analysis of calculated position of TOAC nitroxide in the complex of peptide ETDDpYAEI-Toac-DEED with Src SH2. Spin-label to amide distances derived from the NMR data are shown as white squares, with the allowed distance range (error margins used in calculations) shown as a shaded area. Distances in the converged structure are shown as black circles, black circles outside the shaded area signify violations of the distance restraints. For comparison predicted amide-spin label distances based on a structure of peptide pYEEIE in complex with the SH2 domain (PDB entry 1HCS, from [182]) are shown as white circles connected by a dotted line. Predicted distances were obtained by placing the TOAC in the Y+4 position in this peptide, which corresponds to the position of TOAC in ETDDpYAEI-Toac-DEED.

Analysis of the docking calculations shows that for neither the phosphorylated nor unphosphorylated peptides is a single position of the spin-label relative to the protein sufficient to account for the observed paramagnetic effects, indicating that the peptide samples the surface of the SH2 domain in a dynamic fashion, despite the very high affinity of the long phosphopeptide for the SH2 domain. A possible explanation for this is that peptide and protein are first attracted to each other based on their opposite charges, and that the peptide subsequently moves over the SH2 surface in search of the specific binding position. This view is in line with the two-

step model for protein complex formation [183]. The encounter complex is thought to be dominated by electrostatic interactions. The highly negative peptide is strongly attracted by the positive surface of the SH2 domain, enhancing the formation of the encounter complex and thus the affinity. It has been shown that electrostatic interactions stabilize the encounter complex more than the final complex [184] and, consequently, the introduction of the negative charges not only enhances the affinity of complex formation, but also shifts the equilibrium between encounter state and final complex towards the former (Fig. 3.11). The electrostatic interactions between the charged patches on the protein and the peptide result in an ensemble of rapidly exchanging orientations, making the encounter state dynamic and explaining the spread of the PREs over the SH2 domain. This is supported by

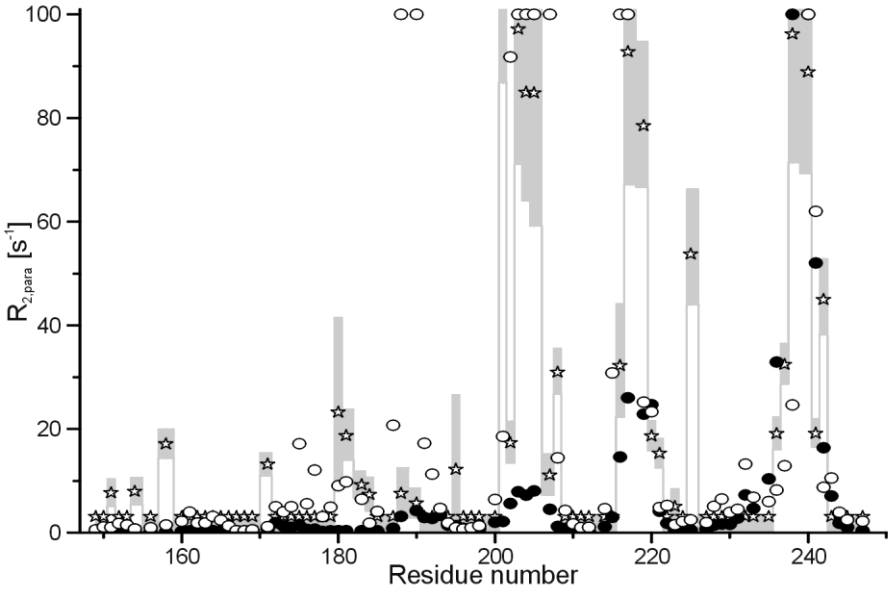

Figure 3.9. Violations analysis of calculated position of TOAC in ETDDYAEI-Toac-DEED in complex with SH2. Stars: $R_{2,para}$ values derived from NMR data; open circles: $R_{2,para}$ values in calculated structure; shaded area: error margins used in calculations. Filled circles show the expected $R_{2,para}$ values based on the position of the residue in peptide pYEEIE [185] corresponding to TOAC in the above peptides. Values exceeding 100 s^{-1} are shown as 100 s^{-1}.

the observation that many of the residues showing high $R_{2,para}$ values are either positively charged or close to residues with a positive charge, whereas the peptide is highly negatively charged.

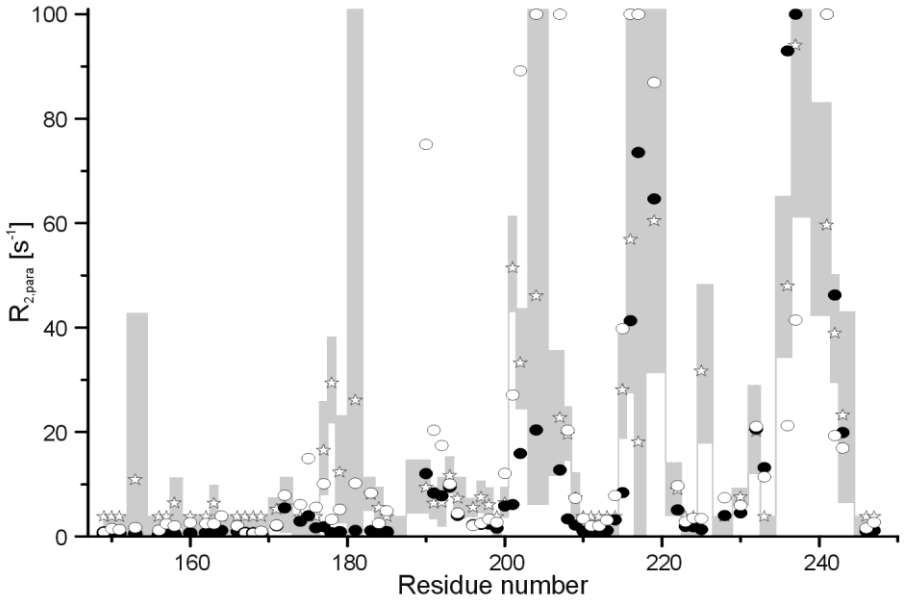

Figure 3.10. Violations analysis of calculated position of TOAC in ETDDpYAEI-Toac-DEED in complex with SH2. Stars: $R_{2,para}$ values derived from NMR data; open circles: $R_{2,para}$ values in calculated structure; shaded area: error margins used in calculations. Filled circles show the expected $R_{2,para}$ values based on the position of the residue in peptide pYEEIE [186] corresponding to TOAC in the above peptides. Values exceeding 100 s^{-1} are shown as 100 s^{-1}.

The advantage of PRE NMR over other methods for studying dynamics in protein complexes is the possibility to detect complex orientations that are only populated for a small fraction of the time. For example, it is not likely that any intermolecular NOEs could be observed for the encounter state, due to its dynamic nature. Previous studies of the Src SH3 domain in complex with spin-labelled peptides derived from FAK have shown that in interactions of weak binding affinity the position of the peptide relative to the protein can still be remarkably well-defined

(chapter 2) with the effects of the spin-label on the protein concentrated to relatively small, well-defined areas (Fig 3.5C, D). The results presented here show that high-affinity binding can be surprisingly dynamic, and that residues outside the central SH2 binding site in FAK may also be important for the Src-FAK interaction.

Conclusions

The negatively charged residues surrounding the Y397 SH2 binding site in FAK increase the binding affinity for the SH2 domain to peptides derived from this site by more than an order of magnitude, demonstrating that residues outside the SH2 core binding motif can have a large influence on SH2-mediated protein interactions. Despite the high binding affinity for the phosphorylated peptide to the SH2 domain, the interaction exhibits dynamics. Previous work has shown that a low binding affinity in itself does not imply mobility in a peptide-protein complex, whereas this study shows that a high binding affinity does not necessarily imply a static way of binding. The strong electrostatic interactions enhance the affinity, but simultaneously appear to favour a more dynamic interaction.

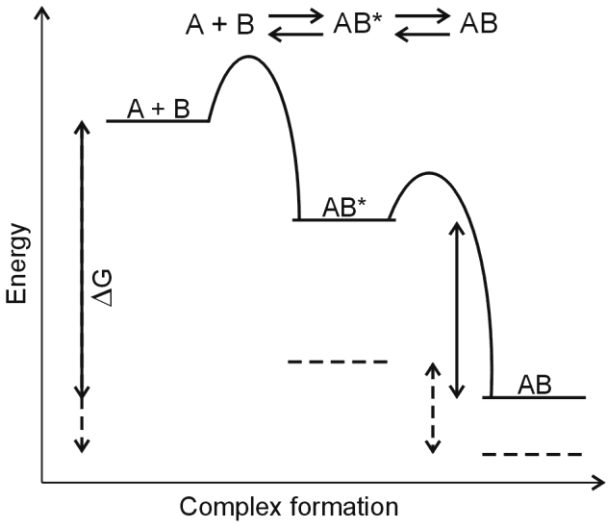

Figure 3.11. Energy diagram of two-step model of peptide-SH2 domain complex formation, with the encounter complex denoted by an asterisk. Electrostatic interactions promote encounter complex formation and stabilize the encounter complex relative to the final complex, thereby shifting the equilibrium towards a more dynamic state (illustrated here by the dashed lines).

Chapter 4

A dynamic intermediate state in peptide-binding to the combined Src SH3 and SH2 domains

Abstract

The interaction of peptides derived from FAK with the SH32 domain of Src has been studied using NMR and ITC. The SH3- and SH2-binding sites in FAK are separated by more amino acid residues than what is required to simply span the distance between the peptide-binding faces on the SH3 and SH2 domains. Here, the length of the linker separating the SH3- and SH2-binding sites in FAK peptides has been reduced and the effect on the interaction with the SH32 domains has been investigated. Peptides in which the distance between the SH2- and SH3-binding sites is not sufficient for simultaneous SH2 and SH3 domain-binding were expected to almost exclusively bind to the SH2 domain, due to the high-affinity nature of SH2 domain-mediated interactions compared to SH3-peptide interactions. Contrary to expectations, a significant fraction of the peptide was found to bind to the SH3 domain at low peptide-to-protein ratios. In order to explain these observations we propose a model for the peptide-SH32 interaction in which long-range electrostatic interactions between charges in the peptide and the SH2 domain help recruit the peptide into a dynamic encounter complex, from which the peptide can either bind the SH3 or SH2 domain, thereby increasing the affinity for the SH3 domain compared to peptide interactions involving the isolated domain.

This chapter will be published as part of:

Lindfors et al (2010). A dynamic intermediate state in peptide-binding to the combined Src SH3 and SH2 domains. *Manuscript in preparation.*

Introduction

A general feature of most signalling proteins is their modular architecture, meaning that they are constructed from several individually folded domains. The domains can either have catalytic functions or be interaction domains, involved in binding to other proteins, lipids or nucleic acids. Recognition of short peptide sequences by protein interaction domains plays an important role in the regulation of cellular behaviour by facilitating the assembly of the signalling protein complexes and larger protein networks involved [15;187]. The protein interaction domains do not only function to recruit the catalytic domain to its appropriate substrates in the cell, but are often also involved in the regulation of protein activity via domain rearrangements [188].

The Src family kinases (SFKs) are prototypical modular signalling proteins. These non-receptor protein tyrosine kinases are involved in the regulation of a number of cellular processes, including cell survival, proliferation, differentiation and motility [189]. SFKs share a common domain structure with an N-terminal myristoylation site, followed by a region that is unique for each family member, a Src homology 3 (SH3) domain, a Src homology 2 (SH2) domain, a tyrosine kinase domain and a C-terminal region containing a negative-regulatory tyrosine residue (Y529 in Src, using mouse Src numbering) [190]. The SH3 and SH2 domains are protein-interaction domains found in a large number of signalling proteins [191]. SH3 domains, first discovered in 1988 [192], bind to proline-rich sequences that adopt a left-handed helical conformation [15], whereas SH2 domains recognize phosphorylated tyrosine residues. Since the original discovery in 1986 [193], SH2 domains have been identified in over 100 different protein sequences in humans [155]. The SH3 and SH2 domains of SFKs are involved in the regulation of protein activity via intramolecular contacts. Phosphorylation of Y527 in the C-terminal region of the kinase leads to association of this region with the SH2 domain. Together with the interaction of the SH3 domain with residues in the linker

connecting the SH2 domain with the catalytic domain, this intramolecular binding promotes a conformation by which kinase activity is repressed [194-197]. The SH2 and SH3 domains therefore play a direct role in regulating kinase activity, and competition for SH3 or SH2 domain binding by external ligands leads to kinase activation [198;199]. Fragments encompassing the SH3-SH2 domains (SH32) from several SFKs have been characterized biochemically, structurally and computationally [139;144;200-206], because of the importance of these domains for the functioning of SFKs.

Focal adhesion kinase (FAK) can activate Src and Fyn via interactions with their SH2 and SH3 domains [139;207;208]. The linker region between the FERM and catalytic domains of FAK contains a tyrosine residue, Y397, which becomes phosphorylated in connection with FAK activation [209]. N-terminal to the tyrosine, the linker contains a proline-rich region of the sequence RALPSIPKL. These residues contain the SH3 domain binding motif PxxP [210], whereas the phosphotyrosine region with sequence pYAEI is close to the consensus sequence pYEEI for SH2 domain binding [211]. Peptides derived from FAK spanning both the proline-rich and phosphotyrosine sites have been shown to bind to SH32 fragments of Src and Fyn in a bidentate manner with equilibrium dissociation constants of 20-30 nM, which is a higher affinity than those seen for peptides containing an SH3 or SH2 binding site alone [139;212]. It has been shown that the interaction between the FAK peptide and the Fyn SH32 domains is restricted to the canonical SH3 and SH2 binding sites and that the interaction does not affect the dynamic independence of the two domains [213].

The SH3- and SH2- domain binding motifs in the FAK fragment are separated by a ‘spacer’ consisting of 22 aminoacids, which is approximately 10 residues more than what is necessary to span the distance between the peptide-binding faces on the SH3 and SH2 domains [214]. This allows for simultaneous association of the SH3- and SH2 domains with their respective binding sites in the peptide. If the

length of the spacer separating the two binding sites in the peptide is reduced, the peptide-protein interaction would be expected to remain unaffected as long as the peptide can span the distance between the two domains. Upon further reduction of the spacer, the peptide would be expected to predominantly bind to the SH2 domain, due to the much higher affinity of the SH2 domain for the phosphotyrosine sequence compared to the SH3 domain binding to the proline-rich sequence (chapters 2 and 3). Only after saturation of the SH2 domain binding site, would binding to the SH3 domain be expected to occur. To test this hypothesis, we have performed NMR and ITC experiments on the Src SH32 domains interacting with peptides derived from FAK, in which the spacer has been gradually reduced in length. In contrast to the hypothesis, even for short spacers simultaneous binding of both domains is observed, indicative of a SH3-peptide interaction that must have significantly higher affinity than what is observed for the SH3 domain with proline-rich peptides. We propose a model for the interaction in which electrostatic interactions of the peptide with the SH2 domain increase the effective affinity of the peptide for the SH3 domain, via the formation of an intermediate dynamic state.

Experimental procedures

Cloning, protein expression and purification

A DNA fragment encoding the mouse Src SH3 and SH2 domains (SH32), residues 85-250, was amplified by PCR from the full-length Src plasmid pUSE Src wt (kindly provided by Prof. B. van de Water). The PCR product was inserted into the expression vector pET28a using the NcoI and XhoI restriction sites and the resulting construct was verified by DNA sequencing. For production of His-tagged SH32 *Escherichia coli* BL21 (DE3) cells, transformed with SH32-pET28, were incubated overnight at 37°C and 250 rpm in LB medium supplemented with 50

mg/L kanamycin. The preculture was diluted at a volume ratio of 1:100 into fresh LB medium with 50 mg/L kanamycin for production of unlabelled protein or into M9 minimal medium with 50mg/L kanamycin using $^{15}NH_4Cl$ as the only source of nitrogen for production of ^{15}N-labelled protein. Cultures were incubated at 37°C and 250 rpm, and protein production was induced with 0.5 mM IPTG when an OD_{600} of 0.6 was reached. Cells were harvested via centrifugation after 3-5 h, resuspended in 20 mM Tris-HCl pH 8, 0.5 M NaCl and 10 mM imidazole and stored at -80°C until protein purification. Following the addition of 1 mM PMSF and 50 µg/mL DNAse, the thawed cells were lysed using a French pressure cell and the lysate was cleared by centrifugation at 40000 rpm for 30 minutes. The supernatant was loaded onto an immobilized metal affinity column (HisTrap HP, GE Healthcare) equilibrated with 20 mM Tris-HCl pH 8, 0.5 M NaCl and 10 mM imidazole. The column was washed with the same buffer containing 60 mM imidazole before elution with the same buffer containing 300 mM imidazole. The eluted protein was diluted at a volume ratio of 1:5 with 20 mM Tris-HCl pH 7.6, in order to lower the NaCl concentration to 0.1 M. Protein was loaded onto an ion-exchange column (HiTrap Q, GE Healthcare) equilibrated with 20 mM Tris-HCl pH 7.6, 0.1 M NaCl, and eluted using a gradient of 0.1 – 0.8 M NaCl. Fractions were checked by SDS-PAGE, and pure fractions were pooled and concentrated. The purity of the protein was estimated to be above 95%. The buffer was exchanged to NMR buffer for the ^{15}N-labelled protein (20 mM KPi pH 6.5, 100 mM NaCl and 1 mM DTT) and to ITC buffer for the unlabelled protein (20 mM HEPES pH 6.8, 100 mM NaCl and 1 mM TCEP). The protein concentration was determined by the absorbance at 280 nm, using a theoretical extinction coefficient of 31400 M^{-1} cm^{-1} [140].

Peptide synthesis

Peptides were synthesized as described in chapter 2 and were kindly provided by Dr. Jan Wouter Drijfhout. Peptide stock solutions were prepared by weighing out

peptide and dissolving in NMR or ITC buffer and adjusting the pH by the addition of small aliquots of NaOH or HCl.

Nuclear magnetic resonance spectroscopy

All NMR experiments were performed at 303 K on a Bruker DMX600 spectrometer equipped with a TCI-Z-GRAD cryoprobe (Bruker, Karlsruhe, Germany). The data were processed with Azara (http://www.bio.cam.ac.uk/azara/) and analyzed using Ansig For Windows [142].

Backbone amide resonance assignments were performed analogous to what has been described for the Src SH3 domain (chapter 2). Peptide titrations were performed through the addition of microliter aliquots of peptide stock solution with concentration ranging from 1 to 5 mM. Two-dimensional [^{15}N,^{1}H]-HSQC spectra were recorded at the start of the titration and at every step. Chemical shift perturbations were analyzed as has been described in chapter 3.

Isothermal titration calorimetry

Isothermal titration calorimetry (ITC) experiments were carried out at 303 K on a Microcal (Northampton, MA) VP-ITC microcalorimeter. Experiments were performed and data were analyzed as described in chapter 3.

Molecular graphics were generated using PyMol [150].

Results and discussion

NMR titrations were performed with peptides derived from the SH3- and SH2-domain binding sites in FAK, with gradually shorter spacers between the binding sites (Table 1). Previous ITC and NMR binding experiments have shown that a peptide derived from the SH2 binding site in FAK, p2, binds to the SH2 domain

with an equilibrium dissociation constant (K_d) of 73 nM, and that the interaction is in the slow exchange regime on the NMR time scale (chapter 3). In contrast to this high-affinity interaction, a peptide derived from the SH3 binding site in FAK, p3, was found to bind to the SH3 domain with a K_d of 56 μM in the fast-to-intermediate exchange regime (chapter 2).

Table 1. Peptides derived from FAK (SH3- and SH2-binding sequences underlined) with the length of the spacer between the SH3 binding site (RALPSIP) and the SH2 binding site (pYAEI) decreasing. The peptides containing either the SH3 domain or SH2 domain binding site are also shown. pY denotes a phosphotyrosine residue. All peptides were acetylated and amidated on the N-, and C-termini, respectively.

Peptide	Sequence	Number of residues removed compared to FAK sequence
p32	RALPSIPKLANSEKQGMRTHAVSVSETDDpYAEIIDEED	0
p-3	RALPSIPKLANSEKQGMAVSVSETDDpYAEIIDEED	3
p-7	RALPSIPKLANSEKQSVSETDDpYAEIIDEED	7
p-11	RALPSIPKLANSESETDDpYAEIIDEED	11
p-15	RALPSIPKLANTDDpYAEIIDEED	15
p-16	RALPSIPKLANDDpYAEIIDEED	16
p-17	RALPSIPKLADDpYAEIIDEED	17
p-19	RALPSIPKDDpYAEIIDEED	19
p2	ETDDpYAEIIDEED	-
p3	RALPSIPKL	-

Titrations of Src SH32 with peptide p32, which contains both the SH3- and SH2-binding motifs separated by the full-length sequence as it is present in FAK, leads to chemical shift perturbations in the SH3 and SH2 domains that are similar to those caused by peptides p3 and p2 (Fig. 4.1), indicating that the peptide-protein

interaction is confined to the SH3 and SH2 peptide binding faces on the protein. The chemical exchange behaviour for SH3 amides in the titration with p32 differs from that observed in the titration with p3. When p32 binds to Src SH32 both the resonances in the SH2 and SH3 domain show slow-exchange behaviour, whereas for p3 fast-to-intermediate chemical exchange is seen for all SH3 resonances affected by binding. This observation is illustrated in Fig. 4.2 for residues T17. Residue G155 is part of the SH2 binding site.

Peptides containing the SH2-binding region in FAK bind too tightly to the Src SH2 domain for the binding affinity to be determined with NMR (see chapter 3) and, thus, ITC was used instead. Due to solubility problems for the longest peptides p32 and p-3, no high-quality ITC data could be obtained for these peptides. For peptide p-7, which is still long enough to span the distance between the SH3 domain and SH2 domain peptide-binding faces, ITC data were fitted to a one-site binding model, yielding a K_d of 28 nM (Fig. 4.3). This agrees well with values determined with surface plasmon resonance and ITC by Thomas et al. [139] and Arold et al. [215], for the binding of the Src and Fyn SH32 domains to a FAK peptide containing both the SH3 and SH2 binding sites. Comparison with results from ITC experiments involving binding of p3 or p2 to SH32 shows that the free energy change upon binding the peptide containing both an SH3- and SH2-binding site is less than the sum of the free energy changes upon binding p2 and p3 (Table 2), indicating that the binding is anti-cooperative. This is in agreement with what has been shown for the SH32 domains of Fyn, for which it was proposed that restriction of the conformational freedom of the FAK peptide, together with possible binding-induced partial structure in the peptide, causes a small entropic penalty [216]. In the absence of favourable contributions from additional contacts outside the SH3- and SH2-binding sites, this leads to anti-cooperative binding.

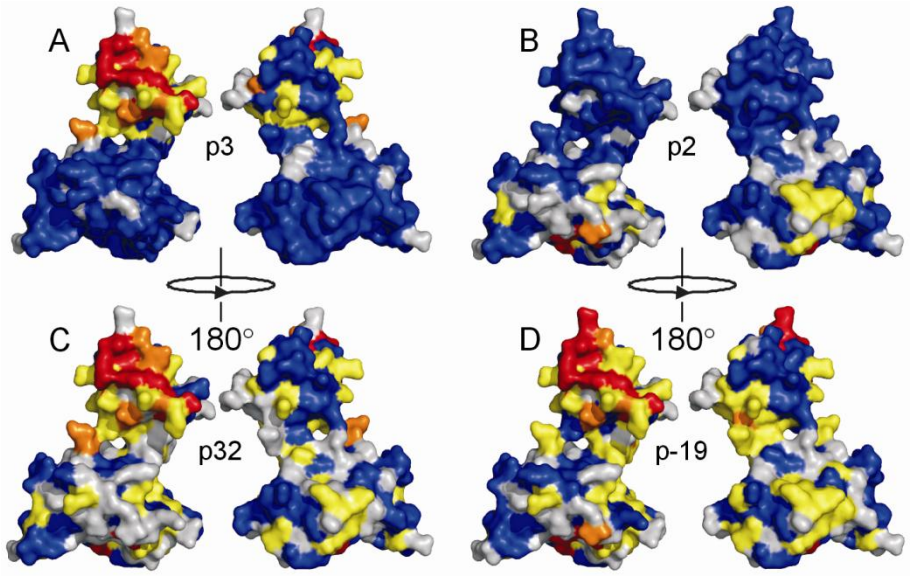

Figure 4.1. Average chemical shift perturbations ($\Delta\delta_{avg}$, Eq. 1, chapter 1) in Src SH32 caused by peptide titrations. **A)** Shifts caused by peptide p3 at a peptide-to-protein molar ratio of 10:1 **B)** shifts caused by peptide p2 at a ratio of 5:1 **C)** Shifts caused by peptide p32, ratio 1.5:1 **D)** Shifts caused by peptide p-19 at a peptide-to-protein ratio of 10:1. Chemical shift perturbations are coloured according to size and mapped onto the surface of SH32 taken from a structure of nearly full-length Src in the inactive state, PDB entry 1FMK [217]. Red: $\Delta\delta_{avg}\geq 0.3$ ppm; orange: $0.3>\Delta\delta_{avg}\geq 0.1$ ppm; yellow: $0.1>\Delta\delta_{avg}\geq 0.04$ ppm; blue: $\Delta\delta_{avg}<0.04$ ppm. Non-assigned residues are shown in grey.

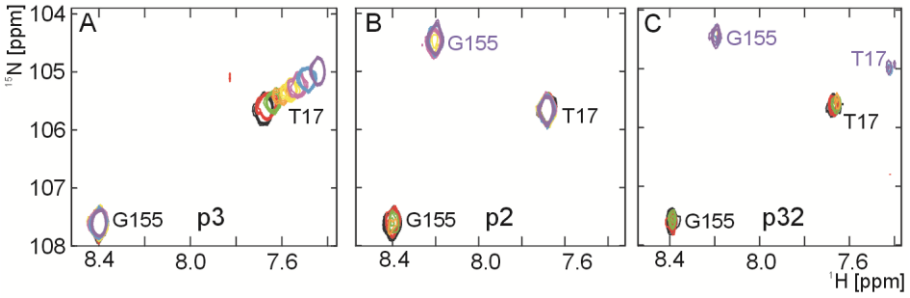

Figure 4.2. Detail from HSQC spectra of Src SH32 in titrations with peptides **A)** p3, **B)** p2 and **C)** p32. Spectra from a few titration points are shown overlaid, with starting points (free protein) in black and titration end points shown in purple.

Table 2. Thermodynamic parameters for peptides binding to Src SH32. Uncertainties in K, ΔH and ΔG are the standard deviations of three experiments, the uncertainty in TΔS was calculated using standard error propagation.

Peptide	**K_a (M^{-1})**	**ΔH (kcal*mol^{-1})**	**TΔS (kcal*mol^{-1})**	**ΔG (kcal*mol^{-1})**	**Fitting model**
p3	10.0±0.3 x 10^4	-14.0 ±0.7	-8.5±0.7	-5.6±0.1	One-site
p2	6.5±1.6 x 10^6	-9.4±0.3	0.1±0.4	-9.4±0.1	One-site
p-7	3.6±0.4 x 10^7	-20.5±0.3	-10.1±0.3	-10.5±0.1	One-site
p-19	2.4±0.1 x 10^6	-12.1±0.1	-3.2±0.1	-8.8±0.1	One-site

ITC data for peptide p-19 interacting with SH32 was fitted to a one-site binding model, yielding a K_a of 2.4 ± 0.1 x 10^6 M^{-1} (Table 2 and Fig. 4.3D). The determined equilibrium association constant is comparable to the affinity of the SH32 domains for peptide p2, containing only the SH2-binding site. In addition to the one-site binding model a two-site binding model was tried, but this did not improve the fit.

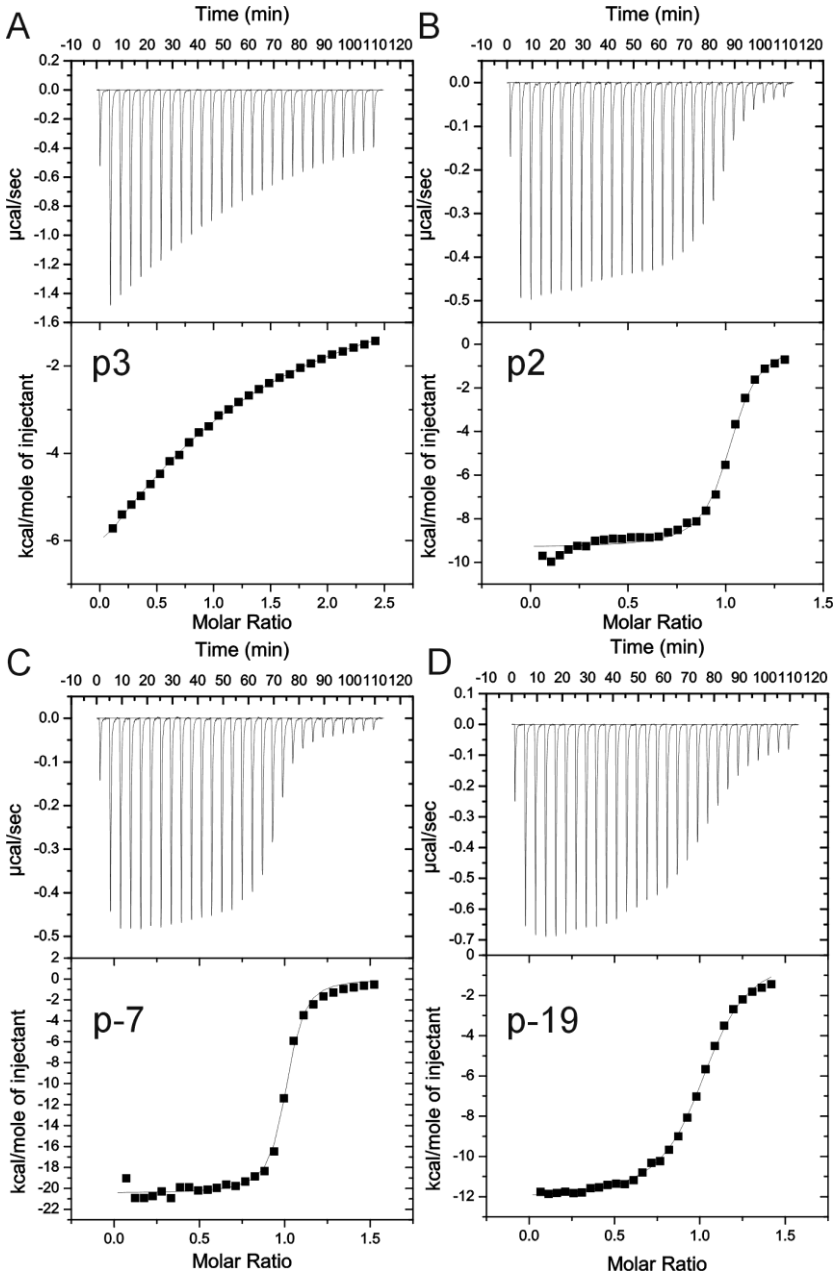

Figure 4.3. Representative isothermal titration calorimetry curves for the binding of Src SH32 to peptides A) p3, B) p2, C) p-7 and D) p-19. Top panel: raw data after baseline correction. Bottom panel: integrated data corrected for the heat of dilution of the peptide. The solid line in the bottom panel represents the best fit to a one-site binding model.

Examination of the exchange characteristics of SH2 and SH3 resonances in NMR titrations with gradually shorter peptides into an SH32 sample shows that for all peptides containing the phosphotyrosine the SH2 domain resonances remain in slow exchange. For the longer peptides the SH3 resonances also show slow exchange between free and bound forms, but for peptides with more than 15 amino acid residues removed from the linker the exchange becomes faster. For peptide p-16 slow-to-intermediate exchange was observed, for peptide p-17 the SH3 resonances are in intermediate-to-fast exchange, and for the shortest peptide, p-19, fast exchange behaviour is observed for the SH3 resonances (Fig. 4.4).

For the shorter peptides, such as p-19, the distance between the SH3- and SH2-binding sites is too small for the peptide to bind to both domains simultaneously, causing the domains to compete for peptide binding. Positioning the SH3 domain and SH2 domain binding faces close enough together for simultaneous binding would require substantial domain rearrangements, which would be reflected by chemical shift perturbations of the linker residues. The chemical shift perturbations for these residues are all small, however, indicating that the relative orientation of the domains remains unchanged. In light of the large difference in binding affinity between the two domains (about 3 orders of magnitude), it would be expected that virtually all available peptide would bind the SH2 domain until the SH2 domain is saturated, and only then would the excess peptide bind to the SH3 domain. This would yield a sigmoidal binding curve for the SH3 domain. The chemical shift perturbations for a few SH3 resonances in the titration with p-19 are plotted against the molar ratio of peptide to protein in Fig. 4.5.

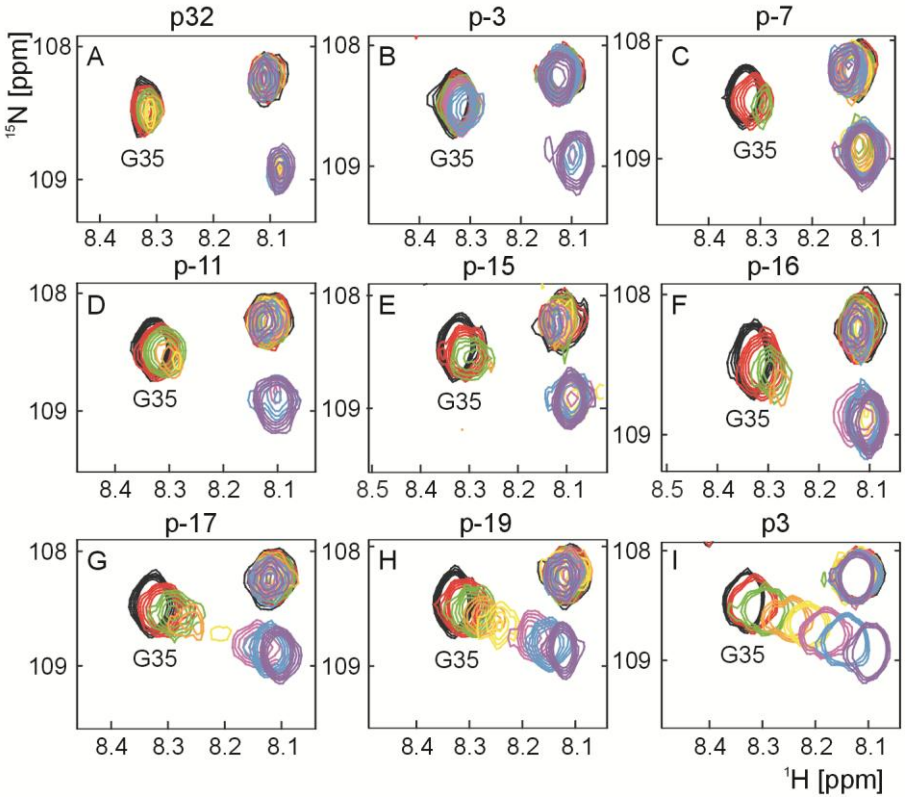

Figure 4.4. Detail from HSQC spectra of Src SH32 in titrations with peptides in which the distance separating the SH2- and SH3-binding sites has been gradually decreased from A) to H). For comparison the titration with peptide p3, containing only the SH3-binding site, is shown in I). Spectra from a few titration points are shown overlaid, with starting points (free protein) in black and titration end points shown in purple.

In contrast to what was expected, the SH3 binding curve for peptide p-19 does not display a sigmoidal binding curve, but chemical shift perturbations are observed for SH3 resonances already at low concentrations. This means that a significant fraction of the peptide binds to the SH3 domain, to an extent that would indicate a considerably larger binding affinity than what has been determined for the proline-rich sequence binding to the SH3 domain. In Fig. 4.5 a fit of the chemical shift perturbations to a 1:1 binding model is shown. It was assumed that the SH2 domain competes for the peptide with the SH3 domain, effectively decreasing the

concentration of the peptide available for binding the SH3 domain, at least at peptide-to-protein ratios smaller than 1. On the basis of this model, a correction factor for the peptide concentration was introduced as an additional parameter (for details see chapter 3). The best fit yields a correction factor of 3.6, with a binding constant of $1.0 \pm 0.4 \times 10^5$ M^{-1} for the peptide interacting with the SH3 domain within SH32. This could suggest that about 30% of the peptide binds to the SH3 domain and 70% to the SH2 domain, which would imply a remarkably high affinity of the p-19 peptide for the SH3 domain, only about 2.5-fold less than for the SH2 domain.

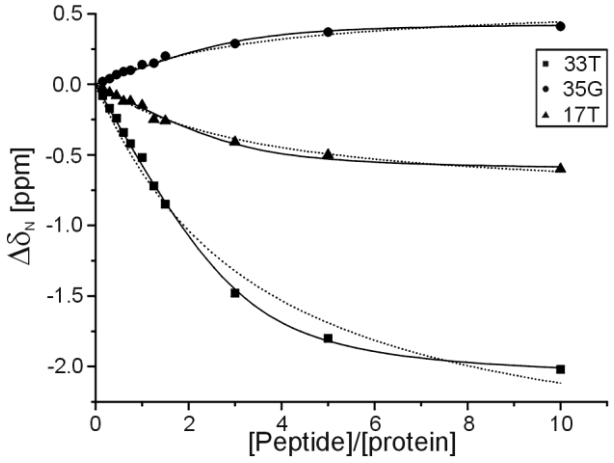

Figure 4.5. Chemical shift perturbations for a few SH3 domain amides within the SH32 tandem upon titration with peptide p-19. The solid line represents a fit to a 1:1 binding model, yielding a correction factor for the peptide concentration of 3.6, $K_a = 1.0 \pm 0.4 \times 10^5$ M^{-1}. For comparison the best fit without a correction factor is shown (dotted line), $K_a = 1.3 \times 10^3$ M^{-1}.

The data suggest that the apparent affinity of the SH3 domain for its binding motif within the short peptide containing both an SH2- and SH3-binding site, p-19, is higher than the affinity of the SH3 domain for peptide p3, which contains only the SH3 binding site. Thus, the presence of the SH2 binding site in the peptide affects the binding of the SH3 motif to the SH3 domain within the context of the SH32 protein. The increased affinity of peptide p-19 for the SH3 domain cannot be

explained by interactions of the SH3 domain with the SH2 binding site in the peptide because the NMR experiments showed that peptide p2, containing the SH2 binding motif only, does not interact with the SH3 part of SH32. This conclusion is further supported by the fact that chemical shift perturbations in the SH3 domain caused by the interaction with peptide p-19 are very similar to those caused by binding of peptide p3, which does not contain the SH2-binding motif (Fig. 4.1).

Binding of SH32 to short peptides with bindings sites for both domains can be described by a thermodynamic cycle for the free protein and peptide, two 1:1 complexes and the 2:1 peptide-to-protein complex (Fig. 4.6A). Based on the experimental observations it can be concluded that the ratio of K_1 and K_3 is merely 2.5. The values of K_2 and K_4 remain as yet undetermined.

The data indicate a much tighter affinity for the SH3 domain for the peptide with the SH2 binding site than for p3. It is proposed that long-range electrostatic interactions between the negative charges surrounding the SH2 core binding motif and charges in the SH2 domain help recruit the peptide to the SH32. Such interactions have previously been shown to be important for SH2 domain-peptide interactions, increasing the affinity of the SH2 domain for the peptide more than 30-fold and, at the same time, resulting in a dynamic mode of interaction in spite of the high affinity (see chapter 3). Recruitment of the peptide to the SH32 domains via long-range charge-charge interactions leads to a dynamic encounter state, from which the peptide may associate with either the SH2 or the SH3 domain (Fig. 4.6B). Thus, SH3 binding profits from the formation of a relatively stable encounter complex, as has been observed for other complexes [100;218], increasing the affinity of the interaction. In this way the SH3 domain is able to compete effectively with the SH2 domain for peptide binding. The association constants for a second peptide will differ from the first one, because the positive charges on the SH2 domain will be shielded by negative charges on the peptide.

SH2 domains interact with their phosphotyrosine target sequences with a considerably higher binding affinity than SH3 domains interact with proline-rich sequences. For isolated domains the binding affinity of peptides for the SH3 domain-interaction can be around a thousand-fold lower than for the SH2 domain (see chapters 2 and 3). In light of this large difference in binding affinity one might raise the question how much the SH3 domains contributes to the interaction of Src with target proteins. The results presented here show that via a dynamic encounter state, the SH3 domain affinity can be higher in the context of a multidomain protein than what is observed for individual domains.

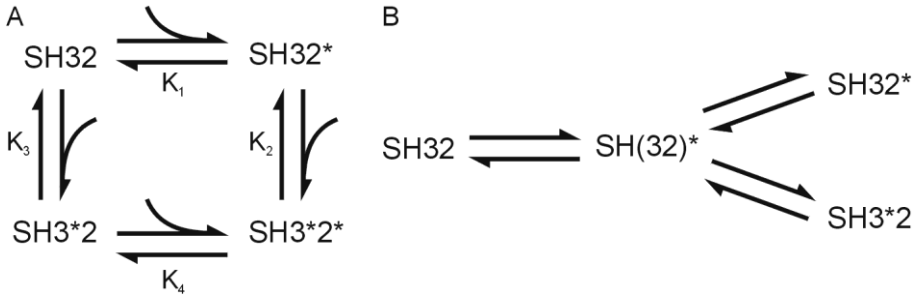

Figure 4.6. A) Model of interaction of Src SH32 with a peptide containing both SH2- and SH3-binding sites in which the distance between the sites is too large for a single peptide to bind simultaneously to both domains. In this model, a peptide first binds the SH32 tandem either via the SH3or the SH2 domain, followed by a second peptide binding the other domain. An asterisk symbolizes the domain bound to peptide, and K_1 to K_4 denote the equilibrium association constants. B) Electrostatic interactions between positively charged residues in the SH2 domain and negatively charged residues at the SH2-binding site in the peptide help recruit the peptide into an encounter complex with the SH32 domains. From the encounter complex the peptide can either bind to the SH2 or the SH3 domain, increasing K_3 compared to peptide binding to an isolated SH3 domain.

Conclusions

Including both the SH3- and SH2- binding motifs in peptides derived from FAK increases the affinity for binding to Src SH32, compared to the individual domains interacting with their respective binding sites. If the distance between the SH3- and

SH2-binding motifs is decreased to a point that the length separating them is no longer sufficient for the peptide to interact simultaneously with the SH3 and SH2 domains, the SH3 domain is still able to compete with the SH2 domain for peptide binding, in spite of the large difference in binding affinity for the isolated domains. We propose a model in which long-range electrostatic interactions between the negative residues surrounding the SH2-binding site and positive charges in the SH2 domain help recruit the peptide into a dynamic encounter complex, from which the peptide can bind either the SH3 or SH2 domain, increasing the affinity of the SH3 domain-peptide interaction. The distance between SH2- and SH3-binding motifs in Src target proteins differ, and, thus, such a dynamic intermediate may be a more general feature of SH3- and SH2 domain-mediated interactions.

Chapter 5

Expression, purification and in vitro phosphorylation of the focal adhesion kinase catalytic domain

Abstract

In this chapter a protocol for the expression of the FAK catalytic domain using a baculovirus expression vector system is presented, together with a protocol for purification and in vitro phosphorylation of the kinase domain.

Introduction

For protein interaction studies or structural biology of proteins, relatively large amounts of pure protein are required. Eukaryotic kinases are notoriously difficult to express in *Escherichia coli*, often showing low expression levels or ending up as insoluble aggregates. In some cases, especially for small proteins, protocols for solubilization and folding can be successfully designed. For kinase domains, however, which in addition to being relatively large also possess catalytic activity, the recovery of properly folded and active protein from inclusion bodies is rarely successful. Recent strategies for improving expression of kinases in *E .coli* include coexpression of chaperones [219] to help with correct folding. In cases where the active kinase is toxic to cells or where the phosphorylated protein is metastable, coexpression of phosphatases can improve yield and solubility [220;221]. In many cases however, it is necessary to look for a more suitable expression system. For structural biology purposes, most tyrosine kinases have been expressed in baculovirus-infected insect cells [222].

The baculovirus expression vector system (BEVS) is widely used in academia and industry for the production of biologically active and functional recombinant proteins. Protein obtained from baculovirus-infected insect cells often shows proper post-translational modifications, such as disulfide-bond formation, glycosylation and acetylation. In general, proteins containing phosphorylation sites will be partially phosphorylated when produced in insect cells.

To date there are no reports of successful large-scale expression of the FAK catalytic domain in bacteria, but both full-length FAK as well as the kinase domain isolated or in combination with the FERM domain have been expressed in insect cells [223-225].

Here, a protocol for expression, purification and in vitro phosphorylation of the FAK kinase domain is presented.

Experimental procedures

Bacmid generation

A DNA fragment corresponding to amino acid residues 390-681 of mouse FAK, followed by 6 C-terminal histidine residues, was generated by PCR using a pET28 vector containing this segment of FAK DNA as a template. The corresponding region of FAK includes the catalytic domain and an N-terminal peptide stretch containing part of the linker connecting the FERM and kinase domains. The PCR product was restricted with *Eco*RI and *Pst*I and ligated into the vector pFastBac Dual, and the integrity of the resulting plasmid, pFastBac Dual-FAK2, was verified by sequencing. Competent *E. coli* DH10Bac cells (Invitrogen) were transformed with pFastBac Dual-FAK2 and plated on LB-agar containing 50 µg/mL kanamycin, 7 µg/mL gentamicin, 10 µg/mL tetracycline, 100 µg/mL X-gal and 40 µg/mL IPTG. Colonies of clones in which successful transposition of FAK DNA into the bacmid had occurred were selected by blue/white screening and the presence of the insert was verified by PCR. The recombinant bacmid was isolated as described in [226] and the DNA concentration was determined via the absorbance at 260 nm.

Insect cell culture and generation of viral stock

Spodoptera frugiperda (Sf9) cells were kept as adherent cultures at 27°C in TNM-FH medium containing 10% FBS (BD biosciences) supplemented with 50 U/mL penicillin and 50 µg/mL streptomycin. Cells were subcultured twice weekly by 1:5 dilution in fresh medium. For recombinant baculovirus generation $2.3x10^6$ cells were seeded in 4 mL TNM-FH medium in a T25 flask. Cells were left to adhere for 30-60 minutes at 27°C. For the transfection mixture 5.2 µg bacmid DNA and 15.6 µL of the liposomal transfection reagent DOTAP were each separately diluted into 300 µL TNM-FH medium without antibiotics, added together in a polystyrene tube and left at room temperature for 45 minutes, allowing nucleic acid/liposomal

complex formation to take place. The attached Sf9 cells were washed once with 2 mL TNM-FH medium without antibiotics, 2.1 mL of the same medium were added to the bacmid/DOTAP mixture and the resulting 2.7 mL were added to the cells. Cells were incubated at 27°C and after 5 h the bacmid/dotap mixture was removed and replaced by 4 mL of normal TNM-FH medium containing antibiotics. Virus was harvested after 5 days, the medium containing the virus was centrifuged at 500 g for 5 minutes, the supernatant was filtered through a 0.4 µm sterile filter and 2% NBS was added to the viral stock before storage at 4°C. For long-term storage an aliquot was kept at -80°C. To increase the titer of the virus the viral stock was amplified by 2-3 further rounds of infection at an estimated MOI of 0.01-0.1, harvesting at 2-4 dpi.

Large scale protein expression

Sf9 cells for protein expression were cultured at 27°C in Insect Xpress medium (BioWhittaker) supplemented with 50 U/mL penicillin and 50 µg/mL streptomycin. For culture scale-up, adherent cultures in T25 flasks were used to seed larger adherent cultures in T75 flasks. Subsequently, 2-3 full T75 flasks were used to start a 100 mL suspension culture in a 250 mL spinner flask, stirring at 55 rpm. To keep cells in the logarithmic growth phase the cell density in suspension cultures was kept between $0.5x10^6$ and $2x10^6$ cells/mL. For further scale-up of cultures, 2 spinner flasks were used to seed a 500-800 mL culture in a 2 l Erlenmeyer flask. The shaker flask culture was incubated at 27°C and 90 rpm. After sufficient increase in cell density, medium was added to a final volume of 800 mL. At a cell density of $2x10^6$ cells/mL recombinant baculovirus was added to the culture at an estimated MOI of 1-10, together with 5 µM leupeptin (Tocris Bioscience) to reduce in-cellprotease activity. Cells were harvested at 5 dpi by centrifugation at 1000 rpm and 4°C for 30 minutes. Cell pellets were gently resuspended by swirling in 20 mM Tris pH8, 500 mM NaCl and 30 mM imidazole kept on ice, and the resuspended cells were stored at -80°C.

Expression and purification of YopH phosphatase

Competent *E. coli* BL21 cells were transformed with the plasmid pCDFDuet containing the YopH tyrosine phosphatase from *Yersinia* [220;227]. The plasmid was generously provided by Dr. Markus Seeliger and Prof. John Kuriyan. Cultures were incubated overnight in LB medium supplemented with 50 µg/mL streptomycin at 37°C while shaking at 250 rpm. The preculture was diluted 1:100 into fresh medium, grown to an OD_{600} of 0.6 and protein expression was induced by the addition of 1 mM IPTG. After 3 h cells were harvested by centrifugation and cell pellets were resuspended in 20 mM HEPES pH 6.8, 50 mM NaCl, 1 mM PMSF and 50 µg/mL DNAse. Cells were lysed by three passages through a French pressure cell and the lysate was cleared by ultracentrifugation (40 000 rpm for 30 minutes at 4°C). The supernatant was loaded onto an ion-exchange column (HiTrap SP, GE Healthcare) equilibrated with 20 mM HEPES pH 6.8, 50 mM NaCl, and protein was eluted with a 50 – 500 mM NaCl gradient. Pure fractions (determined by SDS-PAGE) were pooled and the concentration was determined using a theoretical extinction coefficient at 280 nm of 18910 M^{-1} cm^{-1} [140]. Following the addition of 50% glycerol, the protein was stored at -20°C.

Kinase purification and in vitro phosphorylation

Unless stated otherwise, all purification steps were performed on ice or at 4°C. Cell suspensions were thawed and 1 mM PMSF, 20 µg/mL leupeptin and 50 µg/mL DNAse was added. Cells were lysed by the addition of 0.5% Triton X-100 and the lysate was cleared by ultracentrifugation at 40,000 rpm for 30 minutes. The supernatant was loaded onto an immobilized metal affinity chromatography column (1 mL HisTrap HP, GE Healthcare) using a peristaltic pump. After washing with 20 mM Tris pH8, 500 mM NaCl and 30 mM imidazole, the column was attached to a liquid chromatography system and protein was eluted with the same buffer containing 300 mM imidazole. Protein was dialysed against 50 mM

HEPES pH 7, 100 mM NaCl and 1 mM TCEP. Following dialysis, EDTA to a concentration of 1 mM was added and the protein was treated with YopH phosphatase at a molar ratio of 1:20 for 4 h at RT. Elution buffer containing 300 mM imidazole was added to the phosphatase-treated protein at a volume ratio of 1:15 for a final concentration of 20 mM imidazole, together with 2 mM $MgCl_2$. To remove the phosphatase, protein was again loaded onto an immobilized-metal affinity chromatography column using a peristaltic pump, the column was washed and the protein eluted the same way as before. Protein was dialysed against 20 mM Tris pH 7.4, 150 mM NaCl, 4 mM $MgCl_2$ and 1 mM TCEP for 3h. After dialysis 2 mM ATP and 1 mM activated Na_3VO_4 [228] was added to the kinase domain, which was incubated at RT for 30-45 minutes to allow autophosphorylation of Y397 to take place. The kinase domain was placed at 4°C overnight. In order to separate phosphorylated from unphosphorylated protein, the protein was diluted 2:3 with 20 mM Tris pH 7.6 containing 1 mM Na_3VO_4, bringing the NaCl concentration down to 100 mM, and the protein was loaded onto a 1 mL anion exchange column (1 mL HiTrap Q, GE Healthcare) equilibrated with 20 mM Tris pH 7.6, 100 mM NaCl and 1 mM Na_3VO_4, using a peristaltic pump. Following attachment to a liquid chromatography system the kinase domain was eluted using a gradient of 100-600 mM NaCl.

Kinase domain phosphorylated at Y397 was dialysed against 20 mM HEPES pH 7, 150 mM NaCl, 4 mM $MgCl_2$, 1 mM TCEP and 0.1 mM Na_3VO_4. Protein was concentrated using Spectra/Gel Absorbent (Spectrum laboratories), the protein concentration was determined using a theoretical extinction coefficient at 280 nm of 46870 $MP^{-1}cm^{-1}$ [140] and the protein was stored at -80°C. The final yield of purified protein was around 2 mg per litre culture. For unphosphorylated kinase domain, protein was purified under the same conditions as described above, leaving out the autophosphorylation step (incubation with ATP).

Western blots

Proteins were transferred from SDS-polyacrylamide gels to PVDF membranes and membranes were blocked with 3% BSA in TBS for 1 h at RT. Blots were incubated at RT with primary antibody (1:1000 anti-FAK pY397 from Biosource or 1:2000 anti-His_4 from Qiagen) for 1 h, followed by incubation with horseradish peroxidase-conjugated secondary antibody for 1h. Protein signals were detected by ECL (GE Healthcare).

Results

The purification of the kinase domain and the phosphorylation state of Y397 were monitored by SDS-PAGE and Western blotting of samples taken at different stages of the purification (Fig. 5.1). The western blot against the phosphorylated form of Y397 shows that the kinase domain can become phosphorylated when expressed in Sf9 cells. Treating the protein with YopH phosphatase leads to the complete disappearance of the signal, while incubation with ATP lets the signal reappear. In lane 1-3 in Fig. 5.1, a band is visible below the kinase domain in the SDS-polyacrylamide gel. This band is also visible when western blotting against the His-tag at the C-terminus of the protein, but not visible in the blot against pY397. Most likely this band is the product of proteolytic removal of the N-terminal Y397 linker during protein expression and/or purification. This is further supported by the fact that this band is removed by anion-exchange chromatography, since the region around Y397 provides the dominant contribution to the net negative charge of the protein at the pH used and thus removing this region reduces the affinity of the protein for the anion-exchange column.

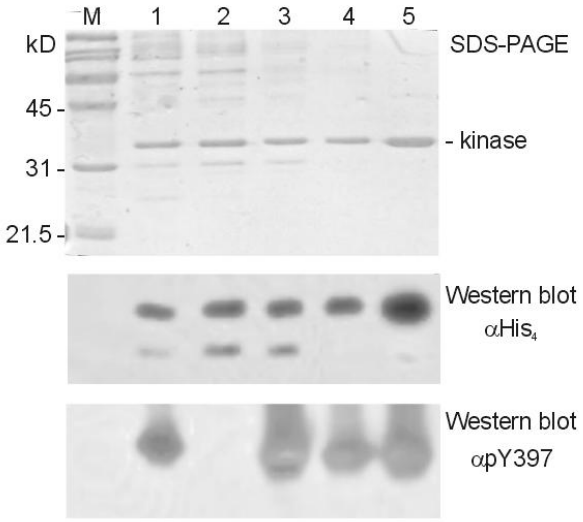

Figure 5.1. Purification and phosphorylation of FAK kinase domain. Top panel: SDS-PAGE, middle panel: western blot against His_4, lower panel: western blot against pY397. Lanes: M: marker, 1: sample after first affinity column, 2: sample after YopH phosphatase treatment, 3: sample after incubation with ATP, 4: sample after ion-exchange column, 5: sample recovered after NMR experiment.

Discussion

The western blots show that, as expected, the protein is at least partly phosphorylated when expressed in insect cells. Under the conditions used, phosphatase treatment is very efficient and no phosphorylation of Y397 can be detected after incubation with YopH. The re-appearance of the pY397 signal shows that the purified kinase domain is active and that the chosen conditions are conducive to autophosphorylation of Y397. This phosphorylation state can be preserved through-out the purification. These results show in a qualitative way that in vitro phosphorylation can be achieved using this protocol. For a more

quantitative analysis another method, such as a radioactivity assay would be required.

Conclusions

The catalytic domain of FAK including the linker containing the SH2 domain binding site Y397 can be expressed in insect cells infected with recombinant baculovirus, purified in an active form, and the phosphorylation state of the protein can be manipulated in vitro.

Chapter 6

The interaction of Src SH2 with the focal adhesion kinase catalytic domain studied by NMR

Abstract

The interaction of the Src SH2 domain with the catalytic domain of FAK, including the Y397 SH2 domain binding site, has been studied using NMR spectroscopy. Analysis of the chemical shift perturbations indicate that the Y397 site is not available for SH2 domain binding. The observed effects are spread over a relatively large area of the SH2 domain and the chemical shift perturbations are small, which is typical for dynamic complexes governed mainly by electrostatic interactions. Competitive binding experiments suggest that although the regular high-affinity SH2 domain binding site in FAK is not involved in the interaction, the binding affinity is still surprisingly high.

Introduction

The interaction of FAK and Src plays a crucial role in a number of signalling pathways, regulating processes such as cell proliferation, survival and migration. The involvement of FAK and Src in many human diseases makes them important drug targets and has made Src and FAK the subject of many structural biology studies. For Src, crystal structures of isolated domains as well as of the full-length protein have been determined, elucidating the mechanism of Src activation [229-233]. Crystal structures also exist of the isolated catalytic domain, FERM domain and FAT domain of FAK [234-237]. More recently, structures of a fragment of FAK comprising both the FERM and kinase domains have been published, suggesting a mechanism of FAK autoinhibition reminiscent of the one for Src [238]. In addition to the crystal structures, NMR structures of the Src SH2 and SH3 domains exist, e.g. [39;239;240], as well as NMR structures of the FAT domain of FAK [241;242]. Examples of FAK and Src structures in the RCSB protein data bank can be found in Table 1.

To date, no NMR studies involving the catalytic domain of FAK have been reported. In spite of the large body of structural biology research on FAK and Src, in vitro studies of the FAK-Src interaction are limited to the study of peptides derived from FAK binding to the SH3 and SH2 domains of Src [139], chapters 2-4 this thesis. In these studies the SH2 and SH3 domains of Src bind to the peptide motifs present in the linker between the FERM and catalytic domains of FAK.

In the regulation of Src and FAK activity intramolecular contacts between domains keep the proteins in an inactive state. In order to investigate whether any intermolecular contacts exist between Src and FAK outside the peptide binding motifs we have studied the interaction of the Src SH2 domain with the catalytic domain of FAK including the part of the FERM domain – kinase linker that contains the Y397 SH2 binding site (Fig. 6.1). Using NMR spectroscopy we find

that although the Y397 site seems unavailable for SH2 binding in the present FAK construct, the SH2 domain still binds the kinase domain, in a way typically seen for dynamic complexes governed mainly by electrostatics.

Table 1. Examples of published structures of Src and FAK.

Fragment	Exp. method	PDB	Reference
Src kinase domain	X-ray diffraction	1YOJ, 1YOL, 1YOM	[243]
Src SH3, SH2 and kinase domains	X-ray diffraction	1Y57	[244]
Src SH2 domain	X-ray diffraction	1SPR, 1SPS	[245]
Src SH2, SH3, kinase domains and c-terminal tail	X-ray diffraction	1FMK	[246]
Src SH2, SH3, kinase domains and c-terminal tail	X-ray diffraction	2SRC	[247]
FAK FAT domain	X-ray diffraction	1K04, 1K05	[248]
FAK FAT domain	X-ray diffraction	1K40	[249]
FAK FERM domain	X-ray diffraction	2AEH, 2AL6	[250]
FAK kinase domain	X-ray diffraction	1MP8	[251]
FAK FERM and kinase domains	X-ray diffraction	2J0J, 2J0L	[252]
Src SH3 domain	NMR	1SRL	[253]
Src SH3 domain	NMR	1RLQ, 1PRM	[39]
Src SH2 domain	NMR	1HCS	[254]
FAK FAT domain	NMR	1KTM	[255]
FAK FAT domain	NMR	1PV3	[256]

Figure 6.1. FAK domain organization. The underlined region corresponds to the fragment of FAK studied in this chapter (the catalytic domain and the linker region containing the SH2-binding site).

Experimental procedures

Protein expression and purification

FAK kinase domain was produced and purified as described in chapter 6, and non-deuterated SH2 domain was produced as described in chapter 3. For production of deuterated SH2 *Escherichia coli* BL21 cells were transformed with SH2-pET28 and incubated overnight in LB medium supplemented with 50 mg/L kanamycin at 37°C while shaking at 250 rpm. The preculture was diluted 1:100 into D_2O-M9 minimal medium with 50 mg/L kanamycin (M9 salts prepared in 100% D_2O, trace elements and other supplements prepared in H_2O, non-deuterated carbon source) using $^{15}NH_4Cl$ as the sole nitrogen source. Cultures were incubated at 37°C and 250 rpm until an OD_{600} of 0.6, the temperature was reduced to 25 °C and protein expression was induced with 0.5 mM IPTG. After 13 h cells were harvested via centrifugation. The SH2 domain was purified as described in chapter 3.

NMR sample preparation and experiments

NMR experiments were recorded at 293 K on a Bruker DMX600 spectrometer equipped with a TCI-Z-GRAD cryoprobe (Bruker, Karlsruhe, Germany). The data were processed with Azara (http://www.bio.cam.ac.uk/azara/) and analyzed using Ansig For Windows [142].

To assess the degree of deuteration of the SH2 domain a 1D NMR spectrum was recorded, from this it was estimated that 70 % of the protein was deuterated (Fig. 6.2). NMR samples contained 40-100 µM $^{2}H,^{15}N$-SH2 in 20 mM HEPES pH 7, 150 mM NaCl, 4 mM $MgCl_2$, 1 mM TCEP (with 0.1 mM Na_3VO_4 for experiments with phosphorylated kinase domain). To the SH2 domain samples phosphorylated or unphosphorylated FAK kinase domain was added and 2D [^{15}N, ^{1}H] TROSY spectra were recorded.

For peptide titrations, a stock solution of 5 mM peptide (for synthesis see chapter 3) was prepared by dissolving peptide in 20 mM HEPES pH 7, 150 mM NaCl, 4 mM $MgCl_2$ and 1 mM TCEP, and adjusting the pH to 7 with small aliquots of 0.1–0.5 M solutions of NaOH. Titrations were performed by the addition of microliter aliquots of peptide to samples containing either 50 µM $^{2}H,^{15}N$ SH2 alone or 50 µM $^{2}H,^{15}N$ SH2 together with 50 µM unlabelled FAK kinase domain in 20 mM HEPES pH 7, 150 mM NaCl, 4 mM $MgCl_2$, 1 mM TCEP. [^{15}N, ^{1}H] TROSY spectra were recorded at the start of the titration and after each addition of peptide.

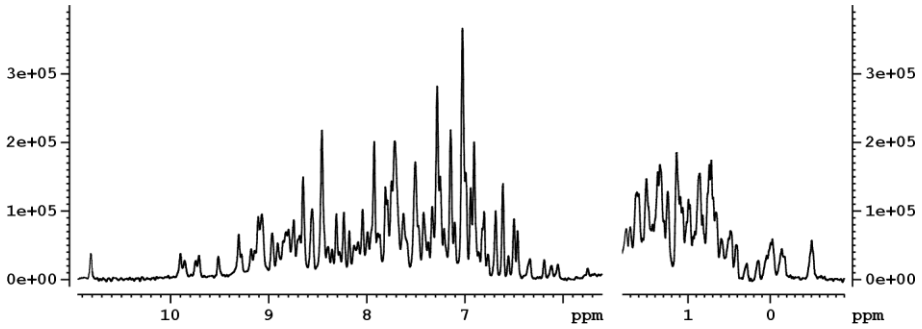

Figure 6.2. ^{1}H NMR spectrum of SH2 domain purified from *E.coli* cultured in deuterated minimal medium (see Exp. Procedures).

Chemical shift perturbation analysis

The average chemical shift perturbations, $\Delta\delta_{avg}$, were calculated according to Eq. 2:

$$\Delta\delta_{avg} = \sqrt{\left(\frac{\left(\Delta\delta^{N}_{binding}/5\right)^2 + \left(\Delta\delta^{H}_{binding}\right)^2}{2}\right)} \quad (1)$$

where $\Delta\delta^{N}_{binding}$ and $\Delta\delta^{H}_{binding}$ are the chemical shift perturbations of the amide nitrogen and amide proton, respectively.

For competitive binding experiments peptides were titrated into samples containing either only SH2 domain or SH2 domain and kinase domain at a 1:1 molar ratio. Chemical shift perturbations of amide resonances were plotted against the molar ratio of peptide-to-protein. A non-linear least-squares global fit to a single-site binding model [145] (Eq. 2) was performed in Origin (OriginLab corporation, Northampton, MA).

$$\Delta\delta_{binding} = \frac{1}{2}\delta_{\infty}\left(A - \sqrt{A^2 - 4R}\right) \quad (2)$$

$$A = 1 + R + \frac{LR + U}{LUK_a}$$

In Eq. 2, R is the molar ratio of peptide-to-protein, $\Delta\delta_{binding}$ is the chemical shift perturbation at a given ratio, $\Delta\delta_{\infty}$ is the chemical shift perturbation at 100% bound protein, L is the initial concentration of ^{15}N-labelled protein, U is the concentration of the peptide stock solution and K_a is the association constant of the complex. The error in K_a was estimated by determining the range of K_a values that produced acceptable fits given the uncertainty in $\Delta\delta_{binding}$. For the peptide titration in the presence of the kinase domain, $\Delta\delta_{\infty}$ values were fixed to the corresponding values obtained from the titration in the absence of the kinase domain.

Competitive binding model and chemical shift perturbation simulations

In order to estimate the dissociation constant of the kinase-SH2 domain complex, chemical shift perturbation simulations were performed and compared to data from the competitive binding experiments. Assuming a model in which the SH2 domain either binds to the peptide or to the kinase domain (Fig. 6.3) the equilibrium association constants can be written:

$$K_1 = \frac{[SH2*P]}{[SH2][P]} \quad (3a), \quad K_2 = \frac{[SH2*K]}{[SH2][K]} \quad (3b)$$

where K_1 is the equilibrium association constant for the SH2-peptide complex, SH2*P denotes SH2 domain bound to peptide, SH2 is free SH2 domain, P is free peptide, K_2 is the equilibrium association constant for the SH2-kinase complex, SH2*K denotes SH2 domain bound to the kinase and K is free kinase domain.

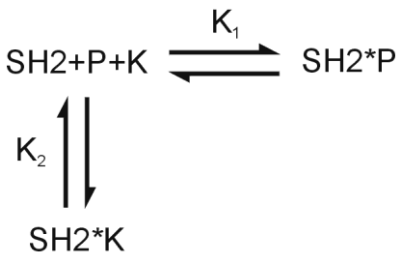

Figure 6.3. Peptide and kinase domain competing for binding to the SH2 domain. SH2 = SH2 domain, P = peptide and K = kinase.

If, at a given point in the titration, we let x be the concentration of SH2 domain bound to peptide, y the concentration of SH2 domain bound to kinase, A, B and C be the total concentration of SH2 domain, peptide and kinase domain, respectively, Eqs. 3a and b can be re-written:

$$K_1 = \frac{x}{(A-x-y)(B-x)} \quad (4a), \quad K_2 = \frac{y}{(A-x-y)(C-y)} \quad (4b)$$

Dividing Eq. 4a by Eq. 4b and solving for x yields:

$$x = \frac{K_1 B y}{C K_2 + y(K_1 - K_2)} \tag{5}$$

In Eq. 5, B and C are known from the experimental parameters, and K_1 can be fixed to the value determined from the titration in the absence of the kinase domain. Using the value of x from Eq. 5 as input in Eq. 4a, y was varied until the value of K_1 calculated from Eq. 4a matched the fixed value used in Eq. 5. This way x, the concentration of SH2 domain bound to peptide, could be determined at each titration point for a given value of K_2, the equilibrium association constant of the SH2 domain-kinase domain complex. The chemical shift perturbation, $\Delta\delta_x$, for an SH2 domain residue at the determined value of x can be predicted using Eq. 6:

$$\Delta\delta_x = \frac{x}{A}\Delta\delta_\infty \tag{6}$$

where x is the concentration of SH2 domain bound to peptide determined using Eqs. 4 and 5, A is the total concentration of SH2 domain in the sample and $\Delta\delta_\infty$ is the chemical shift perturbation for the residue at 100% bound protein, obtained from fitting the data from the titration in the absence of the kinase domain to the model described by Eq. 2. By varying K_2 the predicted chemical shift perturbations for a range of kinase-SH2 domain binding affinities could be compared to the experimental data.

Results

The addition of kinase domain to a sample of $^{1}H,^{15}N$ SH2 domain lead to the majority of the resonances in the HSQC spectrum being broadened beyond detection (Fig. 6.4), indicating that the proteins associate but that the protein

complex is too large to be observed using this method (approximately 48 kDa). To reduce the linewidth of the amide protons deuterated SH2 was produced and TROSY experiments were performed.

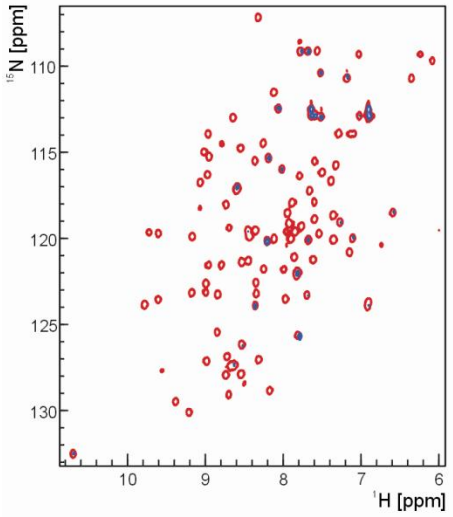

Figure 6.4. Overlaid HSQC spectra of free ^{1}H,^{15}N SH2 domain (red) and ^{1}H,^{15}N SH2 after addition of kinase domain at a ratio of 2:1 kinase to SH2 (blue). The majority of the SH2 peaks disappear upon addition of kinase, indicating binding.

Comparison of the spectrum of free SH2 domain with the spectrum of a sample containing SH2 domain and phosphorylated FAK kinase domain at a molar ratio of 1:1 reveals small chemical shift perturbations for a large number of backbone amide resonances (Fig. 6.5). Although reminiscent of a calibration problem, the chemical shift perturbations were found to be highly reproducible. The shift changes caused by the kinase domain differ from those typically caused both by nonphosphorylated (Fig. 6.6B) and phosphorylated (Fig. 6.6C) peptides binding to the SH2 domain. Chemical shift perturbations caused by the kinase domain are smaller and affect a larger fraction of the SH2 resonances. Mapping the chemical shift perturbations caused by the kinase domain onto the surface of the SH2 domain shows that the general pattern of shifts does not match that seen with peptide binding and that some SH2 domain residues that are strongly affected by peptide binding are not affected by the interaction with the kinase domain (Fig. 6.7). NMR spectra of the SH2 domain together with unphosphorylated kinase domain show a chemical shift perturbation pattern very similar to that caused by

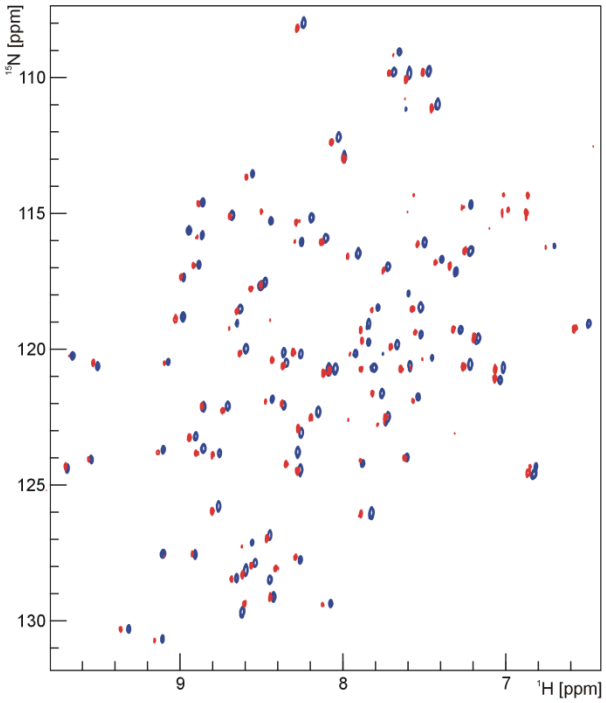

Figure 6.5. Overlaid TROSY spectra of $^{2}H^{,15}N$Src SH2 in the absence of kinase domain (blue) and in the presence of phosphorylated FAK kinase domain at a molar ratio of 1:1 (red).

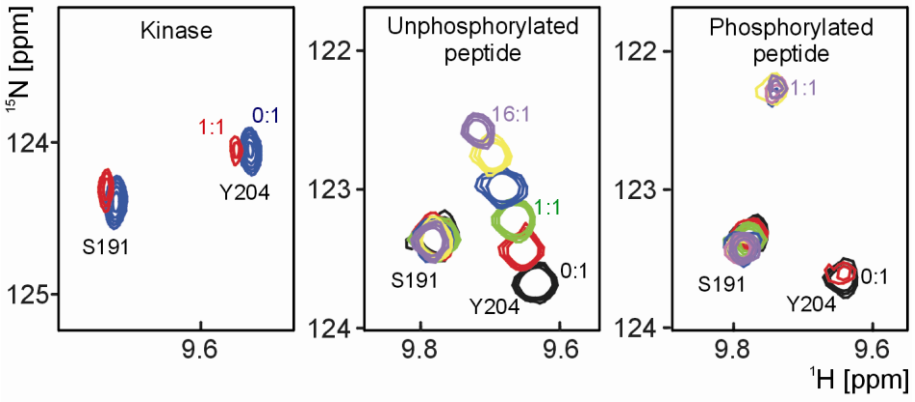

Figure 6.6. A) Detail of TROSY spectrum of free SH2 domain (blue) overlaid with spectrum of a 1:1 mixture of SH2 and FAK kinase domain (red). Spectra recorded at T=293 K and pH=7.0. **B)** Detail of overlaid HSQC spectra from titration of SH2 domain with peptide ETDDYAEIIDEED, T=303K and pH=6.5. **C)** Detail of overlaid HSQC spectra from titration of SH2 domain with peptide ETDDpYAEIIDEED, T=303K and pH=6.5.

the phosphorylated kinase domain, but with generally larger shift changes (Figs. 6.8 and 6.9).

A competitive binding experiment was performed where the unphosphorylated peptide ETDDYAEIIDEED (chapter 3) was titrated into either a 1:1 mixture of SH2 and phosphorylated kinase or into SH2 alone. Titration of peptide into SH2 domain causes significant chemical shift perturbations of some SH2 resonances (Fig. 6.10A), while addition of equal amounts of peptide to the SH2–kinase mixture produced much smaller chemical shift changes (Fig. 6.10B). Some peaks that are shifted in the SH2:kinase complex relative to free SH2 are not affected by peptide binding to SH2 only. When peptide is added to the SH2:kinase complex these resonances start to shift towards the corresponding position in free or peptide bound SH2 (Fig. 6.10C). Both these observations indicate that the peptide is competing with the kinase domain for binding to the SH2 domain. Fitting of the chemical shift perturbations for the titration of SH2 domain with peptide to a 1:1 binding model yields a dissociation constant of 0.17 ± 0.03 mM (Fig 6.11A). This value agrees within the error margins with the previously reported value (chapter 3), despite differences in buffer, pH and temperature. For the titration of SH2 domain with the same peptide in the presence of kinase domain it was assumed that the chemical shift perturbation for fully bound protein, $\Delta\delta_\infty$, for each residue would be the same as in the titration without the kinase domain. By fitting the titration data using fixed $\Delta\delta_\infty$ values obtained from the fit in Fig. 6.11A, an apparent K_d of 2.2 ± 0.4 mM was determined (Fig 6.11B). Including the kinase domain at a ratio of 1:1 with the SH2 domain thus leads to an apparent affinity of the SH2 domain for the peptide that is 13-fold lower than the binding affinity without the kinase domain present.

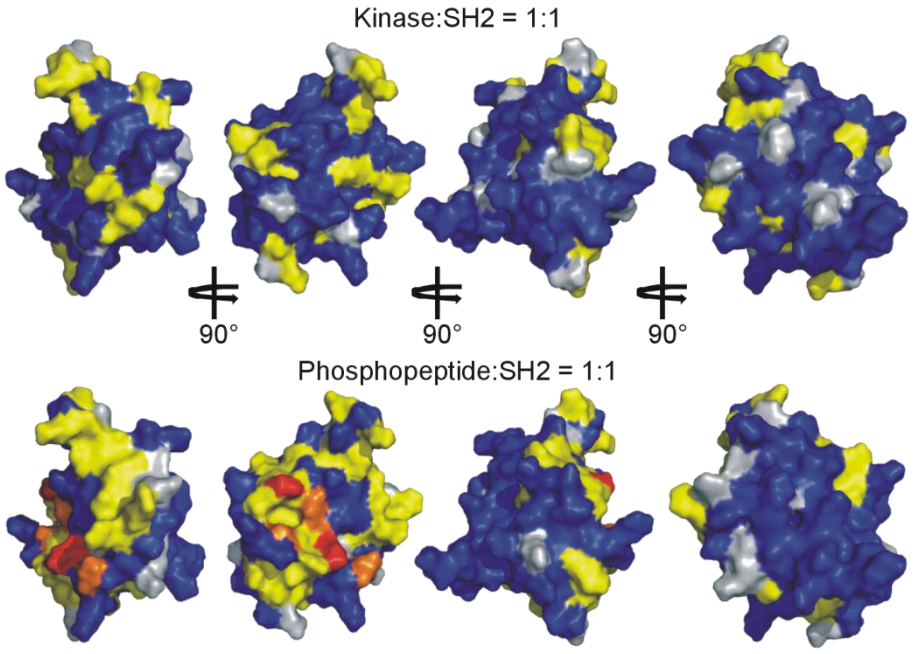

Figure 6.7. Chemical shift perturbations of SH2 domain residues upon addition of phosphorylated FAK kinase domain (top panel) and peptide ETDDpYAEIIDEED (bottom panel), mapped onto the surface of the SH2 domain (PDB structure 1HCS [257]). Residues are coloured according to the size of the average chemical shift perturbation, $\Delta\delta_{avg}$. Red: $\Delta\delta_{avg} \geq 0.3$ ppm; orange: $0.3 > \Delta\delta_{avg} \geq 0.1$ ppm; yellow: $0.1 > \Delta\delta_{avg} \geq 0.04$ ppm; blue: $\Delta\delta_{avg} < 0.04$ ppm. Non-assigned residues are shown in grey.

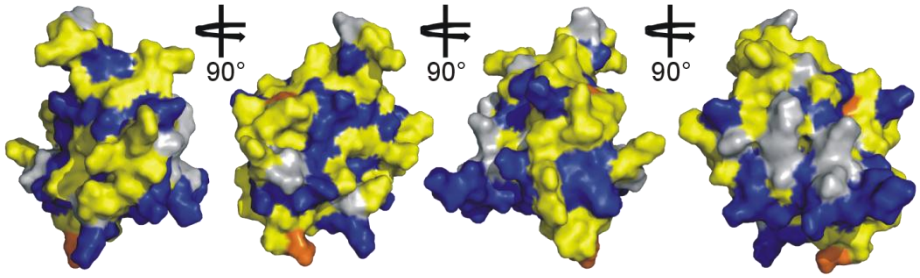

Figure 6.8. Chemical shift perturbations of SH2 domain residues upon addition of unphopshorylated FAK kinase domain at a kinase:SH2 ratio of 1:1, mapped onto the surface of the SH2 domain (PDB structure 1HCS [258]). Residues are coloured according to the size of the average chemical shift perturbation, see Fig. 6.7.

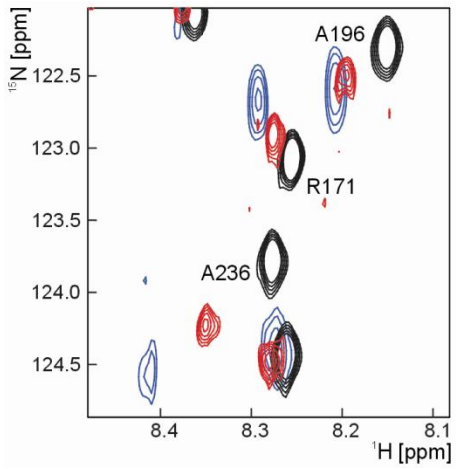

Figure 6.9. Detail of overlaid TROSY spectra of the SH2 domain, showing free SH2 (black), SH2 in complex with phosphorylated kinase (red) and unphosphorylated kinase (blue).

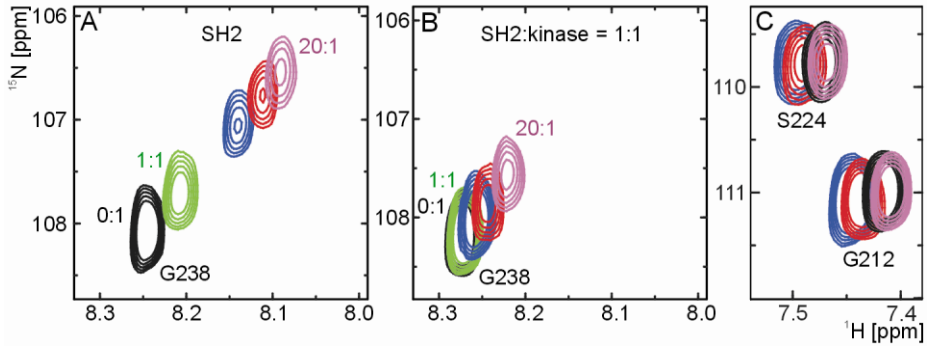

Figure 6.10. Competitive binding experiments, detail of overlaid TROSY spectra of the SH2 domain. **A)** Titration with peptide ETDDYAEIIDEED in the absence of kinase domain. Molar ratios of peptide to SH2 domain are indicated in the figure. **B)** Titration with peptide ETDDYAEIIDEED, in the presence of FAK kinase domain. Molar ratios of peptide to SH2 domain are indicated in the figure. **C)** Black: free SH2 domain. Purple: SH2 domain in presence of peptide, molar ratio 20:1 peptide to protein. Blue: SH2 domain in the presence of kinase domain, molar ratio 1:1. Red: SH2 domain in the presence of kinase domain, molar ratio 1:1 and peptide added at a molar ratio of 20:1 peptide to protein. Resonances that are not affected by peptide binding (black and purple peaks) but that are shifted in the presence of kinase domain (blue peaks) start to shift towards the position they have in free and peptide-bound SH2 domain upon addition of a large excess of peptide (red peaks).

To estimate the affinity of the SH2 domain for the kinase domain, chemical shift perturbation simulations were performed using a competitive binding model (see Exp. Procedures for details). Chemical shift perturbations for a residue in the SH2 domain upon peptide titration in the presence of the kinase domain were simulated for a range of SH2-kinase domain binding affinities (Fig. 6.12). A comparison with the experimental data indicates that the kinase domain binds the SH2 domain with a K_d close to 1 μM (RMSD = 0.03 ppm).

Discussion

The fact that the chemical shift perturbations seen for the interaction of kinase domain with SH2 domain differ completely from the shifts seen for SH2 binding to peptides derived from FAK, suggests that the interaction of the kinase domain with the SH2 domain is independent of the Y397 binding site. The shift changes are small and spread out over a larger portion of the SH2 domain. This is typically observed for dynamic complexes where electrostatics is the main force driving the interaction [259]. The chemical shift perturbations observed for unphosphorylated kinase domain binding to the SH2 domain show the same pattern of shifts, only slightly larger. This difference in size of the chemical shift perturbations may be due to the additional charges on the phosphate group influencing the electrostatics of the interaction. It was already demonstrated that electrostatics play an important role in SH2 domain interactions (chapter 3).

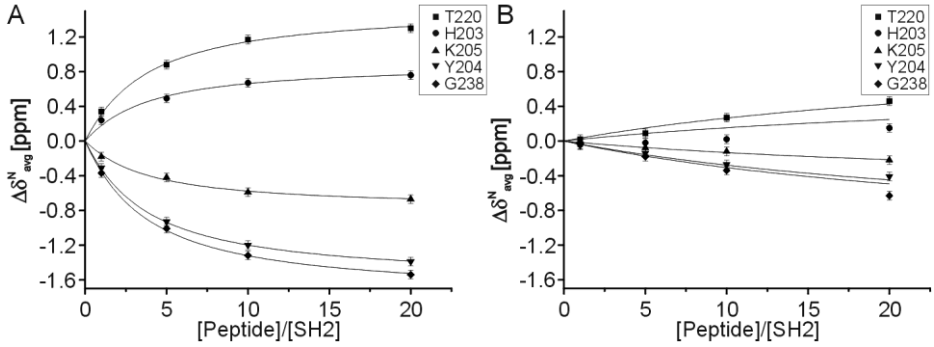

Figure 6.11. ^{15}N chemical shift perturbations of SH2 resonances upon titration with peptide ETDDYAEIIDEED. The curves represent the best global fit to a 1:1 binding model. **A)** peptide added to SH2 domain only, K_d = 0.17 ± 0.03 mM **B)** peptide added to a 1:1 mix of SH2 domain and FAK kinase domain.

Even at a 20:1 molar ratio of peptide to SH2, the chemical shift perturbations of the SH2 amides in the kinase - SH2 mixture are significantly smaller than those seen for the sample with SH2 domain only. In other words the kinase domain is efficiently competing with peptide for binding the SH2 domain, and the SH2 domain displays a considerably higher affinity for the kinase domain than for the unphosphorylated peptide. The K_d of 0.5-1 µM estimated from the chemical shift perturbation simulations indicates a surprisingly high binding affinity, which is unusual for highly dynamic electrostatic complexes. However, previous studies involving the Src SH2 domain binding to peptides have shown that the high-affinity nature of some SH2 domain interactions does not imply that the interaction is static (chapter 3).

There are several possibilities as to why the Y397 binding site is not available for SH2 domain binding. The kinase domain is capable of autophosphorylation of Y397 both in cis and trans in vitro and it is thus possible that the linker is bound to the active site of the kinase domain of the same molecule or of another kinase molecule.

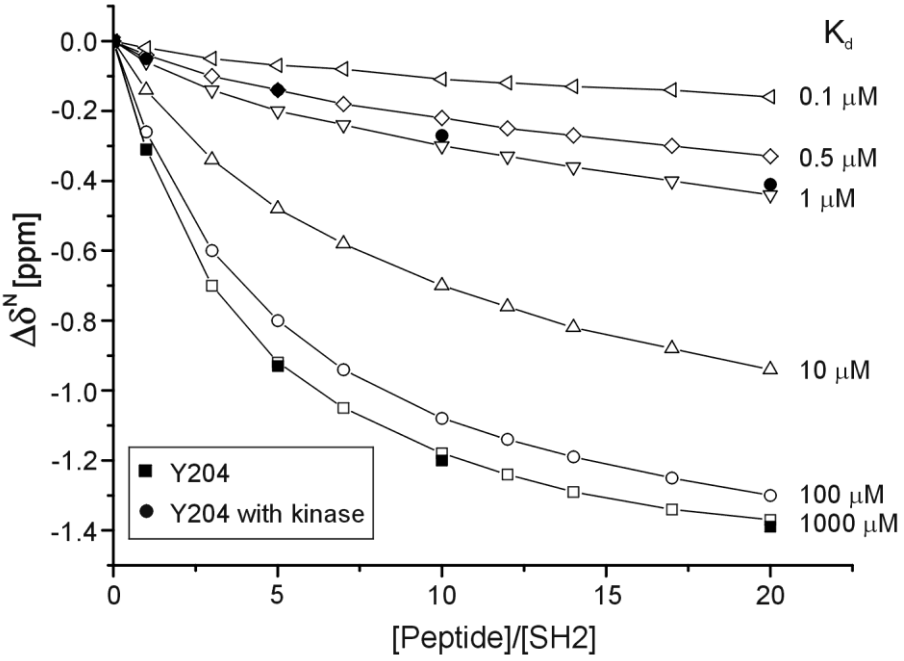

Figure 6.12. ^{15}N chemical shift perturbations of SH2 residue Y204 upon titration with peptide ETDDYAEIIDEED in the presence of the kinase domain (filled circles), together with chemical shift perturbations for the same residue in the presence of the kinase domain simulated for different dissociation constants of the kinase-SH2 domain complex. For comparison, chemical shift perturbations for Y204 upon titration with the same peptide in the absence of the kinase domain are shown as filled squares.

Conclusions

The Src SH2 domain is capable of binding with a high affinity to the catalytic domain of FAK, in a way that does not involve the Y397 region in FAK, and the interaction appears to be highly dynamic and mainly governed by electrostatics. The kinase domain is able to effectively compete with peptides derived from the Y397 binding site for binding to the SH2 domain. The fact that the SH2 domain interacts with the kinase domain with a high affinity independently of the Y397

binding site, suggests that there is still much to be learnt about the interaction of FAK and Src.

Chapter 7

Src-based reporter constructs for fluorescence microscopy of live cells

Abstract

The localization of green fluorescent protein-labelled SH domain constructs in fixed and live cells is studied. Constructs containing two SH2 domains in tandem and constructs containing an SH3 and an SH2 domain in tandem are both found to localize to focal adhesions, although the former shows a clearer localization, reflecting the difference in binding affinity of the SH2 domain and the SH3 domain for focal adhesion components. Overexpression of the phosphotyrosine-binding dual SH2 domain construct is found to lead to increased levels of phosphotyrosine in cells.

Introduction

There is growing interest in the use of fluorescence microscopy in cell biology research, owing to the development of genetically encoded fluorescent markers such as green fluorescent protein (GFP) together with methods such as fluorescence resonance energy transfer (FRET), fluorescence recovery after photobleaching (FRAP), fluorescence loss in photobleaching (FLIP), fluorescence lifetime imaging microscopy (FLIM) and fluorescence correlation spectroscopy (FCS) [260-264]. Using these methods it is possible to study macromolecular mobility and dynamics as well as interactions between macromolecules in live cells [265]. FRET-based biosensors involving a range of serine, threonine and tyrosine kinases have been developed [266-272], including a sensor for monitoring the activation of Src in response to epidermal growth factor or mechanical stimulation [273]. Recently, fluorescence microscopy has been used to study tyrosine phosphorylation in focal adhesions and the dynamics of focal adhesion components [274-276]. Kirchner and co-workers [276] developed an approach for monitoring phosphotyrosine levels in live cells, based on a 'phosphotyrosine reporter', consisting of yellow fluorescent protein (YFP) fused to two Src SH2 domains in tandem. This construct was shown to localize to focal adhesions, and its intensity was linearly correlated with that of an anti-phosphotyrosine antibody labelling. Here, GFP-labelled SH2 domain-SH2 domain (dSH2) and SH3 domain-SH2 domain (SH32) constructs are designed, and their localization in live and fixed LLC-PK1 cells is characterized. We find that both the dSH2 and SH32 constructs localize to focal adhesions, although the dSH2 construct localizes to a higher degree.

Experimental procedures

Using the plasmid pET28-SH32 (Chapter 4) as a template, DNA encoding the SH3 and SH2 domains of mouse Src (residues 147-250) were amplified by PCR. The PCR product was ligated into the vector pEGFP-C1 (Clontech) using the EcoRI and BamHI restriction sites, resulting in the construct GFP-SH32. For the construct GFP-dSH2, comprising GFP followed by two Src SH2 domains in tandem, DNA encoding the SH2 domain was amplified by PCR. In order to facilitate control of the integrity of the construct by restriction two different sets of primers were used, providing a unique restriction site between the SH2 domains as well as on both sides of the tandem domains. The PCR products were restricted with EcoRI and SalI or with SalI and BamHI, and ligated into pEGFP-C1 restricted with EcoRI and BamHI. The GFP-SH32 and GFP-dSH2 constructs were verified by sequencing.

Cells from the porcine renal epithelial cell line LLC-PK1 were cultured in DMEM supplemented with 10% (v/v) fetal calf serum and penicillin/streptomycin, and maintained at 37°C in a humidified atmosphere of 95% air and 5% carbon dioxide. For live-cell imaging, cells were plated in tissue culture dishes with a collagen-coated cover slip bottom and left to adhere for 24 h. For immunofluorescence, cells were plated on collagen-coated glass cover slips in 24-wells plates and incubated for 24 h before transfection. Cells were transfected with 0.8 µg of GFP-SH32 or GFP-dSH2 DNA using Lipofectamine Plus transfection reagent (Invitrogen) following the manufacturer's instructions. YFP-dSH2 DNA [276] was used as a control. Cells were fixed in 3.7% formaldehyde and washed with phosphate buffered saline (PBS), followed by permeabilisation and blocking in 0.1% (v/v) Triton X-100 and 0.5% (w/v) bovine serum albumin in PBS (TBP). Cells were incubated with anti-phosphotyrosine antibody (1:2000 PY99, mouse monoclonal, Santa Cruz Biotechnology), anti-FAK pY397 antibody (1:500 rabbit polyclonal, Biosource) or anti-paxillin pY118 antibody (1:375 rabbit polyclonal, Biosource) in TBP overnight at 4°C. After washing with TBP three times, cells were incubated

with Cy3-labelled secondary antibodies (1:1000 goat anti-mouse or anti-rabbit, Jackson Laboratories) in TBP for 1h at RT. Cover slips were washed twice with TBP and once with PBS, and mounted on glass slides using Aqua-Poly/Mount (Polysciences, Warrington, PA). Cells were analyzed for immunofluorescence using a confocal laser scanning system (Bio-rad Radiance 2100, Bio-Rad, Hercules, CA) equipped with a Nikon Eclipse TE2000-U inverted microscope and a 60x Plan Apo oil-immersion objective (NA 1.4; Nikon, Melville, NY). Images were processed using Corel Draw.

Live cell imaging was performed at 37°C in 5% CO_2 in a climate control unit built up on the stage of a Nikon Eclipse TE2000-U inverted microscope, images were taken using a Bio-Rad Radiance 2100 confocal system with a 60 X Plan Apo (NA 1.4; Nikon) objective lens. Sylvia Le Dévédec is gratefully acknowledged for help with fluorescence microscopy.

Results and discussion

Fluorescence imaging of fixed LLC-PK1 cells after transfection with GFP-dSH2 shows that the construct localizes to focal adhesions (Fig. 7.1a), which are the prime sites of tyrosine phosphorylation in the cell. The GFP-SH32 construct is also found to localize to focal adhesions, although to a lesser extent than the double SH2 domains (Fig. 7.1b), reflecting the higher binding affinity of the SH2 domain for phosphotyrosine sequences compared to the affinity of SH3 domains for their proline-rich target sequences. A single SH2 domain YFP construct has been shown not to exhibit clear localization to focal adhesions [276], but the presence of the SH3 domain in GFP-SH32 contributes sufficiently to the binding affinity for the construct to localize to focal adhesions, albeit to a lesser degree than GFP-dSH2.

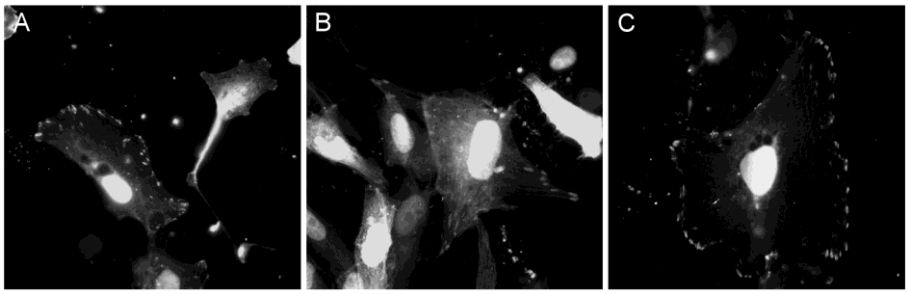

Figure 7.1. Fluorescence images of fixed LLC-PK1 cells transiently transfected with **A)** GFP-dSH2, **B)** GFP-SH32 and **C)** YFP-dSH2. The dSH2 constructs localize more clearly to focal adhesions than the SH32 construct.

The distinct localization of GFP-dSH2 to focal adhesions can also be observed in live cells (Fig. 7.2), making the construct a potentially useful tool for studying dynamic processes involving tyrosine phosphorylation in cells. Immunofluorescence experiments show that the GFP-dSH2 construct colocalizes with anti-phosphotyrosine antibody labelling of fixed cells as well as with labelling with an antibody specific for phosphorylation of Y397 in FAK and Y118 in paxillin (Fig. 7.3). Comparison of phosphotyrosine labelling in cells with different expression levels of GFP-dSH2 shows that the presence of high amounts of GFP-dSH2 leads to higher phosphotyrosine levels at focal adhesions (Fig. 7.4). Most likely, SH2 domain binding protects phosphorylated tyrosine residues from the action of cellular phosphatases, thereby causing the increase in tyrosine phosphorylation. This means that if the GFP-dSH2 construct will be used as phosphotyrosine reporter, care has to be taken to select cells expressing the construct at moderate levels, as to avoid the construct influencing the phosphotyrosine levels [276].

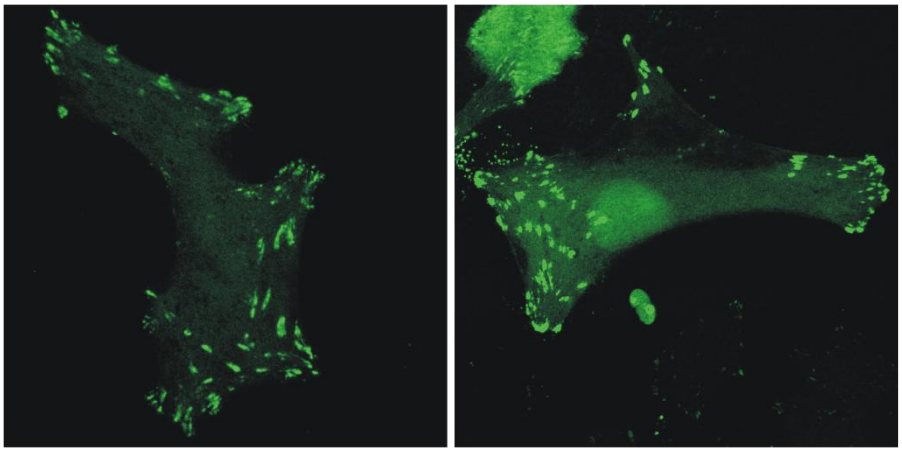

Figure 7.2. Live cell images of LLC-PK1 cells transiently transfected with GFP-dSH2, showing clear localization of GFP-dSH2 to focal adhesions.

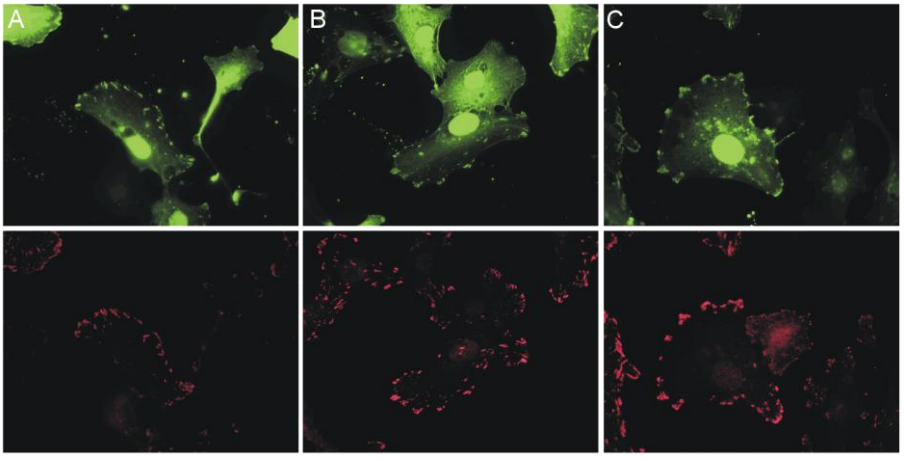

Figure 7.3. Fixed LLC-PK1 cells after transient transfection with GFP-dSH2. **Top panel**: GFP fluorescence **Bottom panel:** Staining with Cy3 using antibodies against **A)** phosphotyrosine **B):** FAK pY397 **C)** Paxillin pY118.

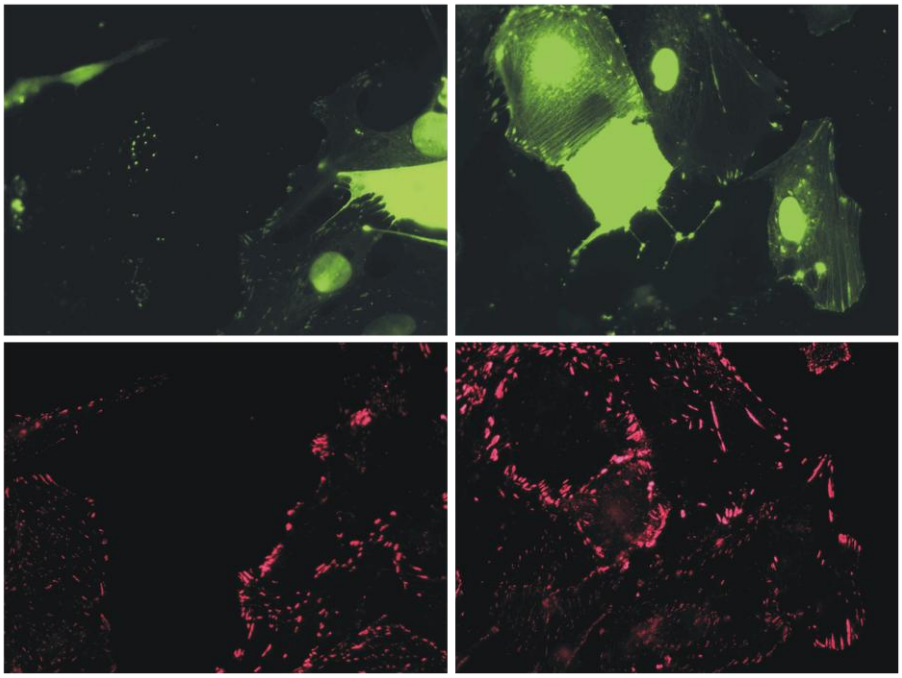

Figure 7.4. Fixed LLC-PK1 cells after transient transfection with GFP-dSH2. **Top panel:** GFP-fluorescence **Bottom panel:** Cy-3 staining using anti-phosphotyrosine antibody. Cells that are expressing GFP-dSH2 at high levels show an increase in phosphotyrosine labelling.

Conclusions

Both the GFP-dSH2 and GFP-SH32 constructs localize to focal adhesions, although the dSH2 construct localizes to a higher degree. High expression levels of GFP-dSH2 influence the phosphotyrosine levels in the cell.

Chapter 8

Interaction between the phosphatidylinositol 3-kinase SH3 domain and a photocleavable cyclic peptide

Abstract

The interaction of the PI3K SH3 domain with a cyclic photocleavable peptide and the linear peptide resulting from UV-irradiation of the cyclic peptide has been studied using NMR spectroscopy. The affinity of the cyclic peptide for the SH3 domain was found to be fourfold lower than the affinity of the photo-irradiated peptide, showing that it is possible to optically modify the strength of the peptide-protein interaction.

This chapter has been published as part of:

I. Takahashi, S. Kuroiwa, H.E. Lindfors, L.A. Ndamba, Y. Hiruma, T. Yajima, N. Okishio, M. Ubbink and S. Hirota (2009). Modulation of protein-ligand interactions by photocleavage of a cyclic peptide using phosphatidylinositol 3-kinase SH3 domain as model system. *J. Pept. Sci.* **15**, 411-416.

Introduction

The use of photoactive molecules as biochemical tools has become increasingly popular in recent years [277-296]. For example, introduction of photocleavable molecules into proteins has enabled studies of the mechanism of protein folding [282;289;290]. In these studies a protein was modified with a photocleavable compound, resulting in partial denaturation. Irradiation with light initiates rapid refolding to the native structure. Photoactive molecules offer the possibility of spatially and temporally controlling peptide-protein interactions inside cells [297]. Caged species can be introduced into the cell in an inactive form, and subsequently be activated by irradiation. This has for example been shown for a phosphorylated peptide that competes with focal adhesion kinase (FAK) for binding to its partner proteins [283]. Phosphate groups in peptides tend to be quickly removed by cellular phosphatases, but by caging the phosphate group the peptides could remain inert until activated. The activated phosphopeptide interferes with the interaction of FAK with downstream signalling proteins, resulting in halting of cell migration.

Phosphoinositide 3-kinase (PI3K) generates 3'-phosphorylated inositol lipids that are key mediators of intracellular signalling [298]. Apart from a catalytical subunit (p110), PI3K also contains a regulatory/adaptor subunit (p85), consisting of two SH2 domains and one SH3 domain. The SH3 domain of PI3K binds to proline-rich motifs with a left-handed type II polyproline (PPII) helix conformation, with the sequence RKLPPRPSK [299].

Here we have studied how the interaction of the SH3 domain of PI3K with its peptide ligand RKLPPRPSK can be controlled optically. To this end we have used a peptide modified with a photocleavable linker which forces the peptide to assume a cyclic conformation [300] (Fig. 8.1). This peptide can be converted into the linear form through light-irradiaton of an appropriate wave-length. Using NMR

spectroscopy we find that the affinity of the SH3 domain for the cyclic peptide is reduced compared to the linear peptide, but surprisingly by a mere factor of four.

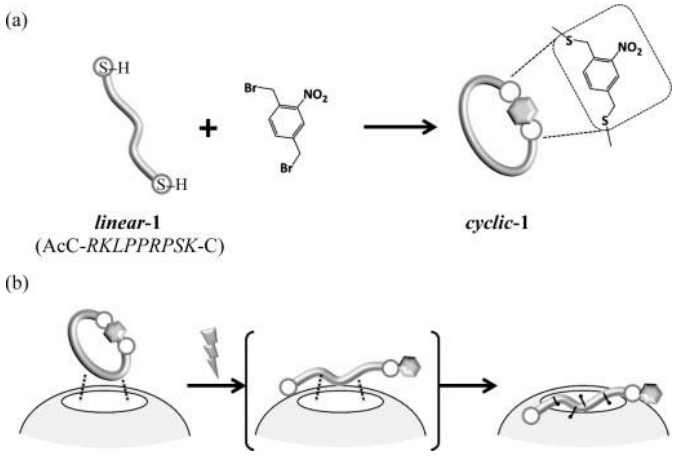

Figure 8.1. Schematic views of **a)** formation of the photocleavable cyclic peptide and **b)** photocontrol of protein-peptide interaction. From [301] copyright (2009), with permission from Wiley Interscience.

Experimental procedures

Peptides

The peptide cyclic-1 consisted of the preferred motif for PI3K SH3 domain binding, RKLPPRPSK, to which cysteines had been added to both termini and the peptide had been further modified with a photolabile linker (2,5-bis(bromomethyl)nitrobenzene), resulting in a photocleavable cyclic peptide. Cyclic-1 peptide and photo-irradiated cyclic-1 peptide (cyclic-1 that had been irradiated with a 355 nm light pulse from a Nd:YAG laser, resulting in a linear peptide) [302] were provided by Prof. Shun Hirota and coworkers (Nara Institute of Science and Technology, Japan). Peptides were received in dry form, with

buffer components already added to yield a 5 mM peptide solution in 50 mM NaP_i pH 7.0 upon addition of 100 µL water. In order for the peptide and protein buffers to match, the peptides were instead dissolved in a 100 mM NaCl solution, yielding peptide stock solutions of 5 mM peptide in 50 mM NaP_i pH 7.0, 100 mM NaCl.

Protein expression and purification

DNA encoding the PI3K SH3 domain, amino acid residues 3-81, with *Escherichia coli* optimized codon usage was purchased from GENEART and ligated into the plasmid pET28a, creating a His-tag at the C-terminus. The resulting construct was verified by sequencing. His-tagged ^{15}N-labelled SH3 domain was produced by culturing freshly transformed *E. coli* BL21 (DE3) cells in M9 minimal medium (50 µg/ml kanamycin) containing $^{15}NH_4Cl$ as the sole nitrogen source. Cells were incubated at 37°C while shaking at 250 rpm until an OD_{600} of 0.8 was reached. Protein expression was induced by the addition of 0.5 mM IPTG and cells were incubated at 22°C for an additional 20 h. Cells were harvested by centrifugation, resuspended in lysis buffer containing 20 mM NaPi pH 7.0, 500 mM NaCl, 1 mM PMSF and 50 µg/ml DNAse, and lysed by sonication. The cell lysate was centrifuged at 15000 rpm and 4°C for 1 h, and the supernatant was loaded onto an immobilized-metal affinity column (HisTrap, GE Health care) equilibrated with 20 mM Tris pH 7.6, 0.5 M NaCl and 5 mM imidazole. After washing with the same buffer containing 60 mM imidazole the protein was eluted using a 500 mM imidazole buffer. The protein was further purified using a size-exclusion chromatography column (Superose 12, GE Healthcare) equilibrated with 50 mM NaPi pH 7.0, 100 mM NaCl. The protein concentration was determined using a theoretical extinction coefficient at 280 nm of 15930 $M^{-1}cm^{-1}$ [140]. The purity was checked by SDS-PAGE and estimated to be above 95%.

NMR experiments

NMR experiments were recorded at 298 K on a Bruker DMX600 spectrometer equipped with a TCI-Z-GRAD cryoprobe (Bruker, Karlsruhe, Germany). The data were processed with Azara (http://www.bio.cam.ac.uk/azara/) and analyzed using Ansig For Windows [142]. For amide backbone resonance assignments 3D [^{15}N,^{1}H] NOESY-HSQC and 3D [^{15}N,^{1}H] TOCSY-HSQC spectra were recorded on a 1 mM ^{15}N SH3 sample in 50 mM NaPi pH 7.0, 100 mM NaCl containing 6% D_2O for lock. Resonances were assigned using published assignments for the PI3K SH3 domain [303]. Lionel Ndamba is gratefully acknowledged for help with resonance assignments. Microliter aliquots of peptide were added to a 0.12 mM sample of ^{15}N SH3 and 2D [^{15}N,^{1}H] HSQC spectra were recorded at each titration point. After titration with cyclic-1 the NMR sample was placed on ice and irradiated with a 365 nm UV/VIS lamp (Spectroline E-series EF-260C) for 20 minutes. An additional 2D [^{15}N,^{1}H] HSQC spectrum was recorded of the irradiated sample.

The chemical shift perturbations were analyzed as described in chapter 6.

Results

Titration of the photocleavable cyclic peptide (cyclic-1) and the linear peptide resulting from light irradiation of cyclic-1 (photo-irradiated cyclic-1) into ^{15}N-labelled SH3 domain both resulted in significant chemical shift perturbations of certain backbone amide resonances in the SH3 domain (Fig. 8.2). At a given peptide-to-protein ratio the linear peptide caused larger shift changes than the cyclic peptide did, indicating a stronger interaction with the SH3 domain for the linear peptide. A comparison of the average chemical shift perturbations in the SH3 domain upon addition of either cyclic-1 or photo-irradiated cyclic-1 at the same

peptide-to-protein ratio shows that all shift changes caused by cyclic-1 are smaller than those caused by photo-irradiated cyclic-1 (Fig. 8.3). The general shift pattern is the same for both peptides; residues displaying the largest chemical shift perturbations in the titration with one peptide also display the largest perturbations in the titration with the other peptide.

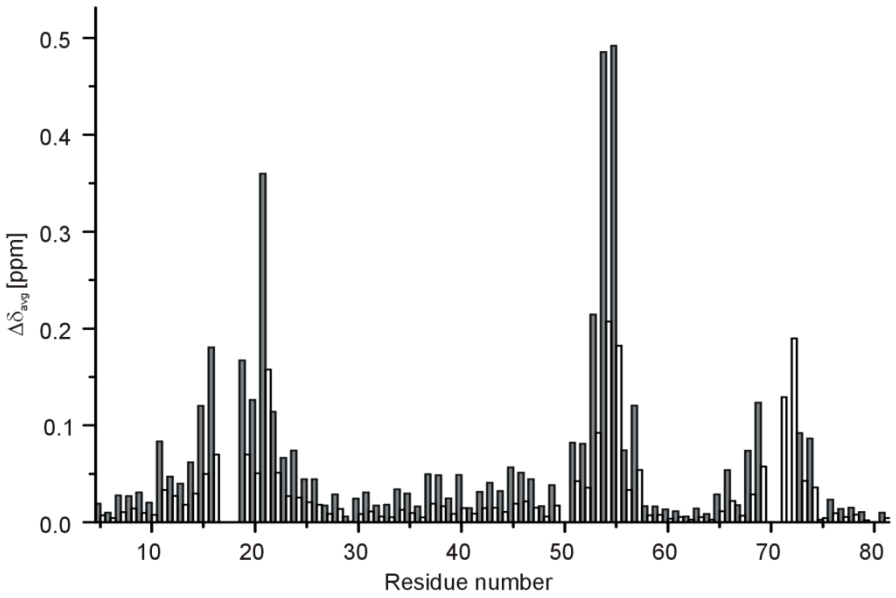

Figure 8.2. Comparison of average chemical shift perturbations of amide nuclei of the PI3K SH3 domain at a molar ratio of peptide to protein of 8.4:1 Open bars: peptide cyclic-1, filled bars: photoirradiated cyclic-1. Missing residues could not be assigned at this point in the titration (prolines or exchange broadened residues).

Fitting the amide nitrogen chemical shift perturbation data for several resonances to a 1:1 binding model yielded dissociation constants (K_d) of 3.4±1.7 mM and 0.9±0.3 mM for cyclic-1 and photo-irradiated cyclic-1, respectively (Fig. 8.4). Thus, linearization of the cyclic peptide by UV-irradiation results in a four-fold stronger binding of the peptide to the SH3 domain. This is further demonstrated by UV-irradiation of the NMR sample containing the SH3 domain and cyclic-1 (see

experimental procedures); a spectrum recorded after UV-irradiation shows much larger chemical shift perturbations than a spectrum recorded of the same sample before irradiation (Fig. 8.5).

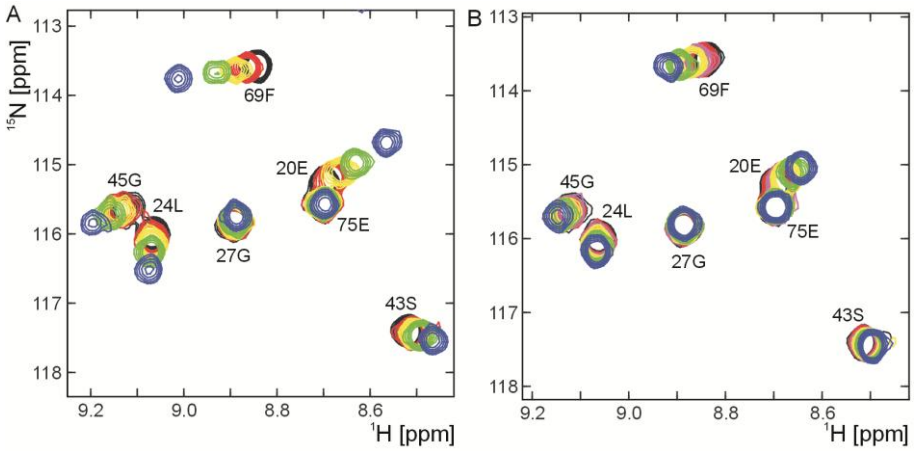

Figure 8.3. Overlay of a region of SH3 domain HSQC spectra from titration with photoirradiated cyclic-1 **(A)** and cyclic-1 **(B)**. Spectra of free SH3 domain are shown in black and spectra of final titration points in blue (final molar ratio of peptide: protein = 8.4:1).

Based on the chemical shift perturbation data fits, the average chemical shift perturbations for all amide resonances were extrapolated to 100% bound protein. A comparison between cyclic-1 and photo-irradiated cyclic-1 shows that although the chemical shift perturbations differ a lot in size at a particular titration point, the values extrapolated to fully bound protein are more similar in size (Fig. 8.6). Mapping of the extrapolated shift changes onto the SH3 domain shows that cyclic-1 and photo-irradiated cyclic-1 bind at the regular peptide-binding face of the SH3 domain, and that the peptides bind in a similar fashion (Fig. 8.7).

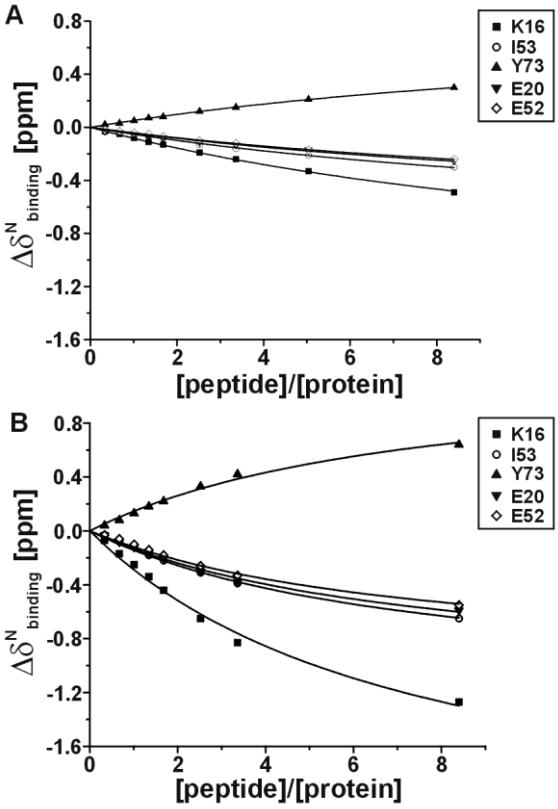

Figure 8.4. Global fit to a one-site binding model (Eq. 1), titration with **(A)** peptide cyclic-1, yielding a dissociation constant of 3.4 ± 1.7 mM and **(B)** photoirradiated cyclic-1 with a dissociation constant of 0.9 ± 0.3 mM.

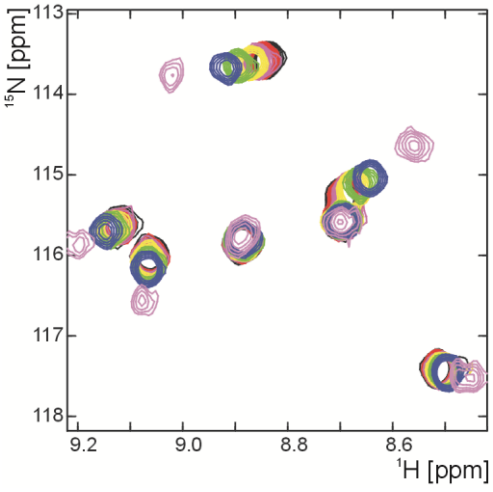

Figure 8.5. Effect of UV-irradiation on chemical shift perturbations of SH3 domain in complex with cyclic-1. Overlay of a region of SH3 domain HSQC spectra from titration with cyclic-1. Spectrum of free SH3 domain is shown in black and the final titration point is shown in blue. In purple is shown the spectrum of the sample from the final titration point, after 20 minutes of UV-irradiation.

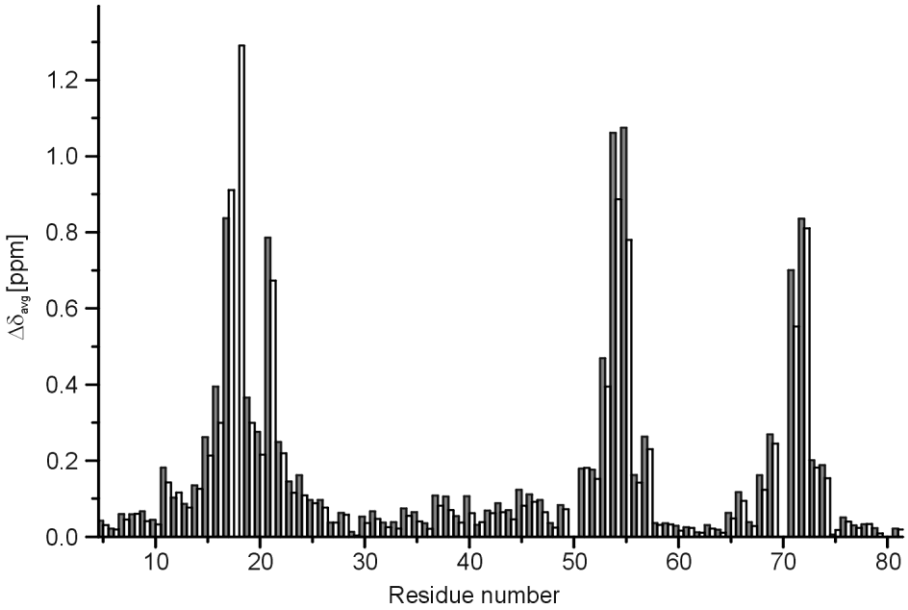

Figure 8.6. Average chemical shift perturbations of amide nuclei of the PI3K SH3 domain extrapolated to fully bound protein. Open bars: peptide cyclic-1, filled bars: photoirradiated cyclic-1. Missing residues could not be assigned at this point in the titration (prolines or exchange broadened residues).

Discussion

Conversion of the cyclic peptide to a linear peptide by light irradiation results in a stronger interaction with the protein (Fig. 8.1B). Whether linear or cyclic, the peptide interacts with the same site on the SH3 domain and seems to bind in a similar way. It is likely that reduced conformational flexibility of the cyclic peptide prevents it from assuming the optimal conformation for interacting with the SH3 domain, leading to the reduced binding affinity. Differences in circular dichroism spectra indicate that the precise binding mode is slightly different for the cyclic and photo-irradiated peptides [304]. The dissociation constant of 0.9±0.3 mM determined for the photo-irradiated peptide binding to the SH3 domain is much larger than the K_d of 9.1 μM reported for the peptide RKLPPRPSK [305]. This

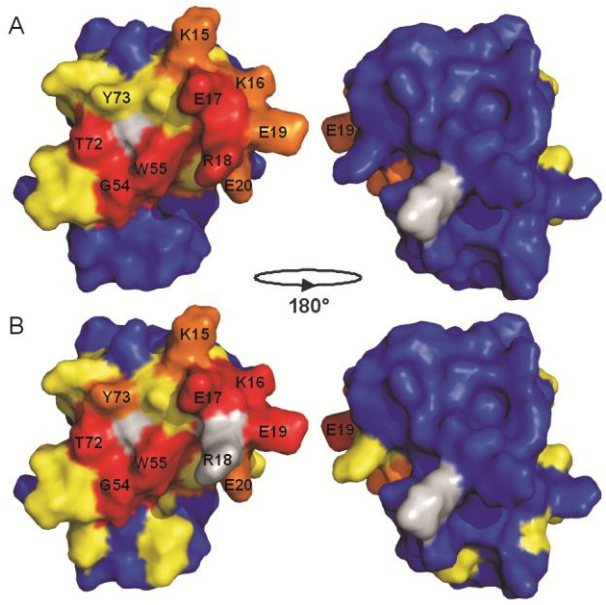

Figure 8.7. Chemical shift perturbations upon titration with peptides cyclic-1 (**A)** and photoirradiated cyclic-1 **(B)** mapped onto the surface of PI3K SH3 domain (PDB entry 1PKS [306]). Shift changes were extrapolated to 100% bound protein and SH3 residues were coloured according to the size of the average chemical shift perturbation (Eq. 2), $\Delta\delta_{avg}$. Red: $\Delta\delta_{avg} \geq 0.3$ ppm; orange: $0.3 > \Delta\delta_{avg} \geq 0.1$ ppm; yellow: $0.1 > \Delta\delta_{avg} \geq 0.04$ ppm; blue: $\Delta\delta_{avg} < 0.04$ ppm. Shown in grey are residues that could not be assigned (proline residues or residues that were exchange-broadened beyond detection at the point of extrapolation).

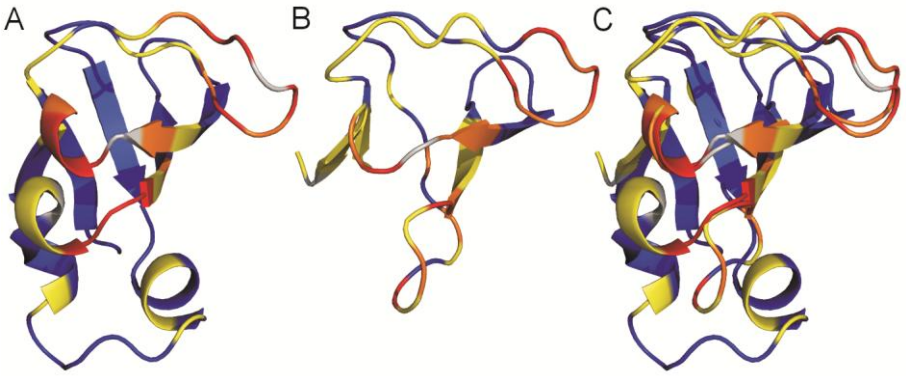

Figure 8.8. Average chemical shift perturbations extrapolated to 100% bound protein and mapped onto the protein structure for titrations of photo-irradiated cyclic-1 peptide into PI3K SH3 (PDB entry 1PKS [307]) **(A)** and peptide P3 (sequence RALPSIPKL, see chapter 2) into Src SH3 (PDB entry 1RLQ [39]) **(B)**. Residues are coloured as described in Fig. 8.7. In **(C)**, (A) and (B) are shown superimposed.

may be the result of steric repulsion between the protein and the attached benzyl derivatives and/or the two cysteine residues of the modified peptide.

The interaction of PI3K SH3 with the linearized peptide can be compared with the interaction of Src SH3 with the proline-rich peptide RALPSIPKL (chapter 2). Alignment of the two SH3 domains with chemical shift perturbations mapped onto the proteins shows that residues in corresponding regions of the proteins are involved in peptide binding (Fig. 8.8), indicating that the peptides bind the respective SH3 domains in a similar way.

Conclusions

The results show that the peptide-protein interaction can be optically controlled by using a photocleavable linker, offering a powerful tool for modulating the interaction between a peptide and a protein. This may also be applicable to other biomolecular interactions. However, the modification lowers the affinity of the peptide, resulting in very weak binding and only a fourfold difference between cyclic and linear peptide.

Chapter 9

General discussion, conclusions and perspectives

The work described in this thesis focuses on protein-peptide and protein-protein interactions mediated by SH2 and SH3 domains. These domains are prototypical protein interaction domains found in cytoplasmic tyrosine kinases, where they are involved both in target recognition and control of kinase activity via intramolecular interactions. Studies of these modular interaction domains and their target sequences has greatly enhanced our understanding of how biological processes are regulated by protein interactions [308-310]. The core peptide sequences recognized by these domains are well-known, but the possibility of interactions outside the core recognition motifs that may modulate binding affinity and protein activity largely remains unexplored, with only a few exceptions [311;312]. The aim of this study was to address this question, to explore the dynamics of SH2 and SH3 mediated interactions, and to investigate how the domains function together with other domains in intra- and intermolecular interactions.

Peptide interactions with isolated SH3 or SH2 domains

The dynamics of peptides derived from FAK interacting with Src SH3 and SH2 domains was investigated in chapters 2 and 3, using paramagnetic NMR methods. Contrary to what might be expected, these experiments demonstrate that although the peptide from the SH3 binding site in FAK binds to the SH3 domain with a low affinity, the peptide binds in a highly specific position and little dynamics is observed. In contrast to this, the peptide derived from SH2-binding site in FAK, which binds to the Src SH2 domain with a very high affinity, interacts with the SH2 domain in a much more dynamic way. This shows that the affinity of an interaction is not necessarily related to the degree of dynamics in the complex.

Peptides binding to SH3 domains can be divided into two groups, depending on the position of an arginine residue relative to the core proline-rich motif. The two classes bind to the SH3 domain in opposite orientations [39]. Paramagnetic effects

observed for a particular aspartic acid residue in the SH3 domain suggest that the peptide derived from FAK, a class I peptide, may for a small fraction of the time also interact with the SH3 domain in the opposite orientation seen for class II peptides. Interestingly, in a recently published molecular dynamics study on the interaction of the N-terminal SH3 domain of C-CRK with a proline-rich motif some simulations also converged to an opposite binding orientation than that seen in the crystal structure of the complex [313]. In these simulations a peptide arginine formed a salt bridge with an aspartic acid residue, in a position where aspartic acid residues are often found for SH3 domains. This corresponds to the same residue for which we noted the unexpected paramagnetic effects, supporting our findings.

The SH2 binding-site in FAK contains a phosphotyrosine in a sequence that conforms to a high-affinity SH2 binding motif. The core binding motif is flanked by a number of negatively charged residues on both sides. Including these residues in a peptide increases the binding affinity around 30-fold compared to a peptide only containing the core binding motif, showing that residues outside the core binding motif can have a significant effect on binding. The increase in binding affinity is most likely due to long-range electrostatic interactions between the negative charges in the peptide and the many positively charged residues in the SH2 domain. This would increase the formation of an encounter complex by recruiting the peptide to the protein, but the charge interactions likely also make the energy difference between the different encounter complex orientations and the specific complex small, which could explain the high degree of dynamics observed for this interaction.

For both the SH2- and SH3-peptide interactions including the spin-label has an effect on the binding affinity. The effect is larger if the spin-label is introduced in the core binding motif, some effect can be seen also when the spin-label is placed outside the core binding sequence. Introducing a spin-label does not affect the observed chemical shift perturbations compared to unlabelled peptides, suggesting

that the mode of binding is still comparable to unlabelled peptide. This is also observed in chapter 8 for the SH3 domain from PI3K binding to a peptide for which the peptide conformation can be optically modified. The peptide can either have a circular structure which prevents the peptide from assuming the optimal conformation for SH3 domain-binding, or a linear structure which binds more efficiently. The introduced modifications are situated outside the core binding motif, but their presence significantly lowers the binding affinity compared to reported values [314].

Interactions involving tandem domains

The SH3- and SH2-binding sites in FAK are separated by a linker that is much longer than what is needed to span the distance between the SH3 and SH2 domains of Src. A long peptide derived from this region of FAK binds to the SH32 tandem with a high affinity (chapter 4), and the interaction is restricted to the canonical SH3- and SH2-binding sites. The binding affinity of the single SH3 domain for its target sequence is low compared to single SH2 domain-peptide interactions (chapters 2 and 3). Including the SH3 domain in tandem with the SH2 domain in a GFP-construct does however improve the localization of the construct to focal adhesions in cells (chapter 7), compared to a single-domain construct, YFP-SH2, that has shown poor localization to focal adhesions [276]. Reflecting the difference in binding affinity, a construct with two SH2 domains in tandem, GFP-dSH2, localizes even more clearly than GFP-SH32 to focal adhesions (chapter 7).

Reducing the length of the linker separating the SH3- and SH2-bidning sites in FAK to a point where the peptide cannot bind simultaneously to both the SH2 and SH3 domain makes the domain compete for peptide binding. Contrary to what would be expected based on the difference in binding affinity, a significant fraction of the peptide still binds to the SH3 domain also at low peptide concentrations

(chapter 4). This suggests that the presence of the SH2 domain and the SH2-binding sequence in the peptide increases the affinity of the SH3 domain for the peptide as well, although the peptide cannot bind both domains at the same time. The model we propose for this is based on the observation that the negative charges surrounding the SH2 core binding site in the peptide increase the affinity of the interaction, but likely also the dynamics. It is perceivable that the peptide and protein forms an encounter complex from which the peptide can either bind the SH3 or SH2 domain, thereby yielding a lower equilibrium dissociation constant for the peptide-SH3 interaction as well. Further experiments and modelling is needed to yield more insights into the process.

Interaction between the Src SH2 domain and the catalytic domain of FAK

Chemical shift perturbations of SH2 domain resonances upon addition of FAK kinase domain show that the SH2 domain binds the kinase domain in a way that differs from how the SH2 domain interacts with peptides derived from FAK (chapter 6). The SH2-binding site in the FERM-kinase linker region of FAK appears to be unavailable for SH2 domain binding in our protein, most likely the linker binds to another region of the kinase domain, either within the same molecule or to another molecule. The observed chemical shift perturbations are small and spread out over a large portion of the SH2 domain, which is typical for dynamic interactions governed by electrostatics. The kinase domain is able to compete with a peptide for binding to the SH2 domain and the estimated binding affinity is surprisingly high. Together this demonstrates that the SH2 domain and the kinase domain can interact in a way that is independent of the SH2-binding site in FAK, with a relatively high affinity, and that domain-domain contacts exist outside the core peptide-binding site. Again, electrostatics appears to be an important factor in interactions mediated by the Src SH2 domain.

Including not only the SH2-binding site but also the part of the linker that contains the proline-rich SH3-binding motif in the kinase construct might make both the SH2- and SH3-binding sites available for SH32 binding and could help shed further light on the FAK-Src interaction.

In conclusion, despite the wealth of information available on the SH-domains, this work illustrates that we still understand surprisingly little of the mechanisms that govern their interactions.

Summary

In order for multicellular life to be possible, cells within an organism need to be able to communicate with each other and respond to signals in their environment. Signal transduction is the process in which a stimulus received from the outside is converted into a response inside the cell. When an external ligand, such as a hormone, binds to a receptor present in the cell membrane a chain of events is initiated in the cell, leading to changes for example in gene expression or enzyme activity. Protein-protein interactions play a central part in signalling cascades and are of vital importance in controlling biological processes.

The work described in this thesis focuses on the interactions mediated by Src homology (SH) domains, a group of protein interaction domains found in proteins involved in phosphotyrosine signalling. Tyrosine phosphorylation, the addition of a phosphate group to tyrosine amino acid residues in proteins, can change the structure and activity of an enzyme and create new protein-interaction sites. This reaction, which is frequently a part of signal transduction pathways, is catalyzed by protein tyrosine kinases, a group of enzymes that often contain SH domains. Src homology 2 (SH2) domains recognise and bind to phosphorylated tyrosine residues, and proteins that contain SH2 domains will therefore be recruited to other proteins that have become phosphorylated in response to an external signal. This can help bring the catalytic domain of the kinase close to its substrate targets for a next round of phosphorylation reactions, transmitting the signal further. Src homology 3 (SH3) domains also function in bringing the appropriate proteins together, by recognizing regions that contain certain sequences rich in the amino acid proline. In addition to recruiting the kinase to the right part of the cell, SH2 and SH3 domains are also involved in regulating the activity of the kinase.

The protein tyrosine kinases focal adhesion kinase (FAK) and Src are involved in processes such as cell proliferation, migration and survival. Their implication in

several types of human cancer makes them important drug targets, and it is thus of general interest to learn more about the details of their interaction. Studying these proteins can also further our understanding of modular signalling proteins in general and of the behaviour of SH domains in protein interactions in particular. Using nuclear magnetic resonance (NMR) spectroscopy and isothermal titration calorimetry (ITC) as the main tools, the interaction of the FAK and Src via the SH2 and SH3 domains of Src has been investigated. To this end, a range of model systems was employed.

Chemical shift perturbation mapping and paramagnetic relaxation enhancement (PRE) NMR was used to study the interaction of the Src SH3 domain with a peptide derived from a proline-rich site in FAK, using peptides containing the spin-labelled amino acid TOAC (chapter 2). Despite the low binding affinity of the peptide for the SH3 domain the peptide was found to bind the SH3 domain in a very well-defined way, with little mobility observed in the complex. The SH2 domain of Src was found to bind with a high-affinity to peptides derived from FAK (chapter 3). Residues flanking the region that is generally regarded as the SH2 binding-motif were found to have a large influence on the binding affinity; including these residues in the peptide lead to a significant increase in binding affinity. Contrary to what was expected for a high-affinity complex, PRE NMR studies with spin-labelled peptides showed that the interaction between the peptide and protein was remarkably dynamic. Given the fact that the flanking residues are mostly negatively charged, whereas the binding face of the SH2 domain contains many positively charged residues, the increase in affinity is likely due to electrostatic interactions that increase the formation of an encounter complex between the peptide and the SH2 domain.

Chemical shift perturbation NMR and ITC studies of peptides containing both the SH3- and SH2-binding sites in FAK together with a Src SH3-SH2 domain tandem (SH32) showed that including both binding sites in the peptide increased the

affinity for the SH32 compared to the individual binding sites (chapter 4). This is also shown in mammalian cells transfected with SH domain constructs, where the SH32 domain tandem localizes to a higher degree to specific regions in the cell, compared to an isolated SH2 domain (chapter 7). The distance between the binding sites as they are present in FAK is much larger than what is required to span the distance between the peptide-binding faces on the SH3 and SH2 domains. We have investigated how decreasing this distance affects the interaction with the SH32. Interestingly, peptides in which the distance between the binding sites is too small to allow simultaneous binding to both the SH2 and SH3 domains, bind the SH3 domain to a much higher extent than what would be expected based on the difference in binding affinity between the isolated SH2 and SH3 domains. Based on these data we have proposed a model for the interaction, describing a new mechanism for peptide-protein complex formation. In this model, the charges on the peptide help recruit the peptide into an encounter complex with the SH32. From the encounter complex the peptide can proceed to form a final complex with either the SH2 domain or the SH3 domain, and this way the charges in the peptide lead to an increase in complex formation with the SH3 domain as well.

A protocol for expressing the catalytic domain of FAK using a baculovirus expression system was developed, together with a purification protocol and a method for manipulating the phosphorylation state of the kinase domain in vitro (chapter 5). This enabled studies of the interaction of the Src SH2 domain together with the entire catalytic domain of FAK, including the SH2 binding site (chapter 6). From chemical shift perturbation data it was shown that the SH2 domain binds the kinase domain, but that the regular SH2-binding site is not available for SH2 binding. Instead, the chemical shift perturbations are typical of dynamic complexes for which the interaction is governed mainly by electrostatics. A competition experiment involving a peptide derived from FAK showed that the apparent binding affinity of the SH2 domain for this peptide is substantially lower in the

presence of the FAK kinase domain than in the absence of the kinase domain. Together these data indicate that the kinase domain binds the SH2 domain tightly, in a way that precludes SH2 domain binding to the added peptide, but that the regular SH2 binding site in FAK is not involved. It is possible that the kinase domain binds (intra- or intermolecularly) to this site itself, thereby sequestering it from SH2 domain binding.

In addition to interactions mediated by the Src SH3 and SH2 domains, the binding of the SH3 domain from the PI3K p85 subunit to proline-rich peptides with different structural conformations has been investigated (chapter 8). The interaction of the SH3 domain with peptides that had been modified with a photo-labile linker to assume a cyclic conformation was compared to the interaction with peptides after photo-irradiation, making the peptides return to a linear conformation. It was found that although the peptides bind in similar ways to the SH3 domain the binding affinity for the linear peptides was increased relative to the cyclic peptides, offering a way to control the affinity of the peptide-protein interaction using photo-irradiation.

From the results presented in this thesis we learn that in macromolecular complexes a high binding affinity does not always correlate with well-defined complex orientation: tight binding can still involve mobility of the molecules relative to each other in the complex, just as weakly interacting molecules can have well-defined relative positions. Furthermore, these studies have increased our understanding of interactions mediated by the Src SH2 domain, and it is shown that these interactions are more complex than what is generally believed. The interactions involve more than the canonical SH2 binding motif: residues outside this region can have a large impact on the binding affinity and electrostatic interactions are important for the binding. Also the combination of SH3 and SH2 domains results in binding behaviour that differs from that expected merely on the basis of the individual binding motifs and isolated domains. The non-additive

nature of the interactions is further illustrated by the observation that the Src SH2 domain can bind the FAK kinase domain independent of the regular SH2 binding site, making contacts with a large area of the SH2 domain surface.

Samenvatting

Meercellig leven is alleen mogelijk als de cellen binnen een organisme in staat zijn om met elkaar te communiceren en te reageren op de signalen uit hun omgeving. Signaaltransductie is een proces waarin een externe prikkel wordt vertaald naar een reactie binnen de cel. Als een extern ligand, zoals een hormoon, aan een receptor in het celmembraan bindt, leidt dit tot een keten van gebeurtenissen. Dit leidt uiteindelijk tot veranderingen in bijvoorbeeld genexpressie of de activiteit van enzymen. Eiwit-eiwitinteracties spelen een centrale rol in signaleringscascades en zijn van vitaal belang in de regulatie van biologische processen.

Dit proefschrift richt zich op interacties gemedieerd door Src homologie (SH) domeinen, een groep eiwitinteractiedomeinen die voorkomen in eiwitten die betrokken zijn bij fosfotyrosine signaaltransductie. Tyrosinefosforylatie, het verbinden van een fosfaatgroep met een tyrosineresidu in een eiwit, kan de structuur en de activiteit van een enzym veranderen en nieuwe locaties voor eiwit-interacties creëren. Deze reactie wordt gekatalyseerd door eiwit-tyrosinekinasen, een groep van enzymen die vaak SH-domeinen bevatten. Tyrosinefosforylatie maakt onderdeel uit van vele signaaltransductieketens.

Src homologie 2 (SH2) domeinen herkennen en binden aan gefosforyleerde tyrosineresiduen. Eiwitten die SH2-domeinen bevatten kunnen daarom andere eiwitten, die gefosforyleerd zijn als resultaat van een externe prikkel, herkennen en binden. Dit kan helpen om het katalytische domein van het tyrosinekinase dicht bij zijn substraat te brengen voor een nieuwe ronde van fosforylatiereacties, wat het signaal doorstuurt. De functie van Src homolgie 3 (SH3) domeinen is ook om de juiste eiwitten bij elkaar te brengen, door bepaalde prolinerijke regio's in eiwitten te herkennen. Naast het sturen van de kinase naar het juiste deel van de cel zijn SH2- en SH3-domeinen ook betrokken bij de regulatie van de activiteit van het kinase.

De eiwit-tyrosinekinasen focal adhesion kinase (FAK) en Src zijn betrokken bij processen zoals celproliferatie, celmigratie en het overleven van de cel. Hun betrokkenheid bij diverse soorten kanker bij de mens maakt hen belangrijke aangrijpingspunten voor geneesmiddelen, en het is dus van algemeen belang om meer over de details van hun interactie te leren. Het bestuderen van deze eiwitten kan in het algemeen ons begrip van modulaire signaleringeiwitten verbeteren en in het bijzonder het gedrag van SH-domeinen in eiwitinteracties. Met behulp van kernspinresonantie (NMR) spectroscopie en isotherme titratie calorimetrie (ITC) als de belangrijkste instrumenten werd de interactie van FAK en Src door middel van de SH2 en SH3 domeinen van Src bestudeerd. Voor dit doeleinde werden een aantal modelsystemen gebruikt.

Het in kaart brengen van verstoringen van de chemische verschuivingen (CSP) werd samen met paramagnetische relaxatie-versnelling (PRE) NMR spectroscopie gebruikt om de interactie van het Src SH3-domein met een peptide afgeleid van een proline-rijke plaats in FAK te bestuderen. Hierbij werd gebruik gemaakt van peptiden die de spin-gelabelde aminozuur TOAC bevatten (hoofstuk 2). Ondanks de lage affiniteit waarmee het peptide bond aan het SH3-domein, bleek het peptide te binden op een zeer specifieke manier en werd er weinig mobiliteit waargenomen in het complex. Het SH2 domein van Src bleek met een hoge affiniteit te binden aan peptiden afgeleid van FAK (hoofdstuk 3). Residuen vlak buiten de regio die in het algemeen wordt beschouwd als het SH2-bindend motief bleken een grote invloed te hebben op de bindingsaffiniteit en het includeren van deze residuen leidde tot een aanzienlijk verhoogde affiniteit. In tegenstelling tot wat werd verwacht voor een complex van hoge affiniteit, is met PRE NMR studies met spin-gelabelde peptiden vastgesteld dat de interactie tussen het peptide en proteïne opmerkelijk dynamisch was. Gezien dat vele van de flankerende residuen negatief geladen zijn, terwijl de plaats waar het peptide bindt aan het SH2-domein overwegend positief geladen is, is de verhoogde affiniteit waarschijnlijk te wijten

aan elektrostatische interacties die de formatie van een ontmoetingscomplex tussen het peptide en het SH2-domein verhogen.

CSP NMR en ITC studies van peptiden die zowel de SH3- als de SH2-bindingsplaatsen van FAK bevatten samen met een Src SH3-SH2 tandem domein (SH32) toonden aan dat het includeren van allebij de bindingsplaatsen in het peptide tot een verhoogde affiniteit voor SH32 leidde, ten opzichte van de individuele bindingsplaatsen (hoofdstuk 4). Dit werd ook aangetoond in zoogdiercellen getransfecteerd met SH-domein constructen, waarin het SH32-tandem domein in een hogere mate lokaliseerde naar specifieke regio's in de cel in vergelijking met een geïsoleerd SH2-domein (hoofdstuk 7). De afstand tussen de bindingsplaatsen zoals aanwezig in FAK is veel groter dan wat nodig is om de afstand tussen de peptide-bindende plaatsen op de SH3- en SH2-domeinen te overbruggen. Wij hebben onderzocht hoe het verminderen van deze afstand in het peptide de interactie met SH32 beïnvloed. Interessant genoeg blijken peptiden, waarin de afstand tussen de bindingsplaatsen te klein is om gelijktijdig aan zowel de SH2- en de SH3-domein te binden, in veel hogere mate aan de SH3-domein te binden dan wat men zou verwachten op basis van het verschil in bindingsaffiniteit tussen de geïsoleerde SH2- en SH3-domeinen. Op basis van deze data hebben wij een model voor de interactie voorgesteld, waarin een nieuw mechanisme voor peptide-eiwit complex formatie wordt beschreven. In dit model helpen de (elektrische) ladingen het peptide naar een ontmoetingscomplex met SH32 te brengen. Vanuit dit ontmoetingscomplex kan het peptide verder met of het SH2-domein of het SH3-domein het uiteindelijke complex vormen. Hierdoor leiden de ladingen in het peptide ook tot een toename in complex formatie met het SH3-domein.

Een protocol voor de expressie van het katalytische domein van FAK door middel van een baculovirus expressie systeem werd ontwikkeld, samen met een zuiveringsprotocol en een methode voor het in vitro manipuleren van de fosforyleringsstaat van het kinase-domein (hoofdstuk 5). Dit maakte studies van de interactie van het Src SH2 domein met het hele katalytische domein van FAK inclusief de SH2 bindingsplaats mogelijk (hoofdstuk 6). Op basis van CSP data werd aangetoond dat het SH2 domein het kinase domein bindt, maar dat de normale SH2-bindingsplaats niet toegankelijk is voor SH2 binding. De verstoringen van de chemische verschuivingen waren typisch voor dynamische complexen waarin de interactie voornamelijk wordt gedreven door elektrostatica. Uit een competitie experiment met een peptide afkomstig van FAK is gebleken dat de schijnbare bindingsaffiniteit van het SH2-domein voor dit peptide aanzienlijk lager is in de aanwezigheid van het FAK kinase-domein dan in de afwezigheid van het kinase-domein. Samen duiden deze gegevens erop dat het kinase-domein het SH2 domein met een hoge affiniteit bindt, waardoor het binden van het SH2-domein aan het toegevoegde peptide onmogelijk is, maar dat de normale SH2 bindingsplaats in FAK er niet bij betrokken is. Het is mogelijk dat het kinase-domein zelf aan deze plaats (intra- of intermoleculair) bindt, waardoor het SH2-domein er niet aan kan binden.

Naast de interacties die gemedieerd worden door de Src SH3- en SH2-domeinen, werd de binding van het SH3-domein van het PI3K p85-onderdeel aan proline-rijke peptiden met verschillende structurele conformaties onderzocht (hoofdstuk 8). De interactie van het SH3-domein met peptiden die gemodificeerd waren met een foto-labiele linker, waardoor zij een cyclische conformatie aan hadden genomen, werd vergeleken met de interactie met de peptiden na bestraling met UV-licht, waardoor de peptiden weer een lineaire conformatie aan hadden genomen. Er werd vastgesteld dat, hoewel de peptiden in soortgelijke manieren aan het SH3-domein bonden, de bindingsaffiniteit voor de lineaire peptiden verhoogd was ten opzichte

van de cyclische peptiden. Deze methode biedt dus een manier om de affiniteit van de peptide-eiwit interacties te controleren met behulp van bestraling met UV-licht.

Uit de resultaten die in dit proefschrift gepresenteerd zijn kunnen we vaststellen dat in macromoleculaire complexen een hoge bindingsaffiniteit niet altijd gecorreleerd is met een duidelijk gedefinieerde oriëntatie in het complex: sterke binding kan alsnog mobiliteit van de moleculen ten opzichte van elkaar met zich mee brengen, net als zwak bindende moleculen duidelijk gedefinieerde relatieve posities in het complex kunnen hebben. Verder hebben deze studies ons begrip van interacties door bemiddeling van het Src SH2-domein bevorderd, en het is aangetoond dat deze interacties complexer zijn dan wat vaak gedacht wordt. De interacties omvatten meer dan het canonieke SH2-bindende motief: residuen buiten dit gebied kunnen een grote invloed hebben op de bindingsaffiniteit en elektrostatische interacties zijn belangrijk voor de binding. Ook resulteerde de combinatie van SH3- en SH2-domeinen in bindingsgedrag dat afwijkt van wat verwacht werd op basis van de individuele bindingsmotieven en geïsoleerde domeinen. De niet-additieve aard van de interacties wordt verder geïllustreerd door de observatie dat het Src SH2-domein onafhankelijk van de normaale SH2 bindingsplaats kan binden aan het FAK-kinase domein, waarbij het kinase-domein contact maakt met een groot deel van het oppervlak van het SH2-domein.

References

[1] Ubbink M (2009) The courtship of proteins: understanding the encounter complex. *FEBS Lett*, **583,** 1060-1066.

[2] Xu X, Reinle W, Hannemann F, Konarev PV, Svergun DI, Bernhardt R, & Ubbink M (2008) Dynamics in a pure encounter complex of two proteins studied by solution scattering and paramagnetic NMR spectroscopy. *J Am Chem Soc*, **130,** 6395-6403.

[3] Manning G, Young SL, Miller WT, & Zhai Y (2008) The protist, *Monosiga brevicollis*, has a tyrosine kinase signaling network more elaborate and diverse than found in any known metazoan. *Proc Natl Acad Sci USA*, **105,** 9674-9679.

[4] Mayer BJ (2008) Clues to the evolution of complex signaling machinery. *Proc Natl Acad Sci USA*, **105,** 9453-9454.

[5] Pincus D, Letunic I, Bork P, & Lim WA (2008) Evolution of the phospho-tyrosine signaling machinery in premetazoan lineages. *Proc Natl Acad Sci USA*, **105,** 9680-9684.

[6] Pincus D, Letunic I, Bork P, & Lim WA (2008) Evolution of the phospho-tyrosine signaling machinery in premetazoan lineages. *Proc Natl Acad Sci USA*, **105,** 9680-9684.

[7] Hunter T & Cooper JA (1981) Epidermal growth factor induces rapid tyrosine phosphorylation of proteins in A431 human tumor cells. *Cell*, **24,** 741-752.

[8] Myers MG, Jr., Grammer TC, Wang LM, Sun XJ, Pierce JH, Blenis J, & White MF (1994) Insulin receptor substrate-1 mediates phosphatidylinositol 3'-kinase and p70S6k signaling during insulin, insulin-like growth factor-1, and interleukin-4 stimulation. *J Biol Chem*, **269,** 28783-28789.

[9] Shattil SJ & Brugge JS (1991) Protein tyrosine phosphorylation and the adhesive functions of platelets. *Curr Opin Cell Biol*, **3,** 869-879.

[10] Weiss A & Littman DR (1994) Signal transduction by lymphocyte antigen receptors. *Cell*, **76,** 263-274.

[11] Ortutay C, Valiaho J, Stenberg K, & Vihinen M (2005) KinMutBase: a registry of disease-causing mutations in protein kinase domains. *Hum Mutat*, **25,** 435-442.

[12] Eckhart W, Hutchinson MA, & Hunter T (1979) An activity phosphorylating tyrosine in polyoma T antigen immunoprecipitates. *Cell*, **18,** 925-933.

[13] Hunter T & Eckhart W (2004) The discovery of tyrosine phosphorylation: it's all in the buffer! *Cell*, **116,** S35-9, 1.

[14] Sastry SK & Burridge K (2000) Focal adhesions: a nexus for intracellular signaling and cytoskeletal dynamics. *Exp Cell Res*, **261,** 25-36.

[15] Li SSC (2005) Specificity and versatility of SH3 and other proline-recognition domains: structural basis and implications for cellular signal transduction. *Biochem J*, **390,** 641-653.

[16] Pawson T & Nash P (2003) Assembly of cell regulatory systems through protein interaction domains. *Science*, **300,** 445-452.

[17] Mitra SK, Hanson DA, & Schlaepfer DD (2005) Focal adhesion kinase: in command and control of cell motility. *Nat Rev Mol Cell Biol*, **6,** 56-68.

[18] Parsons SJ & Parsons JT (2004) Src family kinases, key regulators of signal transduction. *Oncogene*, **23,** 7906-7909.

[19] Cance WG, Harris JE, Iacocca MV, Roche E, Yang X, Chang J, Simkins S, & Xu L (2000) Immunohistochemical analyses of focal adhesion kinase expression in benign and malignant human breast and colon tissues: correlation with preinvasive and invasive phenotypes. *Clin Cancer Res*, **6,** 2417-2423.

[20] Irby RB & Yeatman TJ (2000) Role of Src expression and activation in human cancer. *Oncogene*, **19,** 5636-5642.

[21] Sood AK, Coffin JE, Schneider GB, Fletcher MS, DeYoung BR, Gruman LM, Gershenson DM, Schaller MD, & Hendrix MJ (2004) Biological significance of focal adhesion kinase in ovarian cancer: role in migration and invasion. *Am J Pathol*, **165,** 1087-1095.

[22] Yeatman TJ (2004) A renaissance for SRC. *Nat Rev Cancer*, **4,** 470-480.

[23] Avizienyte E & Frame MC (2005) Src and FAK signalling controls adhesion fate and the epithelial-to-mesenchymal transition. *Curr Opin Cell Biol*, **17,** 542-547.

[24] McLean GW, Carragher NO, Avizienyte E, Evans J, Brunton VG, & Frame MC (2005) The role of focal-adhesion kinase in cancer - a new therapeutic opportunity. *Nat Rev Cancer*, **5,** 505-515.

[25] van Nimwegen MJ, Verkoeijen S, van Buren L, Burg D, & van de WB (2005) Requirement for focal adhesion kinase in the early phase of mammary adenocarcinoma lung metastasis formation. *Cancer Res*, **65,** 4698-4706.

[26] Wu X, Gan B, Yoo Y, & Guan JL (2005) FAK-mediated src phosphorylation of endophilin A2 inhibits endocytosis of MT1-MMP and promotes ECM degradation. *Dev Cell*, **9,** 185-196.

[27] Mitra SK, Lim ST, Chi A, & Schlaepfer DD (2006) Intrinsic focal adhesion kinase activity controls orthotopic breast carcinoma metastasis via the regulation of urokinase plasminogen activator expression in a syngeneic tumor model. *Oncogene*, **25,** 4429-4440.

[28] Mitra SK, Mikolon D, Molina JE, Hsia DA, Hanson DA, Chi A, Lim ST, Bernard-Trifilo JA, Ilic D, Stupack DG, Cheresh DA, & Schlaepfer DD (2006) Intrinsic FAK activity and Y925 phosphorylation facilitate an angiogenic switch in tumors. *Oncogene*, **25,** 5969-5984.

[29] Rous P (1911) A sarcoma of the fowl transmissible by an agent separable from the tumor cells. *J Exp Med*, **13,** 397-411.

[30] Martin GS (1970) Rous sarcoma virus: a function required for the maintenance of the transformed state. *Nature*, **227,** 1021-1023.

[31] Yeatman TJ (2004) A renaissance for SRC. *Nat Rev Cancer*, **4,** 470-480.

[32] Martin GS (2001) The hunting of the Src. *Nat Rev Mol Cell Biol*, **2,** 467-475.

[33] Martin GS (2004) The road to Src. *Oncogene*, **23,** 7910-7917.

[34] Yeatman TJ (2004) A renaissance for SRC. *Nat Rev Cancer*, **4,** 470-480.

[35] Roskoski R (2004) Src protein-tyrosine kinase structure and regulation. *Biochem Biophys Res Commun*, **324,** 1155-1164.

[36] Manning G, Whyte DB, Martinez R, Hunter T, & Sudarsanam S (2002) The protein kinase complement of the human genome. *Science*, **298,** 1912-1934.

[37] Boggon TJ & Eck MJ (2004) Structure and regulation of Src family kinases. *Oncogene*, **23,** 7918-7927.

[38] Yu H, Rosen MK, Shin TB, Seidel-Dugan C, Brugge JS, & Schreiber SL (1992) Solution structure of the SH3 domain of Src and identification of its ligand-binding site. *Science*, **258,** 1665-1668.

[39] Feng S, Chen JK, Yu H, Simon JA, & Schreiber SL (1994) Two binding orientations for peptides to the Src SH3 domain: Development of a general model for SH3-ligand interactions. *Science*, **266,** 1241-1247.

[40] Yu H, Rosen MK, & Schreiber SL (1993) 1H and 15N assignments and secondary structure of the Src SH3 domain. *FEBS Lett.*, **324,** 87-92.

[41] Waksman G, Kominos D, Robertson SC, Pant N, Baltimore D, Birge RB, Cowburn D, Hanafusa H, Mayer BJ, Overduin M, Resh MD, Rios CB, Silverman L, & Kuriyan J (1992) Crystal structure of the phosphotyrosine recognition domain SH2 of v-src complexed with tyrosine-phosphorylated peptides. *Nature*, **358,** 646-653.

[42] Songyang Z, Shoelson SE, Chaudhuri M, Gish G, Pawson T, Haser WG, King F, Roberts T, Ratnofsky S, Lechleider RJ, Neel BG, Birge RB, Fajardo JE, Chou MM, Hanafusa H, Schaffhausen B, & Cantley LC (1993) SH2 domains recognize specific phosphopeptide sequences. *Cell*, **72,** 767-778.

[43] Waksman G, Shoelson SE, Pant N, Cowburn D, & Kuriyan J (1993) Binding of a high affinity phosphotyrosyl peptide to the Src SH2 domain: crystal structures of the complexed and peptide-free forms. *Cell*, **72,** 779-790.

[44] Roskoski R (2004) Src protein-tyrosine kinase structure and regulation. *Biochem Biophys Res Commun*, **324,** 1155-1164.

[45] Xu RX, Word JM, Davis DG, Rink MJ, Willard DH, & Gampe RT (1995) Solution structure of the human pp60(C-Src) SH2 domain complexed with a phosphorylated tyrosine pentapeptide. *Biochemistry*, **34,** 2107-2121.

[46] Parsons SJ & Parsons JT (2004) Src family kinases, key regulators of signal transduction. *Oncogene*, **23,** 7906-7909.

[47] Playford MP & Schaller MD (2004) The interplay between Src and integrins in normal and tumor biology. *Oncogene*, **23,** 7928-7946.

[48] Williams JC, Weijland A, Gonfloni S, Thompson A, Courtneidge SA, Superti-Furga G, & Wierenga RK (1997) The 2.35 A crystal structure of the inactivated form of chicken Src: a dynamic molecule with multiple regulatory interactions. *J Mol Biol*, **274,** 757-775.

[49] Xu WQ, Harrison SC, & Eck MJ (1997) Three-dimensional structure of the tyrosine kinase c-Src. *Nature*, **385,** 595-602.

[50] Yeatman TJ (2004) A renaissance for SRC. *Nat Rev Cancer*, **4,** 470-480.

[51] Yeatman TJ (2004) A renaissance for SRC. *Nat Rev Cancer*, **4,** 470-480.

[52] Bjorge JD, Pang A, & Fujita DJ (2000) Identification of protein-tyrosine phosphatase 1B as the major tyrosine phosphatase activity capable of dephosphorylating and activating c-Src in several human breast cancer cell lines. *J Biol Chem*, **275,** 41439-41446.

[53] Boggon TJ & Eck MJ (2004) Structure and regulation of Src family kinases. *Oncogene*, **23,** 7918-7927.

[54] Hanks SK, Calalb MB, Harper MC, & Patel SK (1992) Focal adhesion protein-tyrosine kinase phosphorylated in response to cell attachment to fibronectin. *Proc Natl Acad Sci USA*, **89,** 8487-8491.

[55] Schaller MD, Borgman CA, Cobb BS, Vines RR, Reynolds AB, & Parsons JT (1992) pp125FAK a structurally distinctive protein-tyrosine kinase associated with focal adhesions. *Proc Natl Acad Sci USA*, **89,** 5192-5196.

[56] Parsons JT (2003) Focal adhesion kinase: the first ten years. *Journal of Cell Science*, **116,** 1409-1416.

[57] Nowakowski J, Cronin CN, McRee DE, Knuth MW, Nelson CG, Pavletich NP, Rogers J, Sang BC, Scheibe DN, Swanson RV, & Thompson DA (2002) Structures of the cancer-related Aurora-A, FAK, and EphA2 protein kinases from nanovolume crystallography. *Structure*, **10,** 1659-1667.

[58] Arold ST, Hoellerer MK, & Noble ME (2002) The structural basis of localization and signaling by the focal adhesion targeting domain. *Structure*, **10,** 319-327.

[59] Hayashi I, Vuori K, & Liddington RC (2002) The focal adhesion targeting (FAT) region of focal adhesion kinase is a four-helix bundle that binds paxillin. *Nat. Struct. Biol.*, **9,** 101-106.

[60] Ceccarelli DF, Song HK, Poy F, Schaller MD, & Eck MJ (2006) Crystal structure of the FERM domain of focal adhesion kinase. *J. Biol. Chem.*, **281,** 252-259.

[61] Guan JL & Shalloway D (1992) Regulation of focal adhesion-associated protein tyrosine kinase by both cellular adhesion and oncogenic transformation. *Nature*, **358,** 690-692.

[62] Schaller MD, Borgman CA, Cobb BS, Vines RR, Reynolds AB, & Parsons JT (1992) pp125FAK a structurally distinctive protein-tyrosine kinase associated with focal adhesions. *Proc Natl Acad Sci USA*, **89,** 5192-5196.

[63] Hauck CR, Hunter T, & Schlaepfer DD (2001) The v-Src SH3 domain facilitates a cell adhesion-independent association with focal adhesion kinase. *J Biol Chem*, **276,** 17653-17662.

[64] Thomas JW, Ellis B, Boerner RJ, Knight WB, White GC, & Schaller MD (1998) SH2- and SH3-mediated interactions between focal adhesion kinase and Src. *J. Biol. Chem.*, **273,** 577-583.

[65] Schaller MD, Hildebrand JD, Shannon JD, Fox JW, Vines RR, & Parsons JT (1994) Autophosphorylation of the focal adhesion kinase, pp125FAK, directs SH2-dependent binding of pp60src. *Mol Cell Biol*, **14,** 1680-1688.

[66] Xing Z, Chen HC, Nowlen JK, Taylor SJ, Shalloway D, & Guan JL (1994) Direct interaction of v-Src with the focal adhesion kinase mediated by the Src SH2 domain. *Mol Biol Cell*, **5,** 413-421.

[67] Cobb BS, Schaller MD, Leu TH, & Parsons JT (1994) Stable association of pp60src and pp59fyn with the focal adhesion-associated protein tyrosine kinase, pp125FAK. *Mol Cell Biol*, **14,** 147-155.

[68] Chen HC, Appeddu PA, Isoda H, & Guan JL (1996) Phosphorylation of tyrosine 397 in focal adhesion kinase is required for binding phosphatidylinositol 3-kinase. *J Biol Chem*, **271,** 26329-26334.

[69] Han DC & Guan JL (1999) Association of focal adhesion kinase with Grb7 and its role in cell migration. *J Biol Chem*, **274,** 24425-24430.

[70] Nowakowski J, Cronin CN, McRee DE, Knuth MW, Nelson CG, Pavletich NP, Rogers J, Sang BC, Scheibe DN, Swanson RV, & Thompson DA (2002) Structures of the cancer-related Aurora-A, FAK, and EphA2 protein kinases from nanovolume crystallography. *Structure*, **10,** 1659-1667.

[71] Cooper LA, Shen TL, & Guan JL (2003) Regulation of focal adhesion kinase by its amino-terminal domain through an autoinhibitory interaction. *Mol Cell Biol*, **23,** 8030-8041.

[72] Dunty JM, Gabarra-Niecko V, King ML, Ceccarelli DF, Eck MJ, & Schaller MD (2004) FERM domain interaction promotes FAK signaling. *Mol Cell Biol*, **24,** 5353-5368.

[73] Cohen LA & Guan JL (2005) Residues within the first subdomain of the FERM-like domain in focal adhesion kinase are important in its regulation. *J Biol Chem*, **280,** 8197-8207.

[74] Jacamo RO & Rozengurt E (2005) A truncated FAK lacking the FERM domain displays high catalytic activity but retains responsiveness to adhesion-mediated signals. *Biochem Biophys Res Commun*, **334,** 1299-1304.

[75] Lietha D, Cai X, Ceccarelli DF, Li Y, Schaller MD, & Eck MJ (2007) Structural basis for the autoinhibition of focal adhesion kinase. *Cell*, **129,** 1177-1187.

[76] Mitra SK & Schlaepfer DD (2006) Integrin-regulated FAK-Src signaling in normal and cancer cells. *Curr. Opin. Cell Biol.*, **18,** 516-523.

[77] Leevers SJ, Vanhaesebroeck B, & Waterfield MD (1999) Signalling through phosphoinositide 3-kinases: the lipids take centre stage. *Curr Opin Cell Biol*, **11,** 219-225.

[78] Katso R, Okkenhaug K, Ahmadi K, White S, Timms J, & Waterfield MD (2001) Cellular function of phosphoinositide 3-kinases: implications for development, homeostasis, and cancer. *Annu Rev Cell Dev Biol*, **17,** 615-675.

[79] Lietha D, Cai X, Ceccarelli DF, Li Y, Schaller MD, & Eck MJ (2007) Structural basis for the autoinhibition of focal adhesion kinase. *Cell*, **129,** 1177-1187.

[80] Vanhaesebroeck B & Waterfield MD (1999) Signaling by distinct classes of phosphoinositide 3-kinases. *Exp Cell Res*, **253,** 239-254.

[81] Koyama S, Yu H, Dalgarno DC, Shin TB, Zydowsky LD, & Schreiber SL (1993) Structure of the PI3K SH3 domain and analysis of the SH3 family. *Cell*, **72,** 945-952.

[82] Booker GW, Gout I, Downing AK, Driscoll PC, Boyd J, Waterfield MD, & Campbell ID (1993) Solution structure and ligand-binding site of the SH3 domain of the p85 alpha subunit of phosphatidylinositol 3-kinase. *Cell*, **73,** 813-822.

[83] Chen JK, Lane WS, Brauer AW, Tanaka A, & Schreiber SL (1993) Biased combinatorial libraries: novel ligands for the SH3 domain of phosphatidylinositol 3-kinase. *Journal of the American. Chemical. Society.*, **115,** 12591-12592.

[84] Yu H, Chen JK, Feng S, Dalgarno DC, Brauer AW, & Schreiber SL (1994) Structural basis for the binding of proline-rich peptides to SH3 domains. *Cell*, **76,** 933-945.

[85] Pellecchia M (2005) Solution nuclear magnetic resonance spectroscopy techniques for probing intermolecular interactions. *Chem Biol*, **12,** 961-971.

[86] Zuiderweg ER (2002) Mapping protein-protein interactions in solution by NMR spectroscopy. *Biochemistry*, **41,** 1-7.

[87] Fernandez C & Wider G (2003) TROSY in NMR studies of the structure and function of large biological macromolecules. *Curr Opin Struct Biol*, **13,** 570-580.

[88] Bloembergen N & Morgan LO (1961) Proton relaxation times in paramagnetic solutions: effects of electron spin relaxation. *J Chem Phys*, **34,** 842-850.

[89] Clore GM, Tang C, & Iwahara J (2007) Elucidating transient macromolecular interactions using paramagnetic relaxation enhancement. *Curr Opin Struct Biol*, **17,** 603-616.

[90] Hansen DF, Hass MAS, Christensen HM, Ulstrup J, & Led JJ (2003) Detection of short-lived transient protein-protein interactions by intermolecular nuclear paramagnetic relaxation: Plastocyanin from *Anabaena variabilis*. *J Am Chem Soc*, **125,** 6858-6859.

[91] Iwahara J & Clore GM (2006) Detecting transient intermediates in macromolecular binding by paramagnetic NMR. *Nature*, **440,** 1227-1230.

[92] Tang C, Iwahara J, & Clore GM (2006) Visualization of transient encounter complexes in protein-protein association. *Nature*, **444,** 383-386.

[93] Volkov AN, Worrall JAR, Holtzmann E, & Ubbink M (2006) Solution structure and dynamics of the complex between cytochrome c and cytochrome c peroxidase determined by paramagnetic NMR. *Proceedings of the National Academy of Sciences of the United States of America*, **103,** 18945-18950.

[94] Clore GM (2008) Visualizing lowly-populated regions of the free energy landscape of macromolecular complexes by paramagnetic relaxation enhancement. *Mol Biosyst*, **4,** 1058-1069.

[95] Velazquez-Campoy A, Leavitt SA, & Freire E (2004) Characterization of protein-protein interactions by isothermal titration calorimetry. *Methods Mol Biol*, **261,** 35-54.

[96] Velazquez CA & Freire E (2005) ITC in the post-genomic era...? Priceless. *Biophys Chem*, **115,** 115-124.

[97] Tang C, Iwahara J, & Clore GM (2006) Visualization of transient encounter complexes in protein-protein association. *Nature*, **444,** 383-386.

[98] Iwahara J & Clore GM (2006) Detecting transient intermediates in macromolecular binding by paramagnetic NMR. *Nature*, **440,** 1227-1230.

[99] Iwahara J, Schwieters CD, & Clore GM (2004) Characterization of nonspecific protein-DNA interactions by ^{1}H paramagnetic relaxation enhancement. *J Am Chem Soc*, **126,** 12800-12808.

[100] Volkov AN, Worrall JAR, Holtzmann E, & Ubbink M (2006) Solution structure and dynamics of the complex between cytochrome c and cytochrome c peroxidase determined by paramagnetic NMR. *Proc Natl Acad Sci USA*, **103,** 18945-18950.

[101] Mahoney NM, Rastogi VK, Cahill SM, Girvin ME, & Almo SC (2000) Binding orientation of proline-rich peptides in solution: Polarity of the profilin-ligand interaction. *J Am Chem Soc*, **122,** 7851-7852.

[102] Mal TK, Ikura M, & Kay LE (2002) The ATCUN domain as a probe of intermolecular interactions: Application to calmodulin-peptide complexes. *J Am Chem Soc*, **124,** 14002-14003.

[103] Gross JD, Moerke NJ, von der Haar T, Lugovskoy AA, Sachs AB, McCarthy JEG, & Wagner G (2003) Ribosome loading onto the mRNA cap is driven by conformational coupling between eIF4G and eIF4E. *Cell*, **115,** 739-750.

[104] Card PB, Erbel PJA, & Gardner KH (2005) Structural basis of ARNT PAS-B dimerization: Use of a common beta-sheet interface for hetero- and homodimerization. *J Mol Biol*, **353,** 664-677.

[105] Johnson PE, Brun E, MacKenzie LF, Withers SG, & McIntosh LP (1999) The cellulose-binding domains from *Cellulomonas fimi* b-1,4-glucanase CenC bind nitroxide spin-labeled cellooligosaccharides in multiple orientations. *J Mol Biol*, **287,** 609-625.

[106] Jain NU, Venot A, Umemoto K, Leffler H, & Prestegard JH (2001) Distance mapping of protein-binding sites using spin-labeled oligosaccharide ligands. *Protein Sci*, **10,** 2393-2400.

[107] Macnaughtan MA, Kamar M, Alvarez-Manilla G, Venot A, Glushka J, Pierce JM, & Prestegard JH (2007) NMR structural characterization of substrates bound to N-acetylglucosaminyltransferase V. *J Mol Biol*, **366,** 1266-1281.

[108] Ramos A & Varani G (1998) A new method to detect long-range protein-RNA contacts: NMR detection of electron-proton relaxation induced by nitroxide spin-labeled RNA. *J Am Chem Soc*, **120,** 10992-10993.

[109] Varani L, Gunderson SI, Mattaj IW, Kay LE, Neuhaus D, & Varani G (2000) The NMR structure of the 38 kDa U1A protein - PIE RNA complex reveals the basis of cooperativity in regulation of polyadenylation by human U1A protein. *Nat Struct Biol*, **7,** 329-335.

[110] Ueda T, Kato A, Ogawa Y, Torizawa T, Kuramitsu S, Iwai S, Terasawa H, & Shimada I (2004) NMR study of repair mechanism of DNA photolyase by FAD-induced paramagnetic relaxation enhancement. *J Biol Chem*, **279,** 52574-52579.

[111] Tang C, Schwieters CD, & Clore GM (2007) Open-to-closed transition in apo maltose-binding protein observed by paramagnetic NMR. *Nature*, **449,** 1078-1082.

[112] Gaponenko V, Howarth JW, Columbus L, Gasmi-Seabrook G, Yuan J, Hubbell WL, & Rosevear PR (2000) Protein global fold determination using site-directed spin and isotope labeling. *Protein Sci*, **9,** 302-309.

[113] Gillespie JR & Shortle D (1997) Characterization of long-range structure in the denatured state of staphylococcal nuclease. 1. Paramagnetic relaxation enhancement by nitroxide spin labels. *J Mol Biol*, **268,** 158-169.

[114] Battiste JL & Wagner G (2000) Utilization of site-directed spin labeling and high-resolution heteronuclear nuclear magnetic resonance for global fold determination of large proteins with limited nuclear overhauser effect data. *Biochemistry*, **39,** 5355-5365.

[115] Dedmon MM, Lindorff-Larsen K, Christodoulou J, Vendruscolo M, & Dobson CM (2005) Mapping long-range interactions in alpha-synuclein using spin-label NMR and ensemble molecular dynamics simulations. *J Am Chem Soc*, **127,** 476-477.

[116] Liang B, Bushweller JH, & Tamm LK (2006) Site-directed parallel spin-labeling and paramagnetic relaxation enhancement in structure determination of membrane proteins by solution NMR spectroscopy. *J Am Chem Soc*, **128,** 4389-4397.

[117] Iwahara J, Anderson DE, Murphy EC, & Clore GM (2003) EDTA-derivatized deoxythymidine as a tool for rapid determination of protein binding polarity to DNA by intermolecular paramagnetic relaxation enhancement. *J Am Chem Soc*, **125,** 6634-6635.

[118] Gaponenko V, Sarma SP, Altieri AS, Horita DA, Li J, & Byrd RA (2004) Improving the accuracy of NMR structures of large proteins using pseudocontact shifts as long-range restraints. *J Biomol NMR*, **28,** 205-212.

[119] Vlasie MD, Comuzzi C, van den Nieuwendijk AM, Prudêncio M, Overhand M, & Ubbink M (2007) Long-range-distance NMR effects in a protein labeled with a lanthanide-DOTA chelate. *Chem Eur J*, **13,** 1715-1723.

[120] Vlasie MD, Fernández-Busnadiego R, Prudêncio M, & Ubbink M (2008) Conformation of pseudoazurin in the 152 kDa electron transfer complex with nitrite reductase determined by paramagnetic NMR. *J Mol Biol*, **375,** 1405-1415.

[121] Toniolo C, Valente E, Formaggio F, Crisma M, Pilloni G, Corvaja C, Toffoletti A, Martinez GV, Hanson MP, Millhauser GL, George C, & Flippen-Anderson JL (1995) Synthesis and conformational studies of peptides containing TOAC, a spin-labelled $C^{a,a}$-disubstituted glycine. *J Pept Sci*, **1,** 45-57.

[122] Marchetto R, Schreier S, & Nakaie CR (1993) A novel spin-labeled amino acid derivative for use in peptide-synthesis: (9-fluorenylmethyloxycarbonyl)-2,2,6,6-tetramethylpiperidine-N-oxyl-4-amino-4-carboxylic acid. *J Am Chem Soc*, **115,** 11042-11043.

[123] Martin L, Ivancich A, Vita C, Formaggio F, & Toniolo C (2001) Solid-phase synthesis of peptides containing the spin-labeled 2,2,6,6-tetramethylpiperidine-1-oxyl-4-amino-4-carboxylic acid (TOAC). *J Pept Res*, **58,** 424-432.

[124] Nilsson BL, Soellner MB, & Raines RT (2005) Chemical synthesis of proteins. *Annu Rev Biophys Biomol Struct*, **34,** 91-118.

[125] Marsh D (2006) Orientation of TOAC amino-acid spin labels in a-helices and b-strands. *J Magn Reson*, **180,** 305-310.

[126] de Deus Teixeira LG, Bersanetti PA, Schreier S, Carmona AK, & Nakaie CR (2007) Analogues containing the paramagnetic amino acid TOAC as substrates for angiotensin I-converting enzyme. *FEBS Lett*, **581,** 2411-2415.

[127] Schreier S, Barbosa SR, Casallanovo F, Vieira RFF, Cilli EM, Paiva ACM, & Nakaie CR (2004) Conformational basis for the biological activity of TOAC-labeled angiotensin II and bradykinin: Electron paramagnetic resonance, circular dichroism, and fluorescence studies. *Biopolymers*, **74,** 389-402.

[128] D'Amore M, Improta R, & Barone V (2003) Conformational behavior and magnetic properties of a nitroxide amino acid derivative in vacuo and in aqueous solution. *J Phys Chem A*, **107,** 6264-6269.

[129] Bettio A, Gutewort V, Pöppl A, Dinger MC, Zschörnig O, Arnold K, Toniolo C, & Beck-Sickinger AG (2002) Electron paramagnetic resonance backbone dynamics studies on spin-labelled neuropeptide Y analogues. *J Pept Sci*, **8,** 671-682.

[130] Nakaie CR, Silva EG, Cilli EM, Marchetto R, Schreier S, Paiva TB, & Paiva ACM (2002) Synthesis and pharmacological properties of TOAC-labeled angiotensin and bradykinin analogs. *Peptides*, **23,** 65-70.

[131] Victor KG & Cafiso DS (2001) Location and dynamics of basic peptides at the membrane interface: Electron paramagnetic resonance spectroscopy of tetramethyl-piperidine-N-oxyl-4-amino-4-carboxylic acid-labeled peptides. *Biophys J*, **81,** 2241-2250.

[132] McNulty JC, Silapie JL, Carnevali M, Farrar CT, Griffin RG, Formaggio F, Crisma M, Toniolo C, & Milhauser GL (2000) Electron spin resonance of TOAC labeled peptides: Folding transitions and high frequency spectroscopy. *Biopolymers*, **55,** 479-485.

[133] Barbosa SR, Cilli EM, Lamy-Freund MT, Castrucci AML, & Nakaie CR (1999) First synthesis of a fully active spin-labeled peptide hormone. *FEBS Lett*, **446,** 45-48.

[134] Karim CB, Kirby TL, Zhang Z, Nesmelov Y, & Thomas DD (2004) Phospholamban structural dynamics in lipid bilayers probed by a spin label rigidly coupled to the peptide backbone. *Proc Natl Acad Sci USA*, **101,** 14437-14442.

[135] Smythe ML, Nakaie CR, & Marshall GR (1995) a-helical versus 3_{10}-helical conformation of alanine-based peptides in aqueous solution: An electron spin resonance investigation. *J Am Chem Soc*, **117,** 10555-10562.

[136] Toniolo C, Crisma M, & Formaggio F (1998) TOAC, a nitroxide spin-labeled, achiral C^{a}-tetrasubstituted a-amino acid, is an excellent tool in material science and biochemistry. *Biopolymers*, **47,** 153-158.

[137] Pertinhez TA, Nakaie CR, Paiva ACM, & Schreier S (1997) Spin-labeled extracellular loop from a seven-transmembrane helix receptor: Studies in solution and interaction with model membranes. *Biopolymers*, **42,** 821-829.

[138] Inbaraj JJ, Laryukhin M, & Lorigan GA (2007) Determining the helical tilt angle of a transmembrane helix in mechanically aligned lipid bilayers using EPR spectroscopy. *J Am Chem Soc*, **129,** 7710-7711.

[139] Thomas JW, Ellis B, Boerner RJ, Knight WB, White II GC, & Schaller MD (1998) SH2- and SH3-mediated interactions between focal adhesion kinase and Src. *J Biol Chem*, **273,** 577-583.

[140] Gasteiger E, Hoogland C, Gattiker A, Duvaud S, Wilkins MR, Appel RD, & Bairoch A (2005) Protein identification and analysis tools on the ExPASy server. In *The proteomics protocols handbook* (Walker JM, ed), pp. 571-607. Humana Press.

[141] Hiemstra HS, Duinkerken G, Benckhuijsen WE, Amons R, de Vries RRP, Roep BO, & Drijfhout JW (1997) The identification of $CD4^+$ T cell epitopes with dedicated synthetic peptide libraries. *Proc Natl Acad Sci USA*, **94,** 10313-10318.

[142] Helgstrand M, Kraulis P, Allard P, & Härd T (2000) Ansig for Windows: An interactive computer program for semiautomatic assignment of protein NMR spectra. *J Biomol NMR*, **18,** 329-336.

[143] Kraulis PJ (1989) Ansig - A program for the assignment of protein ^1H and 2D NMR spectra by interactive computer graphics. *J Magn Reson*, **84,** 627-633.

[144] Tessari M, Gentile LN, Taylor SJ, Shalloway DI, Nicholson LK, & Vuister GW (1997) Heteronuclear NMR studies of the combined Src homology domains 2 and 3 of pp60 c-Src: Effects of phosphopeptide binding. *Biochemistry*, **36,** 14561-14571.

[145] Kannt A, Young S, & Bendall DS (1996) The role of acidic residues of plastocyanin in its interaction with cytochrome f. *BBA - Bioenergetics*, **1277,** 115-126.

[146] Cobas JC & Sardina FJ (2003) Nuclear magnetic resonance data processing. MestRe-C: A software package for desktop computers. *Concept Magn Reson A*, **19A,** 80-96.

[147] García de la Torre J, Huertas ML, & Carrasco B (2000) HYDRONMR: Prediction of NMR relaxation of globular proteins from atomic-level structures and hydrodynamic calculations. *J Magn Reson*, **147,** 138-146.

[148] Schwieters CD, Kuszewski JJ, Tjandra N, & Clore GM (2003) The Xplor-NIH NMR molecular structure determination package. *J Magn Reson*, **160,** 65-73.

[149] Iwahara J, Schwieters CD, & Clore GM (2004) Ensemble approach for NMR structure refinement against ^{1}H paramagnetic relaxation enhancement data arising from a flexible paramagnetic group attached to a macromolecule. *J Am Chem Soc*, **126,** 5879-5896.

[150] DeLano WL. The PyMol molecular graphics system, DeLano scientific, Palo Alto, CA, USA. 2002.
Ref Type: Computer Program

[151] Hanson P, Anderson DJ, Martinez G, Millhauser G, Formaggio F, Crisma M, Toniolo C, & Vita C (1998) Electron spin resonance and structural analysis of water soluble, alanine-rich peptides incorporating TOAC. *Mol Phys*, **95,** 957-966.

[152] Iwahara J, Tang C, & Clore GM (2007) Practical aspects of ^{1}H transverse paramagnetic relaxation enhancement measurements on macromolecules. *J Magn Reson*, **184,** 185-195.

[153] Parsons JT (2003) Focal adhesion kinase: the first ten years. *J Cell Sci*, **116,** 1409-1416.

[154] Boggon TJ & Eck MJ (2004) Structure and regulation of Src family kinases. *Oncogene*, **23,** 7918-7927.

[155] Bradshaw JM & Waksman G (2003) Molecular recognition by SH2 domains. In *Protein modules and protein-protein interactions* (Janin J & Wodak SJ, eds), pp. 161-210.

[156] Songyang Z, Shoelson SE, Chaudhuri M, Gish G, Pawson T, Haser WG, King F, Roberts T, Ratnofsky S, Lechleider RJ, Neel BG, Birge RB, Fajardo JE, Chou MM, Hanafusa H, Schaffhausen B, & Cantley LC (1993) SH2 domains recognize specific phosphopeptide sequences. *Cell*, **72,** 767-778.

[157] Songyang Z, Shoelson SE, Chaudhuri M, Gish G, Pawson T, Haser WG, King F, Roberts T, Ratnofsky S, Lechleider RJ, Neel BG, Birge RB, Fajardo JE, Chou MM, Hanafusa H, Schaffhausen B, & Cantley LC (1993) SH2 domains recognize specific phosphopeptide sequences. *Cell*, **72,** 767-778.

[158] Waksman G, Shoelson SE, Pant N, Cowburn D, & Kuriyan J (1993) Binding of a high affinity phosphotyrosyl peptide to the Src SH2 domain: crystal structures of the complexed and peptide-free forms. *Cell*, **72,** 779-790.

[159] Xu WQ, Harrison SC, & Eck MJ (1997) Three-dimensional structure of the tyrosine kinase c-Src. *Nature*, **385,** 595-602.

[160] Mitra SK & Schlaepfer DD (2006) Integrin-regulated FAK-Src signaling in normal and cancer cells. *Curr Opin Cell Biol*, **18,** 516-523.

[161] Eide BL, Turck CW, & Escobedo JA (1995) Identification of Tyr-397 as the primary site of tyrosine phosphorylation and pp60src association in the focal adhesion kinase, pp125FAK. *Mol Cell Biol*, **15,** 2819-2827.

[162] Schaller MD, Hildebrand JD, Shannon JD, Fox JW, Vines RR, & Parsons JT (1994) Autophosphorylation of the focal adhesion kinase, pp125FAK, directs SH2-dependent binding of pp60src. *Mol Cell Biol*, **14,** 1680-1688.

[163] Xing Z, Chen HC, Nowlen JK, Taylor SJ, Shalloway D, & Guan JL (1994) Direct interaction of v-Src with the focal adhesion kinase mediated by the Src SH2 domain. *Mol Biol Cell*, **5,** 413-421.

[164] Hulsker R, Baranova MV, Bullerjahn GS, & Ubbink M (2008) Dynamics in the Transient Complex of Plastocyanin-Cytochrome f from Prochlorothrix hollandica. *J Am Chem Soc*, **130,** 1985-1991.

[165] Liang ZX, Jiang M, Ning Q, & Hoffman BM (2002) Dynamic docking and electron transfer between myoglobin and cytochrome b(5). *J Biol Inorg Chem*, **7,** 580-588.

[166] Volkov AN, Ferrari D, Worrall JAR, Bonvin AMJJ, & Ubbink M (2005) The orientations of cytochrome c in the highly dynamic complex with cytochrome b(5) visualized by NMR and docking using HADDOCK. *Protein Sci*, **14,** 799-811.

[167] Worrall JAR, Liu YJ, Crowley PB, Nocek JM, Hoffman BM, & Ubbink M (2002) Myoglobin and cytochrome b(5): A nuclear magnetic resonance study of a highly dynamic protein complex. *Biochemistry*, **41,** 11721-11730.

[168] Ubbink M (2009) The courtship of proteins: understanding the encounter complex. *FEBS Lett*, **583,** 1060-1066.

[169] Schreiber G & Fersht AR (1996) Rapid, electrostatically assisted association of proteins. *Nat Struct Biol*, **3,** 427-431.

[170] Sheinerman FB, Norel R, & Honig B (2000) Electrostatic aspects of protein-protein interactions. *Curr Opin Struct Biol*, **10,** 153-159.

[171] Delbrück M & Adam G (1968) Reduction of dimensionality in biological diffusion processes. In *Structural chemistry and molecular biology* (Rich A & Davidson N, eds), pp. 198-215. Freeman, San Francisco.

[172] Xu X, Reinle W, Hannemann F, Konarev PV, Svergun DI, Bernhardt R, & Ubbink M (2008) Dynamics in a pure encounter complex of two proteins studied by solution scattering and paramagnetic NMR spectroscopy. *J Am Chem Soc*, **130,** 6395-6403.

[173] Tang C, Louis JM, Aniana A, Suh JY, & Clore GM (2008) Visualizing transient events in amino-terminal autoprocessing of HIV-1 protease. *Nature*, **455,** 693-696.

[174] Xu RX, Word JM, Davis DG, Rink MJ, Willard DH, & Gampe RT (1995) Solution structure of the human pp60(C-Src) SH2 domain complexed with a phosphorylated tyrosine pentapeptide. *Biochemistry*, **34,** 2107-2121.

[175] Xu RX, Word JM, Davis DG, Rink MJ, Willard DH, & Gampe RT (1995) Solution structure of the human pp60(C-Src) SH2 domain complexed with a phosphorylated tyrosine pentapeptide. *Biochemistry*, **34,** 2107-2121.

[176] Bradshaw JM & Waksman G (1999) Calorimetric examination of high-affinity Src SH2 domain-tyrosyl phosphopeptide binding: Dissection of the phosphopeptide sequence specificity and coupling energetics. *Biochemistry*, **38,** 5147-5154.

[177] Bradshaw JM & Waksman G (1999) Calorimetric examination of high-affinity Src SH2 domain-tyrosyl phosphopeptide binding: Dissection of the phosphopeptide sequence specificity and coupling energetics. *Biochemistry*, **38,** 5147-5154.

[178] Xu RX, Word JM, Davis DG, Rink MJ, Willard DH, & Gampe RT (1995) Solution structure of the human pp60(C-Src) SH2 domain complexed with a phosphorylated tyrosine pentapeptide. *Biochemistry*, **34,** 2107-2121.

[179] Xu RX, Word JM, Davis DG, Rink MJ, Willard DH, & Gampe RT (1995) Solution structure of the human pp60(C-Src) SH2 domain complexed with a phosphorylated tyrosine pentapeptide. *Biochemistry*, **34,** 2107-2121.

[180] Xu RX, Word JM, Davis DG, Rink MJ, Willard DH, & Gampe RT (1995) Solution structure of the human pp60(C-Src) SH2 domain complexed with a phosphorylated tyrosine pentapeptide. *Biochemistry*, **34,** 2107-2121.

[181] Xu RX, Word JM, Davis DG, Rink MJ, Willard DH, & Gampe RT (1995) Solution structure of the human pp60(C-Src) SH2 domain complexed with a phosphorylated tyrosine pentapeptide. *Biochemistry*, **34,** 2107-2121.

[182] Xu RX, Word JM, Davis DG, Rink MJ, Willard DH, & Gampe RT (1995) Solution structure of the human pp60(C-Src) SH2 domain complexed with a phosphorylated tyrosine pentapeptide. *Biochemistry*, **34,** 2107-2121.

[183] Ubbink M (2009) The courtship of proteins: understanding the encounter complex. *FEBS Lett*, **583,** 1060-1066.

[184] Suh JY, Tang C, & Clore GM (2007) Role of electrostatic interactions in transient encounter complexes in protein-protein association investigated by paramagnetic relaxation enhancement. *J Am Chem Soc*, **129,** 12954-12955.

[185] Xu RX, Word JM, Davis DG, Rink MJ, Willard DH, & Gampe RT (1995) Solution structure of the human pp60(C-Src) SH2 domain complexed with a phosphorylated tyrosine pentapeptide. *Biochemistry*, **34,** 2107-2121.

[186] Xu RX, Word JM, Davis DG, Rink MJ, Willard DH, & Gampe RT (1995) Solution structure of the human pp60(C-Src) SH2 domain complexed with a phosphorylated tyrosine pentapeptide. *Biochemistry*, **34,** 2107-2121.

[187] Pawson T & Nash P (2003) Assembly of cell regulatory systems through protein interaction domains. *Science*, **300,** 445-452.

[188] Campbell ID (2003) Modular proteins at the cell surface. *Biochem Soc Trans*, **31,** 1107-1114.

[189] Roskoski R (2004) Src protein-tyrosine kinase structure and regulation. *Biochem Biophys Res Commun*, **324,** 1155-1164.

[190] Boggon TJ & Eck MJ (2004) Structure and regulation of Src family kinases. *Oncogene*, **23,** 7918-7927.

[191] Campbell ID (2003) Modular proteins at the cell surface. *Biochem Soc Trans*, **31,** 1107-1114.

[192] Mayer BJ, Hamaguchi M, & Hanafusa H (1988) A novel viral oncogene with structural similarity to phospholipase C. *Nature*, **332,** 272-275.

[193] Sadowski I, Stone JC, & Pawson T (1986) A noncatalytic domain conserved among cytoplasmic protein-tyrosine kinases modifies the kinase function and transforming activity of fujinami sarcoma-virus p130Gag-Fps. *Mol Cell Biol*, **6,** 4396-4408.

[194] Sicheri F, Moarefi I, & Kuriyan J (1997) Crystal structure of the Src family tyrosine kinase Hck. *Nature*, **385,** 602-609.

[195] Williams JC, Weijland A, Gonfloni S, Thompson A, Courtneidge SA, Superti-Furga G, & Wierenga RK (1997) The 2.35 A crystal structure of the inactivated form of chicken Src: a dynamic molecule with multiple regulatory interactions. *J Mol Biol*, **274,** 757-775.

[196] Xu WQ, Harrison SC, & Eck MJ (1997) Three-dimensional structure of the tyrosine kinase c-Src. *Nature*, **385,** 595-602.

[197] Xu WQ, Doshi A, Lei M, Eck MJ, & Harrison SC (1999) Crystal structures of c-Src reveal features of its autoinhibitory mechanism. *Mol Cell*, **3,** 629-638.

[198] Moarefi I, LaFevre-Bernt M, Sicheri F, Huse M, Lee CH, Kuriyan J, & Miller WT (1997) Activation of the Src-family tyrosine kinase Hck by SH3 domain displacement. *Nature*, **385,** 650-653.

[199] Stover DR, Liebetanz J, & Lydon NB (1994) Cdc2-mediated modulation of pp60c-src activity. *J Biol Chem*, **269,** 26885-26889.

[200] Arold ST, Ulmer TS, Mulhern TD, Werner JM, Ladbury JE, Campbell ID, & Noble ME (2001) The role of the Src homology 3-Src homology 2 interface in the regulation of Src kinases. *J Biol Chem*, **276,** 17199-17205.

[201] Faraldo-Gomez JD & Roux B (2007) On the importance of a funneled energy landscape for the assembly and regulation of multidomain Src tyrosine kinases. *Proc Natl Acad Sci USA*, **104,** 13643-13648.

[202] Hochrein JM, Lerner EC, Schiavone AP, Smithgall TE, & Engen JR (2006) An examination of dynamics crosstalk between SH2 and SH3 domains by hydrogen/deuterium exchange and mass spectrometry. *Protein Sci*, **15,** 65-73.

[203] Hofmann G, Schweimer K, Kiessling A, Hofinger E, Bauer F, Hoffmann S, Rosch P, Campbell ID, Werner JM, & Sticht H (2005) Binding, domain orientation, and dynamics of the Lck SH3-SH2 domain pair and comparison with other Src-family kinases. *Biochemistry*, **44,** 13043-13050.

[204] Panchamoorthy G, Fukazawa T, Stolz L, Payne G, Reedquist K, Shoelson S, Songyang Z, Cantley L, Walsh C, & Band H (1994) Physical and functional interactions between SH2 and SH3 domains of the Src family protein tyrosine kinase p59fyn. *Mol Cell Biol*, **14,** 6372-6385.

[205] Ulmer TS, Werner JM, & Campbell ID (2002) SH3-SH2 domain orientation in Src kinases: NMR studies of Fyn. *Structure*, **10,** 901-911.

[206] Young MA, Gonfloni S, Superti-Furga G, Roux B, & Kuriyan J (2001) Dynamic coupling between the SH2 and SH3 domains of c-Src and hck underlies their inactivation by C-terminal tyrosine phosphorylation. *Cell*, **105,** 115-126.

[207] Arold ST, Ulmer TS, Mulhern TD, Werner JM, Ladbury JE, Campbell ID, & Noble ME (2001) The role of the Src homology 3-Src homology 2 interface in the regulation of Src kinases. *J Biol Chem*, **276,** 17199-17205.

[208] Cobb BS, Schaller MD, Leu TH, & Parsons JT (1994) Stable association of pp60src and pp59fyn with the focal adhesion-associated protein tyrosine kinase, pp125FAK. *Mol Cell Biol*, **14,** 147-155.

[209] Mitra SK, Hanson DA, & Schlaepfer DD (2005) Focal adhesion kinase: in command and control of cell motility. *Nat Rev Mol Cell Biol*, **6,** 56-68.

[210] Cohen GB, Ren R, & Baltimore D (1995) Modular binding domains in signal transduction proteins. *Cell*, **80,** 237-248.

[211] Songyang Z, Shoelson SE, Chaudhuri M, Gish G, Pawson T, Haser WG, King F, Roberts T, Ratnofsky S, Lechleider RJ, Neel BG, Birge RB, Fajardo JE, Chou MM, Hanafusa H, Schaffhausen B, & Cantley LC (1993) SH2 domains recognize specific phosphopeptide sequences. *Cell*, **72,** 767-778.

[212] Arold ST, Ulmer TS, Mulhern TD, Werner JM, Ladbury JE, Campbell ID, & Noble ME (2001) The role of the Src homology 3-Src homology 2 interface in the regulation of Src kinases. *J Biol Chem*, **276,** 17199-17205.

[213] Arold ST, Ulmer TS, Mulhern TD, Werner JM, Ladbury JE, Campbell ID, & Noble ME (2001) The role of the Src homology 3-Src homology 2 interface in the regulation of Src kinases. *J Biol Chem*, **276,** 17199-17205.

[214] Arold ST, Ulmer TS, Mulhern TD, Werner JM, Ladbury JE, Campbell ID, & Noble ME (2001) The role of the Src homology 3-Src homology 2 interface in the regulation of Src kinases. *J Biol Chem*, **276,** 17199-17205.

[215] Arold ST, Ulmer TS, Mulhern TD, Werner JM, Ladbury JE, Campbell ID, & Noble ME (2001) The role of the Src homology 3-Src homology 2 interface in the regulation of Src kinases. *J Biol Chem*, **276,** 17199-17205.

[216] Arold ST, Ulmer TS, Mulhern TD, Werner JM, Ladbury JE, Campbell ID, & Noble ME (2001) The role of the Src homology 3-Src homology 2 interface in the regulation of Src kinases. *J Biol Chem*, **276,** 17199-17205.

[217] Xu WQ, Harrison SC, & Eck MJ (1997) Three-dimensional structure of the tyrosine kinase c-Src. *Nature*, **385,** 595-602.

[218] Xu X, Reinle W, Hannemann F, Konarev PV, Svergun DI, Bernhardt R, & Ubbink M (2008) Dynamics in a pure encounter complex of two proteins studied by solution scattering and paramagnetic NMR spectroscopy. *J Am Chem Soc*, **130,** 6395-6403.

[219] Caspers P, Stieger M, & Burn P (1994) Overproduction of Bacterial Chaperones Improves the Solubility of Recombinant Protein-Tyrosine Kinases in Escherichia-Coli. *Cell Mol Biol*, **40,** 635-644.

[220] Seeliger MA, Young M, Henderson MN, Pellicena P, King DS, Falick AM, & Kuriyan J (2005) High yield bacterial expression of active c-Abl and c-Src tyrosine kinases. *Protein Sci*, **14,** 3135-3139.

[221] Wang WR, Marimuthu A, Tsai J, Kumar A, Krupka HI, Zhang C, Powell B, Suzuki Y, Nguyen H, Tabrizizad M, Luu C, & West BL (2006) Structural

characterization of autoinhibited c-Met kinase produced by coexpression in bacteria with phosphatase. *Proc Natl Acad Sci USA*, **103,** 3563-3568.

[222] Cowan-Jacob SW (2006) Structural biology of protein tyrosine kinases. *Cell Mol Life Sci*, **63,** 2608-2625.

[223] Lietha D, Cai X, Ceccarelli DF, Li Y, Schaller MD, & Eck MJ (2007) Structural basis for the autoinhibition of focal adhesion kinase. *Cell*, **129,** 1177-1187.

[224] Nowakowski J, Cronin CN, McRee DE, Knuth MW, Nelson CG, Pavletich NP, Rogers J, Sang BC, Scheibe DN, Swanson RV, & Thompson DA (2002) Structures of the cancer-related Aurora-A, FAK, and EphA2 protein kinases from nanovolume crystallography. *Structure*, **10,** 1659-1667.

[225] Withers BE, Keller PR, & Fry DW (1996) Expression, purification, and characterization of focal adhesion kinase using a baculovirus system. *Protein Expr Purif*, **7,** 12-18.

[226] Invitrogen life technologies (2002) Instruction manual, Bac-to-Bac Baculovirus expression system, http://tools.invitrogen.com/content/sfs/manuals/bac.pdf.

[227] Bliska JB, Guan KL, Dixon JE, & Falkow S (1991) Tyrosine Phosphate Hydrolysis of Host Proteins by An Essential Yersinia-Virulence Determinant. *Proc Natl Acad Sci USA*, **88,** 1187-1191.

[228] Gordon JA (1991) Use of Vanadate As Protein-Phosphotyrosine Phosphatase Inhibitor. *Methods Enzymol*, **201,** 477-482.

[229] Breitenlechner CB, Kairies NA, Honold K, Scheiblich S, Koll H, Greiter E, Koch S, Schafer W, Huber R, & Engh RA (2005) Crystal structures of active SRC kinase domain complexes. *J Mol Biol*, **353,** 222-231.

[230] Cowan-Jacob SW, Fendrich G, Manley PW, Jahnke W, Fabbro D, Liebetanz J, & Meyer T (2005) The crystal structure of a c-Src complex in an active conformation suggests possible steps in c-Src activation. *Structure*, **13,** 861-871.

[231] Waksman G, Shoelson SE, Pant N, Cowburn D, & Kuriyan J (1993) Binding of a high affinity phosphotyrosyl peptide to the Src SH2 domain: crystal structures of the complexed and peptide-free forms. *Cell*, **72,** 779-790.

[232] Xu WQ, Harrison SC, & Eck MJ (1997) Three-dimensional structure of the tyrosine kinase c-Src. *Nature*, **385,** 595-602.

[233] Xu WQ, Doshi A, Lei M, Eck MJ, & Harrison SC (1999) Crystal structures of c-Src reveal features of its autoinhibitory mechanism. *Mol Cell*, **3,** 629-638.

[234] Arold ST, Hoellerer MK, & Noble ME (2002) The structural basis of localization and signaling by the focal adhesion targeting domain. *Structure*, **10,** 319-327.

[235] Ceccarelli DF, Song HK, Poy F, Schaller MD, & Eck MJ (2006) Crystal structure of the FERM domain of focal adhesion kinase. *J Biol Chem*, **281,** 252-259.

[236] Hayashi I, Vuori K, & Liddington RC (2002) The focal adhesion targeting (FAT) region of focal adhesion kinase is a four-helix bundle that binds paxillin. *Nat Struct Biol*, **9,** 101-106.

[237] Nowakowski J, Cronin CN, McRee DE, Knuth MW, Nelson CG, Pavletich NP, Rogers J, Sang BC, Scheibe DN, Swanson RV, & Thompson DA (2002) Structures of the cancer-related Aurora-A, FAK, and EphA2 protein kinases from nanovolume crystallography. *Structure*, **10,** 1659-1667.

[238] Lietha D, Cai X, Ceccarelli DF, Li Y, Schaller MD, & Eck MJ (2007) Structural basis for the autoinhibition of focal adhesion kinase. *Cell*, **129,** 1177-1187.

[239] Xu RX, Word JM, Davis DG, Rink MJ, Willard DH, & Gampe RT (1995) Solution structure of the human pp60(C-Src) SH2 domain complexed with a phosphorylated tyrosine pentapeptide. *Biochemistry*, **34,** 2107-2121.

[240] Yu H, Rosen MK, & Schreiber SL (1993) 1H and 15N assignments and secondary structure of the Src SH3 domain. *FEBS Lett*, **324,** 87-92.

[241] Liu G, Guibao CD, & Zheng J (2002) Structural insight into the mechanisms of targeting and signaling of focal adhesion kinase. *Mol Cell Biol*, **22,** 2751-2760.

[242] Prutzman KC, Gao G, King ML, Iyer VV, Mueller GA, Schaller MD, & Campbell SL (2004) The focal adhesion targeting domain of focal adhesion kinase contains a hinge region that modulates tyrosine 926 phosphorylation. *Structure*, **12,** 881-891.

[243] Breitenlechner CB, Kairies NA, Honold K, Scheiblich S, Koll H, Greiter E, Koch S, Schafer W, Huber R, & Engh RA (2005) Crystal structures of active SRC kinase domain complexes. *J Mol Biol*, **353,** 222-231.

[244] Cowan-Jacob SW, Fendrich G, Manley PW, Jahnke W, Fabbro D, Liebetanz J, & Meyer T (2005) The crystal structure of a c-Src complex in an active conformation suggests possible steps in c-Src activation. *Structure*, **13,** 861-871.

[245] Waksman G, Shoelson SE, Pant N, Cowburn D, & Kuriyan J (1993) Binding of a high affinity phosphotyrosyl peptide to the Src SH2 domain: crystal structures of the complexed and peptide-free forms. *Cell*, **72,** 779-790.

[246] Xu WQ, Harrison SC, & Eck MJ (1997) Three-dimensional structure of the tyrosine kinase c-Src. *Nature*, **385,** 595-602.

[247] Xu WQ, Doshi A, Lei M, Eck MJ, & Harrison SC (1999) Crystal structures of c-Src reveal features of its autoinhibitory mechanism. *Mol Cell*, **3,** 629-638.

[248] Arold ST, Hoellerer MK, & Noble ME (2002) The structural basis of localization and signaling by the focal adhesion targeting domain. *Structure*, **10,** 319-327.

[249] Hayashi I, Vuori K, & Liddington RC (2002) The focal adhesion targeting (FAT) region of focal adhesion kinase is a four-helix bundle that binds paxillin. *Nat Struct Biol*, **9,** 101-106.

[250] Ceccarelli DF, Song HK, Poy F, Schaller MD, & Eck MJ (2006) Crystal structure of the FERM domain of focal adhesion kinase. *J Biol Chem*, **281,** 252-259.

[251] Nowakowski J, Cronin CN, McRee DE, Knuth MW, Nelson CG, Pavletich NP, Rogers J, Sang BC, Scheibe DN, Swanson RV, & Thompson DA (2002) Structures of the cancer-related Aurora-A, FAK, and EphA2 protein kinases from nanovolume crystallography. *Structure*, **10,** 1659-1667.

[252] Lietha D, Cai X, Ceccarelli DF, Li Y, Schaller MD, & Eck MJ (2007) Structural basis for the autoinhibition of focal adhesion kinase. *Cell*, **129,** 1177-1187.

[253] Yu H, Rosen MK, & Schreiber SL (1993) 1H and 15N assignments and secondary structure of the Src SH3 domain. *FEBS Lett*, **324,** 87-92.

[254] Xu RX, Word JM, Davis DG, Rink MJ, Willard DH, & Gampe RT (1995) Solution structure of the human pp60(C-Src) SH2 domain complexed with a phosphorylated tyrosine pentapeptide. *Biochemistry*, **34,** 2107-2121.

[255] Liu G, Guibao CD, & Zheng J (2002) Structural insight into the mechanisms of targeting and signaling of focal adhesion kinase. *Mol Cell Biol*, **22,** 2751-2760.

[256] Prutzman KC, Gao G, King ML, Iyer VV, Mueller GA, Schaller MD, & Campbell SL (2004) The focal adhesion targeting domain of focal adhesion kinase contains a hinge region that modulates tyrosine 926 phosphorylation. *Structure*, **12,** 881-891.

[257] Xu RX, Word JM, Davis DG, Rink MJ, Willard DH, & Gampe RT (1995) Solution structure of the human pp60(C-Src) SH2 domain complexed with a phosphorylated tyrosine pentapeptide. *Biochemistry*, **34,** 2107-2121.

[258] Xu RX, Word JM, Davis DG, Rink MJ, Willard DH, & Gampe RT (1995) Solution structure of the human pp60(C-Src) SH2 domain complexed with a phosphorylated tyrosine pentapeptide. *Biochemistry*, **34,** 2107-2121.

[259] Worrall JAR, Reinle W, Bernhardt R, & Ubbink M (2003) Transient protein interactions studied by NMR spectroscopy: The case of cytochrome C and adrenodoxin. *Biochemistry*, **42,** 7068-7076.

[260] Giepmans BNG, Adams SR, Ellisman MH, & Tsien RY (2006) Review - The fluorescent toolbox for assessing protein location and function. *Science*, **312,** 217-224.

[261] Huebsch ND & Mooney DJ (2007) Fluorescent resonance energy transfer: A tool for probing molecular cell-biomaterial interactions in three dimensions. *Biomaterials*, **28,** 2424-2437.

[262] Lichtman JW & Conchello JA (2005) Fluorescence microscopy. *Nat Methods*, **2,** 910-919.

[263] Tsien RY (1998) The green fluorescent protein. *Annu Rev Biochem*, **67,** 509-544.

[264] Zhang J, Campbell RE, Ting AY, & Tsien RY (2002) Creating new fluorescent probes for cell biology. *Nat Rev Mol Cell Biol*, **3,** 906-918.

[265] Wang YX, Shyy JYJ, & Chien S (2008) Fluorescence proteins, live-cell imaging, and mechanobiology: Seeing is believing. *Annu Rev Biomed Eng*, **10,** 1-38.

[266] Fujioka A, Terai K, Itoh RE, Aoki K, Nakamura T, Kuroda S, Nishida E, & Matsuda M (2006) Dynamics of the Ras/ERK MAPK cascade as monitored by fluorescent probes. *J Biol Chem*, **281,** 8917-8926.

[267] Kunkel MT, Ni Q, Tsien RY, Zhang J, & Newton AC (2005) Spatio-temporal dynamics of protein kinase B/Akt signaling revealed by a genetically encoded fluorescent reporter. *J Biol Chem*, **280,** 5581-5587.

[268] Sato M, Ozawa T, Inukai K, Asano T, & Umezawa Y (2002) Fluorescent indicators for imaging protein phosphorylation in single living cells. *Nat Biotechnol*, **20,** 287-294.

[269] Ting AY, Kain KH, Klemke RL, & Tsien RY (2001) Genetically encoded fluorescent reporters of protein tyrosine kinase activities in living cells. *Proc Natl Acad Sci USA*, **98,** 15003-15008.

[270] Violin JD, Zhang J, Tsien RY, & Newton AC (2003) A genetically encoded fluorescent reporter reveals oscillatory phosphorylation by protein kinase C. *J Cell Biol*, **161,** 899-909.

[271] Zhang J, Ma YL, Taylor SS, & Tsien RY (2001) Genetically encoded reporters of protein kinase A activity reveal impact of substrate tethering. *Proc Natl Acad Sci USA*, **98,** 14997-15002.

[272] Zhang J, Hupfeld CJ, Taylor SS, Olefsky JM, & Tsien RY (2005) Insulin disrupts beta-adrenergic signalling to protein kinase A in adipocytes. *Nature*, **437,** 569-573.

[273] Wang YX, Botvinick EL, Zhao YH, Berns MW, Usami S, Tsien RY, & Chien S (2005) Visualizing the mechanical activation of Src. *Nature*, **434,** 1040-1045.

[274] Ballestrem C, Erez N, Kirchner J, Kam Z, Bershadsky A, & Geiger B (2006) Molecular mapping of tyrosine-phosphorylated proteins in focal adhesions using fluorescence resonance energy transfer. *J Cell Sci*, **119,** 866-875.

[275] Hamadi A, Bouali M, Dontenwill M, Stoeckel H, Takeda K, & Ronde P (2005) Regulation of focal adhesion dynamics and disassembly by phosphorylation of FAK at tyrosine 397. *J Cell Sci*, **118,** 4415-4425.

[276] Kirchner J, Kam Z, Tzur G, Bershadsky AD, & Geiger B (2003) Live-cell monitoring of tyrosine phosphorylation in focal adhesions following microtubule disruption. *J Cell Sci*, **116,** 975-986.

[277] Caamano AM, Vazquez ME, Martinez-Costas J, Castedo L, & Mascarenas JL (2000) A light-modulated sequence-specific DNA-binding peptide. *Angew Chem Int Ed Engl*, **39,** 3104-3107.

[278] Guerrero L, Smart OS, Woolley GA, & Allemann RK (2005) Photocontrol of DNA binding specificity of a miniature engrailed homeodomain. *J Am Chem Soc*, **127,** 15624-15629.

[279] Guerrero L, Smart OS, Weston CJ, Burns DC, Woolley GA, & Allemann RK (2005) Photochemical regulation of DNA-binding specificity of MyoD. *Angew Chem Int Ed Engl*, **44,** 7778-7782.

[280] Hansen KC, Rock RS, Larsen RW, & Chan SI (2000) A method for photoinitating protein folding in a nondenaturing environment. *J Am Chem Soc*, **122,** 11567-11568.

[281] Hess GP & Grewer C (1998) Development and application of caged ligands for neurotransmitter receptors in transient kinetic and neuronal circuit mapping studies. *Methods Enzymol*, ***291,*** 443.

[282] Hirota S, Fujimoto Y, Choi J, Baden N, Katagiri N, Akiyama M, Hulsker R, Ubbink M, Okajima T, Takabe T, Funasaki N, Watanabe Y, & Terazima M (2006) Conformational changes during apoplastocyanin folding observed by photocleavable modification and transient grating. *J Am Chem Soc*, **128,** 7551-7558.

[283] Humphrey D, Rajfur Z, Vazquez ME, Scheswohl D, Schaller MD, Jacobson K, & Imperiali B (2005) In Situ photoactivation of a caged phosphotyrosine peptide derived from focal adhesion kinase temporarily halts lamellar extension of single migrating tumor cells. *J Biol Chem*, **280,** 22091-22101.

[284] Kawakami T, Cheng H, Hashiro S, Nomura Y, Tsukiji S, Furuta T, & Nagamune T (2008) A caged phosphopeptide-based approach for photochemical activation of kinases in living cells. *Chembiochem*, **9,** 1583-1586.

[285] Kostiainen MA, Smith DK, & Ikkala O (2007) Optically triggered release of DNA from multivalent dendrons by degrading and charge-switching multivalency. *Angew Chem Int Ed Engl*, **46,** 7600-7604.

[286] Li H, Hah JM, & Lawrence DS (2008) Light-mediated liberation of enzymatic activity: "Small Molecule" caged protein equivalents. *J Am Chem Soc*, **130,** 10474-+.

[287] Lu HSM, Volk M, Kholodenko Y, Gooding E, Hochstrasser RM, & DeGrado WF (1997) Aminothiotyrosine disulfide, an optical trigger for initiation of protein folding. *J Am Chem Soc*, **119,** 7173-7180.

[288] Mccray JA & Trentham DR (1989) Properties and Uses of Photoreactive Caged Compounds. *Annu Rev Biophys Biophys Chem*, **18,** 239-270.

[289] Okuno T, Hirota S, & Yamauchi O (2000) Folding character of cytochrome c studied by o-nitrobenzyl modification of methionine 65 and subsequent ultraviolet light irradiation. *Biochemistry*, **39,** 7538-7545.

[290] Okuno T, Hirota S, & Yamauchi O (2000) Folding properties of cytochrome c studied by photocleavable o-nitrobenzyl modification of methionine 65 and 80. *Chem Lett*, 290-291.

[291] Petersen S, Alonso JM, Specht A, Duodu P, Goeldner M, & del Campo A (2008) Phototriggering of cell adhesion by caged cyclic RGD peptides. *Angew Chem Int Ed Engl*, **47,** 3192-3195.

[292] Renner C & Moroder L (2006) Azobenzene as conformational switch in model peptides. *Chembiochem*, **7,** 869-878.

[293] Schutt M, Krupka SS, Milbradt AG, Deindl S, Sinner EK, Oesterhelt D, Renner C, & Moroder L (2003) Photocontrol of cell adhesion processes: Model studies with cyclic azobenzene-RGD peptides. *Chem Biol*, **10,** 487-490.

[294] Taniguchi A, Sohma Y, Kimura M, Okada T, Ikeda K, Hayashi Y, Kimura T, Hirota S, Matsuzaki K, & Kiso Y (2006) "Click peptide" based on the "O-acyl isopeptide method": Control of A beta 1-42 production from a photo-triggered A beta 1-42 analogue. *J Am Chem Soc*, **128,** 696-697.

[295] Ulysse L, Cubillos J, & Chmielewski J (1995) Photoregulation of Cyclic Peptide Conformation. *J Am Chem Soc*, **117,** 8466-8467.

[296] Woolley GA (2005) Photocontrolling peptide alpha helices. *Acc Chem Res*, **38,** 486-493.

[297] Lawrence DS (2005) The preparation and in vivo applications of caged peptides and proteins. *Curr Opin Chem Biol*, **9,** 570-575.

[298] Vanhaesebroeck B & Waterfield MD (1999) Signaling by distinct classes of phosphoinositide 3-kinases. *Exp Cell Res*, **253,** 239-254.

[299] Yu H, Chen JK, Feng S, Dalgarno DC, Brauer AW, & Schreiber SL (1994) Structural basis for the binding of proline-rich peptides to SH3 domains. *Cell*, **76,** 933-945.

[300] Takahashi I, Kuroiwa S, Lindfors HE, Ndamba LA, Hiruma Y, Yajima T, Okishio N, Ubbink M, & Hirota S (2009) Modulation of protein-ligand interactions by photocleavage of a cyclic peptide using phosphatidylinositol 3-kinase SH3 domain as model system. *J Pept. Sci.*, **15,** 411-416.

[301] Takahashi I, Kuroiwa S, Lindfors HE, Ndamba LA, Hiruma Y, Yajima T, Okishio N, Ubbink M, & Hirota S (2009) Modulation of protein-ligand interactions by photocleavage of a cyclic peptide using phosphatidylinositol 3-kinase SH3 domain as model system. *J Pept. Sci.*, **15,** 411-416.

[302] Takahashi I, Kuroiwa S, Lindfors HE, Ndamba LA, Hiruma Y, Yajima T, Okishio N, Ubbink M, & Hirota S (2009) Modulation of protein-ligand interactions by photocleavage of a cyclic peptide using phosphatidylinositol 3-kinase SH3 domain as model system. *J Pept. Sci.*, **15,** 411-416.

[303] Koyama S, Yu H, Dalgarno DC, Shin TB, Zydowsky LD, & Schreiber SL (1993) H-1 and N-15 Assignments and Secondary Structure of the PI3K-Sh3 Domain. *FEBS Lett*, **324,** 93-98.

[304] Takahashi I, Kuroiwa S, Lindfors HE, Ndamba LA, Hiruma Y, Yajima T, Okishio N, Ubbink M, & Hirota S (2009) Modulation of protein-ligand interactions by photocleavage of a cyclic peptide using phosphatidylinositol 3-kinase SH3 domain as model system. *J Pept. Sci.*, **15,** 411-416.

[305] Yu H, Chen JK, Feng S, Dalgarno DC, Brauer AW, & Schreiber SL (1994) Structural basis for the binding of proline-rich peptides to SH3 domains. *Cell*, **76,** 933-945.

[306] Koyama S, Yu H, Dalgarno DC, Shin TB, Zydowsky LD, & Schreiber SL (1993) H-1 and N-15 Assignments and Secondary Structure of the PI3K-Sh3 Domain. *FEBS Lett*, **324,** 93-98.

[307] Koyama S, Yu H, Dalgarno DC, Shin TB, Zydowsky LD, & Schreiber SL (1993) H-1 and N-15 Assignments and Secondary Structure of the PI3K-Sh3 Domain. *FEBS Lett*, **324,** 93-98.

[308] Donaldson LW, Gish G, Pawson T, Kay LE, & Forman-Kay JD (2002) Structure of a regulatory complex involving the Abl SH3 domain, the Crk SH2 domain, and a Crk-derived phosphopeptide. *Proc Natl Acad Sci USA*, **99,** 14053-14058.

[309] Pawson T & Scott JD (1997) Signaling through scaffold, anchoring, and adaptor proteins. *Science*, **278,** 2075-2080.

[310] Pawson T & Nash P (2000) Protein-protein interactions define specificity in signal transduction. *Genes Dev*, **14,** 1027-1047.

[311] Grzesiek S, Bax A, Clore GM, Gronenborn AM, Hu JS, Kaufman J, Palmer I, Stahl SJ, & Wingfield PT (1996) The solution structure of HIV-1 Nef reveals an unexpected fold and permits delineation of the binding surface for the SH3 domain of Hck tyrosine protein kinase. *Nat Struct Biol*, **3,** 340-345.

[312] Lee CH, Saksela K, Mirza UA, Chait BT, & Kuriyan J (1996) Crystal structure of the conserved core of HIV-1 Nef complexed with a Src family SH3 domain. *Cell*, **85,** 931-942.

[313] Ahmad M, Gu W, & Helms V (2008) Mechanism of fast peptide recognition by SH3 domains. *Angew. Chem Int. Ed Engl.*, **47,** 7626-7630.

[314] Yu H, Chen JK, Feng S, Dalgarno DC, Brauer AW, & Schreiber SL (1994) Structural basis for the binding of proline-rich peptides to SH3 domains. *Cell*, **76,** 933-945.

Appendices

XPLOR-NIH restraint files belonging to chapter 2

```
! Distances derived from R2 data from Src SH3 binding to peptide
P3Tm
! store1 = fixed value for atoms that dissappear
! store2 = fixed distance for atoms that dissappear
! store3 = fixed value for atoms that are unaffected
! store4 = fixed distance for atoms that are unaffected
! store5 = observed R(para) value
! store6 = derived experimental distance

set mess=on end
set echo=off end
eval ($ide =1)
!-------------------------------------------------------------------
------
!----------------DEFINE UPPER-BOUND DISTANCE RESTRAINTS-------------
------
!-------------------------------------------------------------------
------
!Residue numbering as in PDB 1RLQ (+5 compared to our protein)

vector do (store1=96.03) (atom "    "  59 HN)

NOE
   nres=20000
   class CL1
   averaging CL1 R-6
   potential CL1 square
   sqconstant CL1 $a9
   sqoffset CL1 0.0
   scale CL1 $a10
   sqexponent CL1 2
   ceil=30.0
end


for $ide in ID (store1)
loop store_values
        vector show element (STORE1) (ID $ide)
       eval ($dist01= (1E8*((1.23E-
32*(4*$tau_c+(3*$tau_c/(1+(600.1328E6*2*3.14*$tau_c)^2)))*$frl*$frb/
$RESULT)^(1/6)) ) )
       NOE
         assign (ID $ide) (name TC) $dist01 $a4 $a5
       end
       vector do (store2=$dist01) (ID $ide)
end loop store_values
```

```
!--------------------------------------------------------------------
------
!----------------DEFINE LOWER-BOUND DISTANCE RESTRAINTS-------------
------
!--------------------------------------------------------------------
------
 vector do (store3=2.60) (atom "    "  9 HT1) !first aa in pdb, not
in protein, so really an amide
 vector do (store3=2.60) (atom "    "  10 HN)
 vector do (store3=2.60) (atom "    "  11 HN)
 vector do (store3=2.60) (atom "    "  12 HN)
 vector do (store3=2.60) (atom "    "  21 HN)
 vector do (store3=2.60) (atom "    "  22 HN)
 vector do (store3=2.60) (atom "    "  27 HN)
 vector do (store3=2.60) (atom "    "  31 HN)
 vector do (store3=2.60) (atom "    "  32 HN)
 vector do (store3=2.60) (atom "    "  33 HN)
 vector do (store3=2.60) (atom "    "  34 HN)
 vector do (store3=2.60) (atom "    "  35 HN)
 vector do (store3=2.60) (atom "    "  36 HN)
 vector do (store3=2.60) (atom "    "  38 HN)
 vector do (store3=2.60) (atom "    "  39 HN)
 vector do (store3=2.60) (atom "    "  40 HN)
 vector do (store3=2.60) (atom "    "  44 HN)
 vector do (store3=2.60) (atom "    "  45 HN)
 vector do (store3=2.60) (atom "    "  46 HN)
 vector do (store3=2.60) (atom "    "  47 HN)
 vector do (store3=2.60) (atom "    "  48 HN)
 vector do (store3=2.60) (atom "    "  49 HN)
 vector do (store3=2.60) (atom "    "  50 HN)
 vector do (store3=2.60) (atom "    "  51 HN)
 vector do (store3=2.60) (atom "    "  52 HN)
 vector do (store3=2.60) (atom "    "  62 HN)
 vector do (store3=2.60) (atom "    "  55 HN)
 vector do (store3=2.60) (atom "    "  56 HN)


NOE
   class CL2
   averaging CL2 R-6
   potential CL2 square
   sqconstant CL2 $a9
   sqoffset CL2 0.0
   scale CL2 $a11
   sqexponent CL2 2
end


for $ide in ID (store3)
loop store_values
        vector show element (STORE3) (ID $ide)
       eval ($dist01= (1E8*((1.23E-
32*(4*$tau_c+(3*$tau_c/(1+(600.1328E6*2*3.14*$tau_c)^2)))*$frl*$frb/
$RESULT)^(1/6)) ) )
```

```
       NOE
         assign (ID $ide) (name TC) $dist01 $a7 $a8
       end
       vector do (store4=$dist01) (ID $ide)
end loop store_values


!-------------------------------------------------------------------
------
!----------------DEFINE 2-BOUNDED DISTANCE RESTRAINTS---------------
------
!-------------------------------------------------------------------
------


! store R2(para) values as measured

 vector do (store5=27.63) (atom "    "  13 HN)
 vector do (store5=51.42) (atom "    "  14 HN)
 vector do (store5=108.08) (atom "    "  15 HN)
 vector do (store5=21.41) (atom "    "  16 HN)
 vector do (store5=45.32) (atom "    "  17 HN)
 vector do (store5=11.59) (atom "    "  28 HN)
 vector do (store5=6.15) (atom "    "  29 HN)
 vector do (store5=3.73) (atom "    "  30 HN)
 vector do (store5=15.16) (atom "    "  41 HN)
 vector do (store5=55.32) (atom "    "  60 HN)
 vector do (store5=23.55) (atom "    "  61 HN)


 NOE
   class CL3
   averaging CL3 r-6
   potential CL3 square
   sqconstant CL3 $a9
   sqoffset CL3 0.0
   scale CL3 $a12
   sqexponent CL3 2
 end

! calculate distance from R2(para), incl. %bound factors
! store distances

for $ide in ID (store5)
loop store_values
        vector show element (STORE5) (ID $ide)
       eval ($dist01= (1E8*((1.23E-
32*(4*$tau_c+(3*$tau_c/(1+(600.1328E6*2*3.14*$tau_c)^2)))*$frl*$frb/
$RESULT)^(1/6)) ) )
       NOE
         assign (ID $ide) (name TC) $dist01 $a1 $a2
       end
       vector do (store6=$dist01) (ID $ide)
end loop store_values
```

```
! Distances derived from R2 data from Src SH3 binding to peptide
P3Te

! store1 = fixed value for atoms that dissappear
! store2 = fixed distance for atoms that dissappear
! store3 = fixed value for atoms that are unaffected
! store4 = fixed distance for atoms that are unaffected
! store5 = observed R(para) value
! store6 = derived experimental distance

set mess=on end
set echo=off end
eval ($ide =1)
!---------------------------------------------------------------------
------
!----------------DEFINE UPPER-BOUND DISTANCE RESTRAINTS-------------
------
!---------------------------------------------------------------------
------
 !Residue numbering as in PDB 1RLQ (+5 compared to our protein)
 vector do (store1=142.50) (atom "    "  41 HN)
 vector do (store1=125.66) (atom "    "  42 HN)


NOE
   nres=20000
   class CL1
   averaging CL1 R-6
   potential CL1 square
   sqconstant CL1 $a9
   sqoffset CL1 0.0
   scale CL1 $a10
   sqexponent CL1 2
   ceil=30.0
end


for $ide in ID (store1)
loop store_values
        vector show element (STORE1) (ID $ide)
       eval ($dist01= (1E8*((1.23E-
32*(4*$tau_c+(3*$tau_c/(1+(600.1328E6*2*3.14*$tau_c)^2)))*$frl*$frb/
$RESULT)^(1/6)) ) )
       NOE
         assign (ID $ide) (name TC) $dist01 $a4 $a5
       end
       vector do (store2=$dist01) (ID $ide)
end loop store_values

!---------------------------------------------------------------------
------
!----------------DEFINE LOWER-BOUND DISTANCE RESTRAINTS-------------
------
!---------------------------------------------------------------------
```

```
------
 vector do (store3=2.60) (atom "    "  9 HT1) !first aa in pdb, not
in protein, so really an amide
 vector do (store3=2.60) (atom "    "  10 HN)
 vector do (store3=2.60) (atom "    "  11 HN)
 vector do (store3=2.60) (atom "    "  12 HN)
 vector do (store3=2.60) (atom "    "  13 HN)
 vector do (store3=2.60) (atom "    "  14 HN)
 vector do (store3=2.60) (atom "    "  16 HN)
 vector do (store3=2.60) (atom "    "  25 HN)
 vector do (store3=2.60) (atom "    "  27 HN)
 vector do (store3=2.60) (atom "    "  28 HN)
 vector do (store3=2.60) (atom "    "  29 HN)
 vector do (store3=2.60) (atom "    "  30 HN)
 vector do (store3=2.60) (atom "    "  31 HN)
 vector do (store3=2.60) (atom "    "  32 HN)
 vector do (store3=2.60) (atom "    "  33 HN)
 vector do (store3=2.60) (atom "    "  34 HN)
 vector do (store3=2.60) (atom "    "  36 HN)
 vector do (store3=2.60) (atom "    "  46 HN)
 vector do (store3=2.60) (atom "    "  47 HN)
 vector do (store3=2.60) (atom "    "  48 HN)
 vector do (store3=2.60) (atom "    "  49 HN)
 vector do (store3=2.60) (atom "    "  50 HN)
 vector do (store3=2.60) (atom "    "  51 HN)
 vector do (store3=2.60) (atom "    "  52 HN)
 vector do (store3=2.60) (atom "    "  54 HN)
 vector do (store3=2.60) (atom "    "  58 HN)
 vector do (store3=2.60) (atom "    "  59 HN)
 vector do (store3=2.60) (atom "    "  60 HN)
 vector do (store3=2.60) (atom "    "  61 HN)
 vector do (store3=2.60) (atom "    "  62 HN)
 vector do (store3=2.60) (atom "    "  64 HN)



NOE
   class CL2
   averaging CL2 R-6
   potential CL2 square
   sqconstant CL2 $a9
   sqoffset CL2 0.0
   scale CL2 $a11
   sqexponent CL2 2
end


for $ide in ID (store3)
loop store_values
        vector show element (STORE3) (ID $ide)
       eval ($dist01= (1E8*((1.23E-
32*(4*$tau_c+(3*$tau_c/(1+(600.1328E6*2*3.14*$tau_c)^2)))*$frl*$frb/
$RESULT)^(1/6)) ) )
       NOE
```

```
         assign (ID $ide) (name TC) $dist01 $a7 $a8
       end
       vector do (store4=$dist01) (ID $ide)
end loop store_values


!-------------------------------------------------------------------
------
!----------------DEFINE 2-BOUNDED DISTANCE RESTRAINTS---------------
------
!-------------------------------------------------------------------
------


! store R2(para) values as measured


 !vector do (store5=8.38) (atom "    "  15 HN)
 vector do (store5=3.72) (atom "    "  18 HN)
 vector do (store5=14.10) (atom "    "  19 HN)
 vector do (store5=21.12) (atom "    "  20 HN)
 vector do (store5=34.40) (atom "    "  21 HN)
 vector do (store5=91.82) (atom "    "  22 HN)
 vector do (store5=75.26) (atom "    "  23 HN)
 vector do (store5=11.41) (atom "    "  24 HN)
 vector do (store5=5.08) (atom "    "  38 HN)
 vector do (store5=26.81) (atom "    "  39 HN)
 vector do (store5=60.31) (atom "    "  40 HN)
 vector do (store5=5.95) (atom "    "  43 HN)
 vector do (store5=7.66) (atom "    "  44 HN)
 vector do (store5=37.91) (atom "    "  55 HN)
 vector do (store5=11.49) (atom "    "  56 HN)


 NOE
   class CL3
   averaging CL3 r-6
   potential CL3 square
   sqconstant CL3 $a9
   sqoffset CL3 0.0
   scale CL3 $a12
   sqexponent CL3 2
 end

! calculate distance from R2(para), incl. %bound factors
! store distances

for $ide in ID (store5)
loop store_values
        vector show element (STORE5) (ID $ide)
       eval ($dist01= (1E8*((1.23E-
32*(4*$tau_c+(3*$tau_c/(1+(600.1328E6*2*3.14*$tau_c)^2)))*$frl*$frb/
$RESULT)^(1/6)) ) )
       NOE
```

```
        assign (ID $ide) (name TC) $dist01 $a1 $a2
      end
      vector do (store6=$dist01) (ID $ide)
end loop store_values
```

XPLOR-NIH restraint files belonging to chapter 3

```
! Refining using individual error margins
! Distances derived from R2 data from SH2 binding to ETDDYAEI-Toac-
DEED
! this file: restraints.xpl
! store1 = fixed value for atoms that dissappear
! store2 = fixed distance for atoms that dissappear
! store3 = fixed value for atoms that are unaffected
! store4 = fixed distance for atoms that are unaffected
! store5 = observed R(para) value
! store6 = derived experimental distance
! store7 = upper limit R(para)
! store8 = lower limit R(para)

set mess=on end
set echo=on end
eval ($ide =1)
!-------------------------------------------------------------------
------
!----------------DEFINE UPPER-BOUND DISTANCE RESTRAINTS-------------
------
!-------------------------------------------------------------------
------

 !Rpara for target distance to store1


 vector do (store1=97.14) (atom "    "  201 HN)
 vector do (store1=84.84) (atom "    "  203 HN)
 vector do (store1=92.77) (atom "    "  215 HN)
 vector do (store1=96.18) (atom "    "  236 HN)


 !lower Rpara to store 8
 vector do (store8=71.11) (atom "    "  201 HN)
 vector do (store8=59.18) (atom "    "  203 HN)
 vector do (store8=67.20) (atom "    "  215 HN)
 vector do (store8=71.40) (atom "    "  236 HN)

NOE
   nres=20000
   class CL1
   averaging CL1 R-6
   potential CL1 square
   sqconstant CL1 $a9
   sqoffset CL1 0.0
   scale CL1 $a10
   sqexponent CL1 2
   ceil=30.0
end
```

```
for $ide in ID (store1)
loop store_values
        vector show element (STORE1) (ID $ide)
       eval ($dist01= (1E8*((1.23E-
32*(4*$tau_c+(3*$tau_c/(1+(600.1328E6*2*3.14*$tau_c)^2)))*$frl*$frb/
$RESULT)^(1/6)) ) )
        vector show element (STORE8) (ID $ide)
       eval ($r01= (1E8*((1.23E-
32*(4*$tau_c+(3*$tau_c/(1+(600.1328E6*2*3.14*$tau_c)^2)))*$frl*$frb/
$RESULT)^(1/6)) ) )
       eval ($dist02 = $r01 - $dist01)
       eval ($dist03 = $dist01 - 3.5)
       NOE
         assign (ID $ide) (name TC) $dist01 $dist03 $dist02
       end
       vector do (store2=$dist01) (ID $ide)
end loop store_values

!---------------------------------------------------------------------
------
!----------------DEFINE LOWER-BOUND DISTANCE RESTRAINTS-------------
------
!---------------------------------------------------------------------
------


 vector do (store3=3.11) (atom "    "  147 HN)
 vector do (store3=3.11) (atom "    "  148 HN)
 vector do (store3=3.11) (atom "    "  150 HN)
 vector do (store3=3.11) (atom "    "  151 HN)
 vector do (store3=3.11) (atom "    "  154 HN)
 vector do (store3=3.11) (atom "    "  158 HN)
 vector do (store3=3.11) (atom "    "  159 HN)
 vector do (store3=3.11) (atom "    "  160 HN)
 vector do (store3=3.11) (atom "    "  161 HN)
 vector do (store3=3.11) (atom "    "  162 HN)
 vector do (store3=3.11) (atom "    "  163 HN)
 vector do (store3=3.11) (atom "    "  164 HN)
 vector do (store3=3.11) (atom "    "  165 HN)
 vector do (store3=3.11) (atom "    "  166 HN)
 vector do (store3=3.11) (atom "    "  167 HN)
 vector do (store3=3.11) (atom "    "  170 HN)
 vector do (store3=3.11) (atom "    "  171 HN)
 vector do (store3=3.11) (atom "    "  172 HN)
 vector do (store3=3.11) (atom "    "  173 HN)
 vector do (store3=3.11) (atom "    "  174 HN)
 vector do (store3=3.11) (atom "    "  175 HN)
 vector do (store3=3.11) (atom "    "  176 HN)
 vector do (store3=3.11) (atom "    "  177 HN)
 vector do (store3=3.11) (atom "    "  183 HN)
 vector do (store3=3.11) (atom "    "  185 HN)
 vector do (store3=3.11) (atom "    "  189 HN)
 vector do (store3=3.11) (atom "    "  190 HN)
```

```
 vector do (store3=3.11) (atom "    "  191 HN)
 vector do (store3=3.11) (atom "    "  192 HN)
 vector do (store3=3.11) (atom "    "  194 HN)
 vector do (store3=3.11) (atom "    "  195 HN)
 vector do (store3=3.11) (atom "    "  196 HN)
 vector do (store3=3.11) (atom "    "  198 HN)
 vector do (store3=3.11) (atom "    "  207 HN)
 vector do (store3=3.11) (atom "    "  208 HN)
 vector do (store3=3.11) (atom "    "  209 HN)
 vector do (store3=3.11) (atom "    "  210 HN)
 vector do (store3=3.11) (atom "    "  212 HN)
 vector do (store3=3.11) (atom "    "  213 HN)
 vector do (store3=3.11) (atom "    "  220 HN)
 vector do (store3=3.11) (atom "    "  222 HN)
 vector do (store3=3.11) (atom "    "  225 HN)
 vector do (store3=3.11) (atom "    "  226 HN)
 vector do (store3=3.11) (atom "    "  227 HN)
 vector do (store3=3.11) (atom "    "  228 HN)
 vector do (store3=3.11) (atom "    "  229 HN)
 vector do (store3=3.11) (atom "    "  230 HN)
 vector do (store3=3.11) (atom "    "  231 HN)
 vector do (store3=3.11) (atom "    "  233 HN)
 vector do (store3=3.11) (atom "    "  241 HN)
 vector do (store3=3.11) (atom "    "  242 HN)
 vector do (store3=3.11) (atom "    "  243 HN)
 vector do (store3=3.11) (atom "    "  245 HN)



NOE
   class CL2
   averaging CL2 R-6
   potential CL2 square
   sqconstant CL2 $a9
   sqoffset CL2 0.0
   scale CL2 $a11
   sqexponent CL2 2
end

for $ide in ID (store3)
loop store_values
        vector show element (STORE3) (ID $ide)
       eval ($dist01= (1E8*((1.23E-
32*(4*$tau_c+(3*$tau_c/(1+(600.1328E6*2*3.14*$tau_c)^2)))*$frl*$frb/
$RESULT)^(1/6)) ) )
       NOE
         assign (ID $ide) (name TC) $dist01 $a7 $a8
       end
       vector do (store4=$dist01) (ID $ide)
end loop store_values


!-------------------------------------------------------------------
------
```

```
!----------------DEFINE 2-BOUNDED DISTANCE RESTRAINTS---------------
------
!-------------------------------------------------------------------
------


 !store R2(para) values as measured

 vector do (store5=7.66) (atom "    "  149 HN)
 vector do (store5=7.95) (atom "    "  152 HN)
 vector do (store5=17.09) (atom "    "  156 HN)
 vector do (store5=13.16) (atom "    "  169 HN)
 vector do (store5=23.24) (atom "    "  178 HN)
 vector do (store5=18.70) (atom "    "  179 HN)
 vector do (store5=9.19) (atom "    "  181 HN)
 vector do (store5=7.34) (atom "    "  182 HN)
 vector do (store5=7.57) (atom "    "  186 HN)
 vector do (store5=5.66) (atom "    "  188 HN)
 vector do (store5=12.20) (atom "    "  193 HN)
 vector do (store5=110.00) (atom "    "  199 HN)
 vector do (store5=17.34) (atom "    "  200 HN)
 vector do (store5=84.95) (atom "    "  202 HN)
 vector do (store5=11.08) (atom "    "  205 HN)
 vector do (store5=30.97) (atom "    "  206 HN)
 vector do (store5=32.19) (atom "    "  214 HN)
 vector do (store5=78.51) (atom "    "  217 HN)
 vector do (store5=18.65) (atom "    "  218 HN)
 vector do (store5=15.29) (atom "    "  219 HN)
 vector do (store5=5.02) (atom "    "  221 HN)
 vector do (store5=53.74) (atom "    "  223 HN)
 vector do (store5=19.09) (atom "    "  234 HN)
 vector do (store5=32.42) (atom "    "  235 HN)
 vector do (store5=88.88) (atom "    "  238 HN)
 vector do (store5=19.16) (atom "    "  239 HN)
 vector do (store5=44.93) (atom "    "  240 HN)


 !upper Rpara to store 7
 vector do (store7=10.38) (atom "    "  149 HN)
 vector do (store7=10.63) (atom "    "  152 HN)
 vector do (store7=20.03) (atom "    "  156 HN)
 vector do (store7=15.45) (atom "    "  169 HN)
 vector do (store7=41.53) (atom "    "  178 HN)
 vector do (store7=23.87) (atom "    "  179 HN)
 vector do (store7=11.92) (atom "    "  181 HN)
 vector do (store7=10.68) (atom "    "  182 HN)
 vector do (store7=12.52) (atom "    "  186 HN)
 vector do (store7=8.61) (atom "    "  188 HN)
 vector do (store7=26.61) (atom "    "  193 HN)
 vector do (store7=155.24) (atom "    "  199 HN)
 vector do (store7=21.51) (atom "    "  200 HN)
 vector do (store7=121.46) (atom "    "  202 HN)
 vector do (store7=15.21) (atom "    "  205 HN)
 vector do (store7=35.59) (atom "    "  206 HN)
```

```
vector do (store7=44.18) (atom "    "  214 HN)
vector do (store7=94.80) (atom "    "  217 HN)
vector do (store7=21.63) (atom "    "  218 HN)
vector do (store7=18.22) (atom "    "  219 HN)
vector do (store7=8.48) (atom "    "  221 HN)
vector do (store7=66.32) (atom "    "  223 HN)
vector do (store7=22.34) (atom "    "  234 HN)
vector do (store7=36.51) (atom "    "  235 HN)
vector do (store7=123.38) (atom "    "  238 HN)
vector do (store7=22.01) (atom "    "  239 HN)
vector do (store7=52.85) (atom "    "  240 HN)



!lower Rpara to store 8
vector do (store8=5.09) (atom "    "  149 HN)
vector do (store8=5.41) (atom "    "  152 HN)
vector do (store8=14.35) (atom "    "  156 HN)
vector do (store8=11.00) (atom "    "  169 HN)
vector do (store8=8.75) (atom "    "  178 HN)
vector do (store8=14.00) (atom "    "  179 HN)
vector do (store8=6.62) (atom "    "  181 HN)
vector do (store8=4.19) (atom "    "  182 HN)
vector do (store8=3.00) (atom "    "  186 HN)
vector do (store8=2.86) (atom "    "  188 HN)
vector do (store8=0.001) (atom "    "  193 HN)
vector do (store8=86.84) (atom "    "  199 HN)
vector do (store8=13.48) (atom "    "  200 HN)
vector do (store8=64.02) (atom "    "  202 HN)
vector do (store8=7.25) (atom "    "  205 HN)
vector do (store8=26.77) (atom "    "  206 HN)
vector do (store8=22.26) (atom "    "  214 HN)
vector do (store8=66.64) (atom "    "  217 HN)
vector do (store8=15.84) (atom "    "  218 HN)
vector do (store8=12.52) (atom "    "  219 HN)
vector do (store8=1.77) (atom "    "  221 HN)
vector do (store8=43.94) (atom "    "  223 HN)
vector do (store8=16.07) (atom "    "  234 HN)
vector do (store8=28.71) (atom "    "  235 HN)
vector do (store8=69.36) (atom "    "  238 HN)
vector do (store8=16.49) (atom "    "  239 HN)
vector do (store8=38.19) (atom "    "  240 HN)



NOE
  class CL3
  averaging CL3 r-6
  potential CL3 square
  sqconstant CL3 $a9
  sqoffset CL3 0.0
  scale CL3 $a12
  sqexponent CL3 2
```

```
 end

! calculate distance from R2(para), incl. %bound factors
! store distances

for $ide in ID (store5)
loop store_values
        vector show element (STORE5) (ID $ide)
       eval ($dist01= (1E8*((1.23E-
32*(4*$tau_c+(3*$tau_c/(1+(600.1328E6*2*3.14*$tau_c)^2)))*$frl*$frb/
$RESULT)^(1/6)) ) )
        vector show element (STORE7) (ID $ide)
       eval ($r01= (1E8*((1.23E-
32*(4*$tau_c+(3*$tau_c/(1+(600.1328E6*2*3.14*$tau_c)^2)))*$frl*$frb/
$RESULT)^(1/6)) ) )
        vector show element (STORE8) (ID $ide)
       eval ($r02= (1E8*((1.23E-
32*(4*$tau_c+(3*$tau_c/(1+(600.1328E6*2*3.14*$tau_c)^2)))*$frl*$frb/
$RESULT)^(1/6)) ) )
       eval ($dist03 = $dist01 - $r01)
       eval ($dist02 = $r02 - $dist01)
       NOE
         assign (ID $ide) (name TC) $dist01 $dist03 $dist02
       end
       vector do (store6=$dist01) (ID $ide)
end loop store_values
```

```
! Refining using individual error margins
! Distances derived from R2 data from SH2 binding to ETDDpYAEI-Toac-
DEED
! this file: restraints.xpl
! store1 = fixed value for atoms that dissappear
! store2 = fixed distance for atoms that dissappear
! store3 = fixed value for atoms that are unaffected
! store4 = fixed distance for atoms that are unaffected
! store5 = observed R(para) value
! store6 = derived experimental distance
! store7 = upper limit R(para)
! store8 = lower limit R(para)

set mess=on end
set echo=on end
eval ($ide =1)
!---------------------------------------------------------------------
------
!----------------DEFINE UPPER-BOUND DISTANCE RESTRAINTS-------------
------
!---------------------------------------------------------------------
------

 !Rpara for target distance to store1


 vector do (store1=26.08) (atom "    "  179 HN)
 vector do (store1=46.06) (atom "    "  202 HN)
 vector do (store1=18.08) (atom "    "  215 HN)
 vector do (store1=60.45) (atom "    "  217 HN)


 !lower Rpara to store 8
 vector do (store8=0.0001)   (atom "    "  179 HN)
 vector do (store8=6.2)   (atom "    "  202 HN)
 vector do (store8=0.0001)   (atom "    "  215 HN)
 vector do (store8=31.4)  (atom "    "  217 HN)

NOE
   nres=20000
   class CL1
   averaging CL1 R-6
   potential CL1 square
   sqconstant CL1 $a9
   sqoffset CL1 0.0
   scale CL1 $a10
   sqexponent CL1 2
   ceil=30.0
end


for $ide in ID (store1)
loop store_values
        vector show element (STORE1) (ID $ide)
```

```
       eval ($dist01= (1E8*((1.23E-
32*(4*$tau_c+(3*$tau_c/(1+(600.1328E6*2*3.14*$tau_c)^2)))*$frl*$frb/
$RESULT)^(1/6)) ) )
        vector show element (STORE8) (ID $ide)
       eval ($r01= (1E8*((1.23E-
32*(4*$tau_c+(3*$tau_c/(1+(600.1328E6*2*3.14*$tau_c)^2)))*$frl*$frb/
$RESULT)^(1/6)) ) )
       eval ($dist02 = $r01 - $dist01)
       eval ($dist03 = $dist01 - 3.5)
       NOE
         assign (ID $ide) (name TC) $dist01 $dist03 $dist02
       end
       vector do (store2=$dist01) (ID $ide)
end loop store_values

!---------------------------------------------------------------------
------
!----------------DEFINE LOWER-BOUND DISTANCE RESTRAINTS-------------
------
!---------------------------------------------------------------------
------


 vector do (store3=3.80) (atom "    "  147 HN)
 vector do (store3=3.80) (atom "    "  148 HN)
 vector do (store3=3.80) (atom "    "  149 HN)
 vector do (store3=3.80) (atom "    "  154 HN)
 vector do (store3=3.80) (atom "    "  155 HN)
 vector do (store3=3.80) (atom "    "  158 HN)
 vector do (store3=3.80) (atom "    "  160 HN)
 vector do (store3=3.80) (atom "    "  162 HN)
 vector do (store3=3.80) (atom "    "  164 HN)
 vector do (store3=3.80) (atom "    "  165 HN)
 vector do (store3=3.80) (atom "    "  166 HN)
 vector do (store3=3.80) (atom "    "  167 HN)
 vector do (store3=3.80) (atom "    "  172 HN)
 vector do (store3=3.80) (atom "    "  173 HN)
 vector do (store3=3.80) (atom "    "  174 HN)
 vector do (store3=3.80) (atom "    "  183 HN)
 vector do (store3=3.80) (atom "    "  197 HN)
 vector do (store3=3.80) (atom "    "  208 HN)
 vector do (store3=3.80) (atom "    "  209 HN)
 vector do (store3=3.80) (atom "    "  210 HN)
 vector do (store3=3.80) (atom "    "  211 HN)
 vector do (store3=3.80) (atom "    "  212 HN)
 vector do (store3=3.80) (atom "    "  221 HN)
 vector do (store3=3.80) (atom "    "  222 HN)
 vector do (store3=3.80) (atom "    "  226 HN)
 vector do (store3=3.80) (atom "    "  231 HN)
 vector do (store3=3.80) (atom "    "  244 HN)
 vector do (store3=3.80) (atom "    "  245 HN)
```

```
NOE
   class CL2
   averaging CL2 R-6
   potential CL2 square
   sqconstant CL2 $a9
   sqoffset CL2 0.0
   scale CL2 $a11
   sqexponent CL2 2
end

for $ide in ID (store3)
loop store_values
        vector show element (STORE3) (ID $ide)
       eval ($dist01= (1E8*((1.23E-
32*(4*$tau_c+(3*$tau_c/(1+(600.1328E6*2*3.14*$tau_c)^2)))*$frl*$frb/
$RESULT)^(1/6)) ) )
       NOE
         assign (ID $ide) (name TC) $dist01 $a7 $a8
       end
       vector do (store4=$dist01) (ID $ide)
end loop store_values


!-------------------------------------------------------------------
------
!----------------DEFINE 2-BOUNDED DISTANCE RESTRAINTS---------------
------
!-------------------------------------------------------------------
------


 !store R2(para) values as measured

 vector do (store5=10.89) (atom "    "  151 HN)
 vector do (store5=6.38) (atom "    "  156 HN)
 vector do (store5=6.32) (atom "    "  161 HN)
 vector do (store5=5.18) (atom "    "  169 HN)
 vector do (store5=5.86) (atom "    "  170 HN)
 vector do (store5=16.49) (atom "    "  175 HN)
 vector do (store5=29.38) (atom "    "  176 HN)
 vector do (store5=12.29) (atom "    "  177 HN)
 vector do (store5=8.06) (atom "    "  181 HN)
 vector do (store5=5.54) (atom "    "  182 HN)
 vector do (store5=9.38) (atom "    "  188 HN)
 vector do (store5=6.36) (atom "    "  189 HN)
 vector do (store5=6.49) (atom "    "  190 HN)
 vector do (store5=11.66) (atom "    "  191 HN)
 vector do (store5=7.30) (atom "    "  192 HN)
 vector do (store5=5.53) (atom "    "  194 HN)
 vector do (store5=7.49) (atom "    "  195 HN)
 vector do (store5=6.02) (atom "    "  196 HN)
 vector do (store5=6.44) (atom "    "  198 HN)
```

```
vector do (store5=51.43) (atom "    "  199 HN)
vector do (store5=33.27) (atom "    "  200 HN)
vector do (store5=22.70) (atom "    "  205 HN)
vector do (store5=19.51) (atom "    "  206 HN)
vector do (store5=7.38) (atom "    "  207 HN)
vector do (store5=28.07) (atom "    "  213 HN)
vector do (store5=56.88) (atom "    "  214 HN)
vector do (store5=8.91) (atom "    "  220 HN)
vector do (store5=31.64) (atom "    "  223 HN)
vector do (store5=7.57) (atom "    "  228 HN)
vector do (store5=20.06) (atom "    "  230 HN)
vector do (store5=47.91) (atom "    "  234 HN)
vector do (store5=94.03) (atom "    "  235 HN)
vector do (store5=59.61) (atom "    "  239 HN)
vector do (store5=38.91) (atom "    "  240 HN)
vector do (store5=23.23) (atom "    "  241 HN)


!upper Rpara to store 7
vector do (store7=42.7) (atom "    "  151 HN)
vector do (store7=11.2) (atom "    "  156 HN)
vector do (store7=9.8) (atom "    "  161 HN)
vector do (store7=7.4) (atom "    "  169 HN)
vector do (store7=11.3) (atom "    "  170 HN)
vector do (store7=25.8) (atom "    "  175 HN)
vector do (store7=38.1) (atom "    "  176 HN)
vector do (store7=23.1) (atom "    "  177 HN)
vector do (store7=11.3) (atom "    "  181 HN)
vector do (store7=9.4) (atom "    "  182 HN)
vector do (store7=14.6) (atom "    "  188 HN)
vector do (store7=9.5) (atom "    "  189 HN)
vector do (store7=11.3) (atom "    "  190 HN)
vector do (store7=15.2) (atom "    "  191 HN)
vector do (store7=11.3) (atom "    "  192 HN)
vector do (store7=7.3) (atom "    "  194 HN)
vector do (store7=10.6) (atom "    "  195 HN)
vector do (store7=9.3) (atom "    "  196 HN)
vector do (store7=9.4) (atom "    "  198 HN)
vector do (store7=61.3) (atom "    "  199 HN)
vector do (store7=43.6) (atom "    "  200 HN)
vector do (store7=35.6) (atom "    "  205 HN)
vector do (store7=24.8) (atom "    "  206 HN)
vector do (store7=12.2) (atom "    "  207 HN)
vector do (store7=38.6) (atom "    "  213 HN)
vector do (store7=107.0) (atom "    "  214 HN)
vector do (store7=14.1) (atom "    "  220 HN)
vector do (store7=48.2) (atom "    "  223 HN)
vector do (store7=9.2) (atom "    "  228 HN)
vector do (store7=28.9) (atom "    "  230 HN)
vector do (store7=65.1) (atom "    "  234 HN)
vector do (store7=168.8) (atom "    "  235 HN)
vector do (store7=83.1) (atom "    "  239 HN)
vector do (store7=50.1) (atom "    "  240 HN)
```

```
 vector do (store7=43.0) (atom "    "  241 HN)

 !lower Rpara to store 8
 vector do (store8=0.001) (atom "    "  151 HN)
 vector do (store8=1.8) (atom "    "  156 HN)
 vector do (store8=3.0) (atom "    "  161 HN)
 vector do (store8=3.0) (atom "    "  169 HN)
 vector do (store8=0.8) (atom "    "  170 HN)
 vector do (store8=8.0) (atom "    "  175 HN)
 vector do (store8=21.8) (atom "    "  176 HN)
 vector do (store8=2.6) (atom "    "  177 HN)
 vector do (store8=5.0) (atom "    "  181 HN)
 vector do (store8=1.9) (atom "    "  182 HN)
 vector do (store8=4.5) (atom "    "  188 HN)
 vector do (store8=3.4) (atom "    "  189 HN)
 vector do (store8=2.0) (atom "    "  190 HN)
 vector do (store8=8.3) (atom "    "  191 HN)
 vector do (store8=3.5) (atom "    "  192 HN)
 vector do (store8=3.8) (atom "    "  194 HN)
 vector do (store8=4.6) (atom "    "  195 HN)
 vector do (store8=2.9) (atom "    "  196 HN)
 vector do (store8=3.7) (atom "    "  198 HN)
 vector do (store8=43.1) (atom "    "  199 HN)
 vector do (store8=24.5) (atom "    "  200 HN)
 vector do (store8=11.7) (atom "    "  205 HN)
 vector do (store8=14.6) (atom "    "  206 HN)
 vector do (store8=2.8) (atom "    "  207 HN)
 vector do (store8=18.8) (atom "    "  213 HN)
 vector do (store8=27.5) (atom "    "  214 HN)
 vector do (store8=4.0) (atom "    "  220 HN)
 vector do (store8=17.9) (atom "    "  223 HN)
 vector do (store8=6.0) (atom "    "  228 HN)
 vector do (store8=12.1) (atom "    "  230 HN)
 vector do (store8=34.3) (atom "    "  234 HN)
 vector do (store8=61.2) (atom "    "  235 HN)
 vector do (store8=42.3) (atom "    "  239 HN)
 vector do (store8=29.5) (atom "    "  240 HN)
 vector do (store8=6.5) (atom "    "  241 HN)


 NOE
   class CL3
   averaging CL3 r-6
   potential CL3 square
   sqconstant CL3 $a9
   sqoffset CL3 0.0
   scale CL3 $a12
   sqexponent CL3 2
 end

! calculate distance from R2(para), incl. %bound factors
! store distances

for $ide in ID (store5)
```

```
loop store_values
        vector show element (STORE5) (ID $ide)
       eval ($dist01= (1E8*((1.23E-
32*(4*$tau_c+(3*$tau_c/(1+(600.1328E6*2*3.14*$tau_c)^2)))*$frl*$frb/
$RESULT)^(1/6)) ) )
        vector show element (STORE7) (ID $ide)
       eval ($r01= (1E8*((1.23E-
32*(4*$tau_c+(3*$tau_c/(1+(600.1328E6*2*3.14*$tau_c)^2)))*$frl*$frb/
$RESULT)^(1/6)) ) )
        vector show element (STORE8) (ID $ide)
       eval ($r02= (1E8*((1.23E-
32*(4*$tau_c+(3*$tau_c/(1+(600.1328E6*2*3.14*$tau_c)^2)))*$frl*$frb/
$RESULT)^(1/6)) ) )
       eval ($dist03 = $dist01 - $r01)
       eval ($dist02 = $r02 - $dist01)
       NOE
         assign (ID $ide) (name TC) $dist01 $dist03 $dist02
       end
       vector do (store6=$dist01) (ID $ide)
end loop store_values
```

List of publications

Lindfors, H.E., de Koning, P.E., Drijfhout, J.W., Venezia, B. and Ubbink, M. (2008). Mobility of TOAC spin-labelled peptides binding to the Src SH3 domain studied by paramagnetic NMR. *J. Biomol. NMR* **41**, 157-167.

I. Takahashi, S. Kuroiwa, H.E. Lindfors, L.A. Ndamba, Y. Hiruma, T. Yajima, N. Okishio, M. Ubbink and S. Hirota (2009). Modulation of protein-ligand interactions by photocleavage of a cyclic peptide using phosphatidylinositol 3-kinase SH3 domain as model system. *J. Pept. Sci.* **15**, 411-416.

Lindfors, H.E., Drijfhout, J.W., Arendsen, Y. and Ubbink, M (2010). Dynamics in a high-affinity peptide-SH2 domain complex. *Submitted.*

Lindfors et al (2010). A dynamic intermediate state in peptide-binding to the combined Src SH3 and SH2 domains. *Manuscript in preparation.*

Curriculum vitae

Hanna Lindfors was born in Säter, Sweden on the 24th of May 1978. In 2003 she obtained a M.Sc. degree in engineering physics from Uppsala University, having spent one year of the programme at the Swiss federal institute of technology (ETH) in Zurich, Switzerland. Her M.Sc. thesis research focused on the characterisation of magnetic nanoparticles, and was performed at the institutes of materials physics and solid state physics at Uppsala University, under the supervision of Prof. R. Wäppling and Prof. P. Nordblad.

After having completed additional courses in molecular and cellular biology at Uppsala University, in May 2004 Hanna joined the medicinal chemistry group at the Leiden Amsterdam Centre for Drug Research (LACDR) in Leiden for a five-month research project. During this time she worked on the cloning of genes encoding G-protein coupled receptors. In November 2004 Hanna joined the Protein Chemistry and Biophysical Structural Chemistry groups at Leiden University as a PhD student, working under the supervision of Dr. M. Ubbink and Prof. J.P. Abrahams.

As of August 2009 Hanna is employed at the DSM Biotechnology Centre, Delft.

Acknowledgements

I would like to thank all the collaborators and colleagues that have contributed to the work in this thesis.

Marcellus Ubbink and Jan Pieter Abrahams are thanked for their support and advice through-out this project. Margot Beukers, Elisabeth Klaasse and Henk de Vries are thanked for their help with insect cell culture and the baculovirus expression vector system. I am grateful to Jan Wouter Drijfhout for providing me with peptides for the NMR and ITC studies, Francesco Scarpelli for help with EPR experiments, and Shun Hirota and co-workers for collaboration on the PI3 kinase project. Kees Erkelens and Fons Lefeber are thanked for NMR support and Sylvia Le Dévédec for help with mammalian cell culture and fluorescence microscopy. I would also like to thank the students that took part in the research in this thesis: Yoshi Hiruma and Brigida Venezia. I am grateful to Lionel Ndamba for his work on the NMR resonance assignments of the PI3 kinase SH3 domain and to Yvonne Arendsen for the SH2 domain construct.

To all the members of the protchem group: thank you for interesting scientific discussions and for the many laughs we have shared. Anneloes and Lionel, thanks for all the technical support you have provided.

Rinske, Gerhild, Virginie and Monica, thanks for all the good times inside and outside the lab – this journey would not have been the same without you!

My most heartfelt thanks also to my family (in-law), without whom I could not have done this.

Finally, I would like to thank Gabor – without whom I could not do at all.